

PALEOTECTONIC SETTING OF THE TAKLA GROUP VOLCANO-SEDIMENTARY
ASSEMBLAGE, STIKINE TERRANE, McCONNELL CREEK MAP AREA,
NORTH CENTRAL BRITISH COLUMBIA

Vanessa Gale

Submitted in Partial Fulfillment of the Requirements
for the Degree of Bachelor of Sciences, Honours
Department of Earth Sciences
Dalhousie University, Halifax, Nova Scotia
March, 1996



Dalhousie University

Department of Earth Sciences

Halifax, Nova Scotia

Canada B3H 3J5

(902) 494-2358

FAX (902) 494-6889

DATE April 9, 1996

AUTHOR Vanessa Gale

TITLE PALEOTECTONIC SETTING OF THE TAKLA GROUP VOLCANO-
SEDIMENTARY ASSEMBLAGE, STIKINE TERRANE, McCONNELL
CREEK MAP AREA, NORTH CENTRAL BRITISH COLUMBIA

Degree B Sc Convocation Spring, 1996 Year 1996

Permission is herewith granted to Dalhousie University to circulate and to have copied for non-commercial purposes, at its discretion, the above title upon the request of individuals or institutions.

THE AUTHOR RESERVES OTHER PUBLICATION RIGHTS, AND NEITHER THE THESIS NOR EXTENSIVE EXTRACTS FROM IT MAY BE PRINTED OR OTHERWISE REPRODUCED WITHOUT THE AUTHOR'S WRITTEN PERMISSION.

THE AUTHOR ATTESTS THAT PERMISSION HAS BEEN OBTAINED FOR THE USE OF ANY COPYRIGHTED MATERIAL APPEARING IN THIS THESIS (OTHER THAN BRIEF EXCERPTS REQUIRING ONLY PROPER ACKNOWLEDGEMENT IN SCHOLARLY WRITING) AND THAT ALL SUCH USE IS CLEARLY ACKNOWLEDGED.

Distribution License

DalSpace requires agreement to this non-exclusive distribution license before your item can appear on DalSpace.

NON-EXCLUSIVE DISTRIBUTION LICENSE

You (the author(s) or copyright owner) grant to Dalhousie University the non-exclusive right to reproduce and distribute your submission worldwide in any medium.

You agree that Dalhousie University may, without changing the content, reformat the submission for the purpose of preservation.

You also agree that Dalhousie University may keep more than one copy of this submission for purposes of security, back-up and preservation.

You agree that the submission is your original work, and that you have the right to grant the rights contained in this license. You also agree that your submission does not, to the best of your knowledge, infringe upon anyone's copyright.

If the submission contains material for which you do not hold copyright, you agree that you have obtained the unrestricted permission of the copyright owner to grant Dalhousie University the rights required by this license, and that such third-party owned material is clearly identified and acknowledged within the text or content of the submission.

If the submission is based upon work that has been sponsored or supported by an agency or organization other than Dalhousie University, you assert that you have fulfilled any right of review or other obligations required by such contract or agreement.

Dalhousie University will clearly identify your name(s) as the author(s) or owner(s) of the submission, and will not make any alteration to the content of the files that you have submitted.

If you have questions regarding this license please contact the repository manager at dalspace@dal.ca.

Grant the distribution license by signing and dating below.

Name of signatory

Date

Abstract

The Upper Triassic Takla Group volcano-sedimentary assemblage is located within the Stikine Terrane of the Intermontane Belt in the Canadian Cordillera. In the McConnell Creek area, the assemblage consists of clinopyroxene and plagioclase porphyritic basaltic to andesitic effusive and pyroclastic rocks that are interlayered with sandstones, siltstones, argillites and conglomerates. Relatively immobile trace element analysis indicates that rocks are subalkaline and compositionally intermediate between tholeiitic and calc-alkaline. Chondrite normalized rare earth element (REE) plots show minor light REE enrichment consistent with subalkaline tholeiitic to calc-alkaline magmas. Mantle normalized trace element patterns display a pronounced Nb depletion and large ion lithophile element enrichment that suggest magmatism was subduction-related.

A coeval volcano-sedimentary assemblage occurs in fault contact with the Takla Group of the Stikine Terrane. This group, also named Takla, occurs in the adjacent Quesnel terrane and is also subduction-related. In the past, the two have been interpreted as a single cogenetic unit as well as two separate, non-related units. Similarities in relatively immobile trace element abundances indicate that the eastern and western Takla Groups are broadly geochemically alike and may have similar source compositions and melt histories. However, the location of the groups in two different terranes precludes a comagmatic relationship. Nevertheless, the chemical resemblance between the two groups does emphasize larger scale similarities noted between the Stikine and Quesnel terranes.

Key Words: Takla Group, Stikine Terrane, arc-magmatism, REE, Nb-depletion, Quesnel Terrane

Acknowledgments

This thesis is the cumulative result of efforts on the part of many people. Firstly, I owe great thanks to my advisor, Jarda Dostal, for his guidance and patience. I am also grateful to Marcos Zentilli and Martin Gibling for all of the good advice they have given me. The helpful suggestions of Mike Gorton, Rebecca Jamieson, Neil Banerjee and Gunter Muecke have greatly improved the quality of this thesis. I would also like to acknowledge Neil Church and Filippo Ferri, of the British Columbia Ministry of Mines, Energy and Petroleum Resources, as well as Jim Monger, for their insight into Cordilleran geology.

I would like to thank Bob Mackay for his patient and helpful instruction with the microprobe. Randolph Coney also deserves credit for aiding me with his technical support.

I would also like to thank the entire Honours class for their tireless support, in particular Clare Robinson and Jennifer Harding, who rushed to my rescue following an ill-timed computer crash. A thousand thank-yous to Owen Chapman for his final hour assistance in getting this thesis in on time. Lastly, I wish to thank my friends and family for their limitless patience, support and encouragement.

Table of Contents

	Page
Abstract.....	i
Acknowledgments.....	ii
Table of Contents.....	iii
Table of Figures.....	v
Table of Plates.....	vii
Chapter 1 Geological Framework.....	1
1.1 Introductory Statement.....	1
1.2 Purpose and Objectives.....	1
1.3 Scope and Thesis Organization.....	3
1.4 Regional Geological Setting.....	3
1.5 Location and Physiography of Study Area.....	9
1.6 Previous Work.....	9
1.7 Geology of Study Area.....	12
Chapter 2 Petrography and Mineral Chemistry.....	22
2.1 Introduction.....	22
2.2 Effusive Rocks.....	23
2.3 Pyroclastic Rocks.....	38
2.4 Alteration and Metamorphism.....	38
2.5 Petrographic Classification.....	42
2.6 Summary.....	47
Chapter 3 Geochemical Classification.....	48
3.1 Introduction.....	48
3.2 Experimental Methods.....	48
3.3 Element Mobility.....	49
3.4 Normative Calculation.....	53
3.5 Major and Trace Element Classification.....	54
3.6 Petrogenesis and Melt Evolution.....	60
3.7 Summary.....	69

Chapter 4 Paleotectonic Interpretation.....	70
4.1 Introduction.....	70
4.2 Sample Screening.....	71
4.3 Tectonomagmatic Discrimination Diagrams.....	72
4.4 Rare Earth Element Patterns.....	76
4.5 Spider Diagrams.....	76
4.6 Clinopyroxene Analysis.....	79
4.7 Discussion.....	80
4.8 Summary.....	85
Chapter 5 Local and Regional Tectonic Implications.....	87
5.1 Introduction.....	87
5.2 General Comparison.....	88
5.3 Geochemical Comparison.....	90
5.4 Discussion.....	95
5.5 Summary.....	98
Chapter 6 Conclusions.....	103
6.1 Results.....	103
6.2 Recommendations.....	104
References.....	105
Appendices	
A: Petrographic descriptions of Stikinian Takla Group volcanic samples.....	A1
B: Electron microprobe techniques and data.....	B1
C: XRF and ICP-MS data, accuracy and precision.....	C1
D: Quesnellian Takla Group XRF data.....	D1

Table of Figures

Figure	Page
Figure 1.1: Schematic diagram of the major terranes of the Canadian Cordillera.....	5
Figure 1.2: Schematic diagram of terrane amalgamation and accretion.....	6
Figure 1.3: Physiographic belt distribution in the Canadian Cordillera.....	7
Figure 1.4: Map of the McConnell Creek area.....	10
Figure 1.5: Stratigraphic relationships of Takla Group formations.....	13
Figure 2.1: Stratigraphic column showing sample location.....	24
Figure 2.2: Electron microprobe backscatter images of zoned clinopyroxene phenocrysts.....	31
Figure 2.3: Pyroxene quadrilateral diagram.....	32
Figure 2.4: Feldspar ternary diagram.....	35
Figure 2.5: Pyroclastic classification scheme of Easton and Johns (1986).....	39
Figure 3.1a,b: Binary plots of elements against Zr to demonstrate element mobility.....	51
Figure 3.2: SiO ₂ vs. Zr/TiO ₂ diagram to determine alkalinity and differentiation.....	55
Figure 3.3: Nb/Y vs. Zr/TiO ₂ diagram to determine alkalinity.....	56
Figure 3.4: SiO ₂ vs. FeO*/MgO diagram.....	58
Figure 3.5: TiO ₂ vs FeO*/MgO diagram.....	59
Figure 3.6: Spider diagram to determine pyroclastic trace element composition.....	61
Figure 3.7: REE diagram for source depth determination.....	62
Figure 3.8a-h: Binary variation diagrams to test melt evolutionary trends.....	64
Figure 4.1a,b: Tables of samples used for geochemical analysis.....	71
Figure 4.2: MgO-FeO-Al ₂ O ₃ tectonomagmatic discrimination diagram.....	73
Figure 4.3: Ti-Zr-Y tectonomagmatic discrimination diagram.....	74
Figure 4.4: Hf-Th-Nb tectonomagmatic discrimination diagram.....	75
Figure 4.5: REE patterns of selected samples.....	77
Figure 4.6: Spider diagram patterns of selected samples.....	78
Figure 4.7a-c: Clinopyroxene compositional discrimination diagrams.....	81
Figure 5.1: SiO ₂ vs. Zr/TiO ₂ diagram.....	91
Figure 5.2: SiO ₂ vs. Na ₂ O + K ₂ O.....	92

Figure 5.3: SiO ₂ vs. FeO*/MgO diagram.....	93
Figure 5.4: Ti-Zr-Y tectonomagmatic discrimination diagram.....	94
Figure 5.5: Spider diagram patterns to compare trace element abundances and ratios.....	96
Figure 5.6: Map of Canadian Cordillera showing Stikinis, Cache Creek and Quesnellia.....	97
Figure 5.7a-d: Oroclinal entrapment model of Mihalynuk et al., 1994.....	99

Table of Plates

Plate 1.1: Sustut copper property.....	11
Plate 1.2: Savage Mountain and Moosevale Formation units.....	14
Plate 1.3: Pillow basalts of the Mount Savage Formation.....	17
Plate 1.4: Lahar of the Moosevale Formation.....	19
Plate 1.5: Turbidite deposit of the Dewar Formation.....	21
Plate 2.1a-d: Effusive rock textures.....	25
Plate 2.2: Clinopyroxene zoning.....	29
Plate 2.3: Plagioclase phenocryst textures.....	34
Plate 2.4a,b: Olivine textures.....	36
Plate 2.5a-c: Pyroclastic rock textures.....	40
Plate 2.6a,b: Alteration mineralogy and style.....	43
Plate 2.7a,b: Metamorphic minerals.....	45

CHAPTER 1: GEOLOGICAL FRAMEWORK

1.1 Introductory Statement

The volcano-sedimentary Upper Triassic Takla Group is located within the McConnell Creek map area in north-central British Columbia. It consists of basaltic to andesitic effusive and pyroclastic rocks, siltstones, argillites and volcanogenic sandstones deposited under conditions ranging from marine to subaerial (Monger, 1977). The Takla Group is present in both the Stikine and Quesnel allochthonous terranes of the Intermontane Belt in the Canadian Cordillera. These extensive, predominantly subduction-related terranes persist throughout much of the length of this portion of the Cordillera. In the McConnell Creek area, they are bordered by a branch of the major dextral transcurrent Pinchi Fault which separates the Takla Group into two adjacent units. The relationship between these two units in the McConnell Creek area remains uncertain.

1.2 Purpose and Objectives

The purpose of this study is to determine the paleotectonic setting of the Takla Group of Stikinia. In addition, the results of the study will be used for comparison with the Takla Group of Quesnellia. The determination of the relationship between the two groups could test current theories on Stikine and Quesnel terrane history (Mihalynuk et al., 1994; Wernicke and Klepacki, 1988). The two Takla groups are so similar that they have been mapped as a single continuous assemblage (Lord, 1948; Monger, 1977), although they (1) overlie a terrane

boundary, (2) are bordered by a major transcurrent fault, (3) differ in metamorphic grade across the fault from lower greenschist to prehnite-pumpellyite and zeolite facies, and (4) are underlain by different units. Reasons for mapping the two groups as a single unit include (1) lithologic similarity, (2) virtually contemporaneous age and (3) adjacent position. Minehan (1989) studied the paleotectonic setting of the Quesnellian Takla Group and interpreted it as the product of island arc volcanism. Based on major element analyses of the Stikinian Takla Group from Monger (1977), Minehan (1989) suggested that it was erupted in an oceanic island setting. On the basis of proposed differences in tectonic setting, Minehan (1989) recommended that the Quesnellian Takla Group be renamed the Johansen Group. A more detailed geochemical interpretation of the paleotectonic setting of the Stikinian Takla Group (including trace element analysis) and determination of the relationship between the two groups will add to our knowledge of the Mesozoic tectonic history of this part of the Canadian Cordillera.

The objectives of this thesis include: (1) petrographic characterization of the volcanic units of the Stikinian Takla Group, (2) geochemical characterization of these units by major and trace element analysis, (3) evaluation of the petrogenesis of the Stikinian Takla Group volcanic rocks, (4) determination of their paleotectonic setting through major and trace element analysis, (5) determination of the relationship between the two Takla Groups, and (6) discussion of the implications of the paleotectonic interpretation in terms of regional geology.

1.3 Scope and Thesis Organization

This thesis examines the petrology and geochemical characteristics of the Takla Group volcanic rocks of Stikinia. Analysis of structural features, sedimentary units or aspects of physical volcanology is beyond the scope of this thesis.

Chapter 1 continues with descriptions of the regional geology of British Columbia and of the local geology of the Stikinian Takla Group. Chapter 2 contains petrographic descriptions of the major volcanic rock types of this Takla Group. It also focuses on the chemistry of significant minerals in the assemblage, obtained by electron microprobe techniques. In Chapter 3, geochemical data derived by x-ray fluorescence (XRF) and inductively coupled plasma mass spectrometry (ICP-MS) are used to characterize the volcanic rocks of the Stikinian Takla Group. In Chapter 4, the major and trace element analyses obtained by XRF and ICP-MS are used to determine the paleotectonic setting of the group. Chapter 5 consists of a comparison of the Stikinian and Quesnellian Takla Groups based on lithologic and geochemical features. It also raises the implications of the comparison on a regional scale. Chapter 6 concludes the thesis and recommends future work. Appendices contain detailed petrographic descriptions and tables of geochemical data.

1.4 Regional Geological Setting

The review of Canadian Cordilleran tectonics presented here is intended to provide background knowledge related to tectonic concepts presented in later chapters. The Canadian segment of the Cordillera is approximately 2000 km long by 750 km wide and forms the leading edge of the western North American plate (Monger, 1989).

1.4.1 Terminology

The Cordillera can be regarded as being composed of terranes (Gabrielse et al., 1992). A *terrane* is a fault-bound package of rock that may comprise several tectonic assemblages, but represents a geologic history distinct from that of neighbouring terranes (Monger, 1989). A *tectonic assemblage* is a group of rocks that is representative of formation in a specific environmental setting. Those terranes with origins differing from that of ancestral cratonic North America are *allochthonous* terranes. Those with an unknown origin are *suspect* terranes. *Accreted* terranes are those having an extracontinental origin which have been subsequently attached to the North American craton. Terranes composed of several smaller terranes that amalgamated prior to accretion to the North American craton are *superterranes*. Figure 1.1 is a schematic diagram of the major terranes of the Canadian Cordillera.

Terrane *amalgamation* and *accretion* to the craton are accompanied by (1) overlap of sediment cover on several terranes, (2) erosion of rock from one terrane and deposition of the derived sediments as a clastic wedge on another terrane, and (3) welding by igneous intrusive activity (Fig. 1.2). Terrane accretion to ancestral North America occurred mainly during the Mesozoic (Monger, 1989).

1.4.2 Physiography

The Canadian Cordillera is composed of five linear belts which are distinguished on the basis of lithology, structural style and morphology (Gabrielse et al., 1992). From east to west these are the Foreland, Omineca, Intermontane, Coast and Insular belts (Fig. 1.3).

Morphogeological Belts

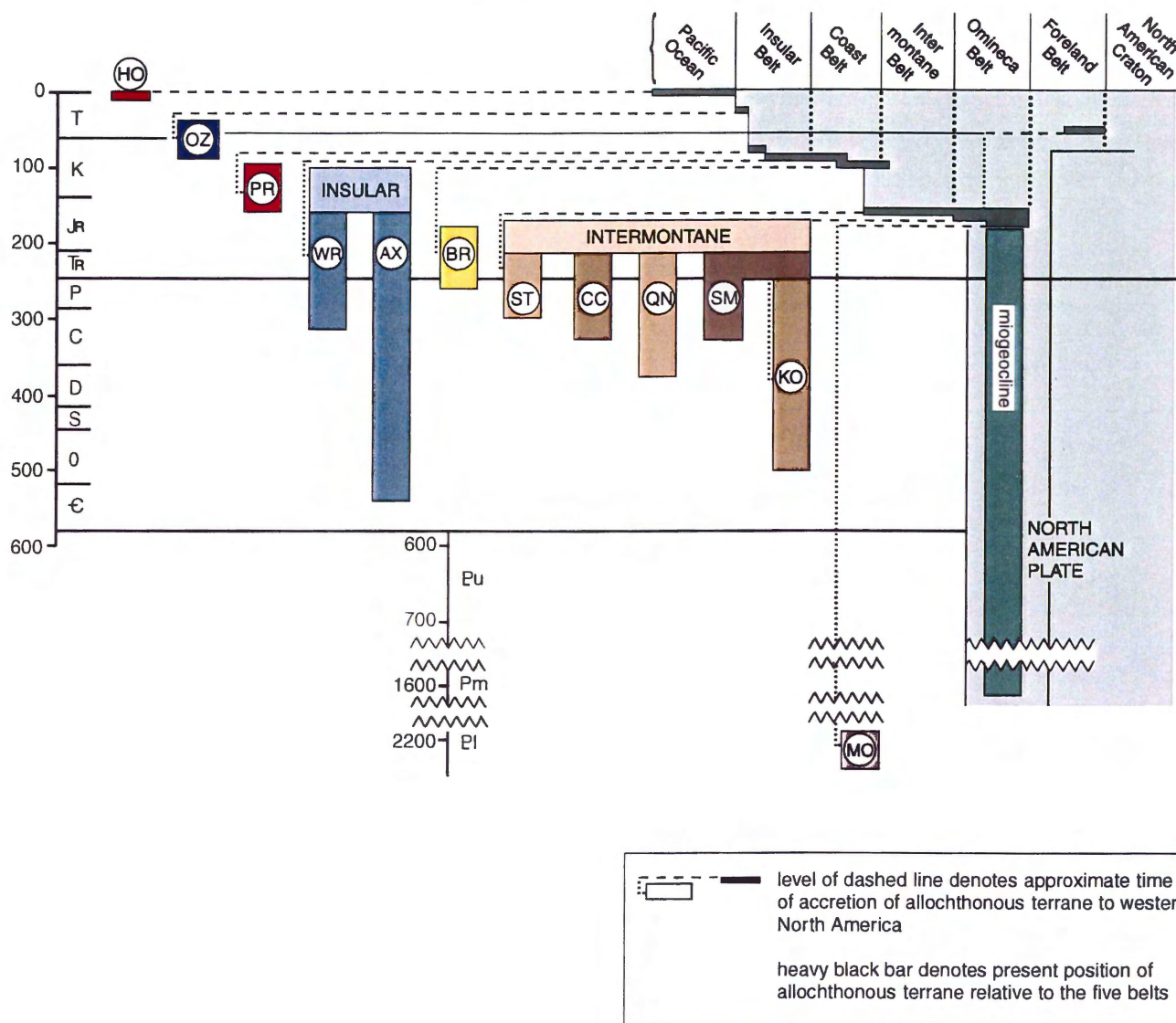


Figure 1.1 Space and time relationships of suspect terranes in the southern Canadian Cordillera with the North American craton. Figure shows (1) depositional time interval spanned by each terrane; (2) gaps between columns indicating unknown spatial relationships; (3) overlap assemblages that define superterranes; (4) green areas showing western margin of continent built westwards by accretion of terranes; (5) spatial relationships of morphogeological belts to North America: accreted terrane boundaries; coincidence of high-grade metamorphic rocks in Omineca and Coast belts with boundaries of Intermontane and Insular superterranes suggests that these belts may be partly collisional in origin (modified from Monger et al., 1982). HO, Hoh terrane; OZ, Ozette terrane; PR, Pacific Rim terrane; WR, Wrangellia terrane; AX, Alexander terrane; BR, Bridge River terrane; ST, Stikinia terrane; CC, Cache Creek terrane; QN, Quesnellia terrane; SM, Slide Mountain terrane; KO, Kootenay terrane; MO, Monashee terrane (Monger, 1989).

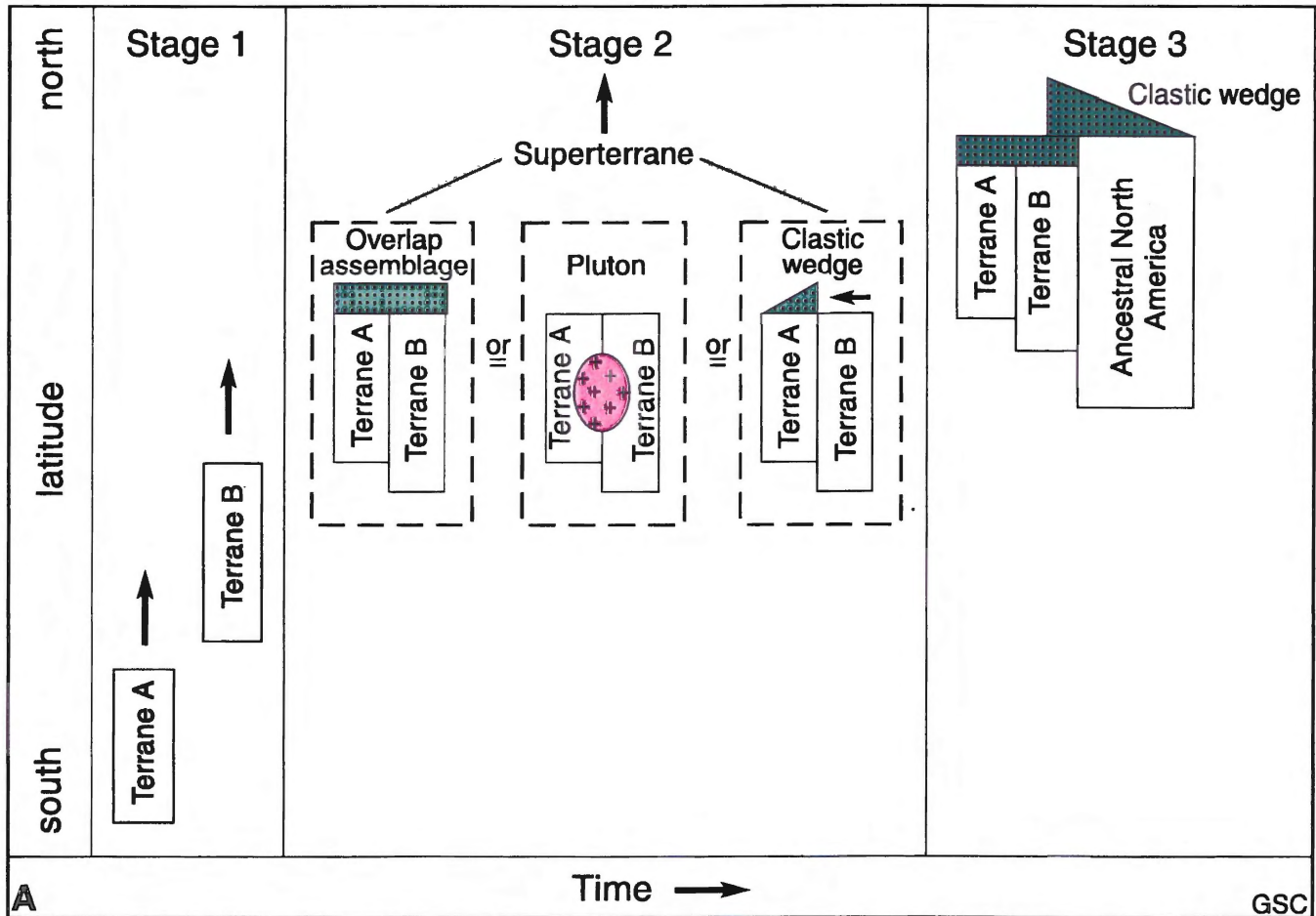


Figure 1.2 Schematic diagram showing stages of terrane amalgamation and accretion with ancestral North America (Gabrielse et al., 1992).

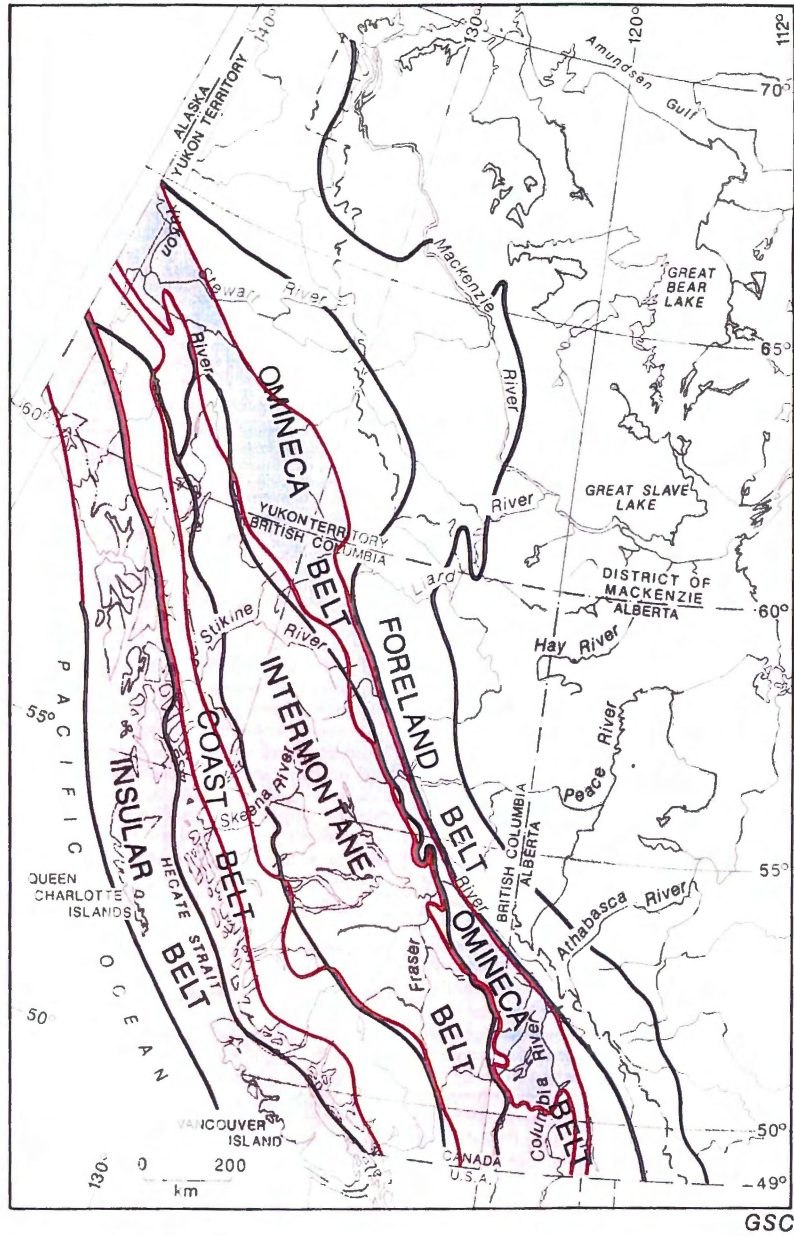


Figure 1.3 Comparison of the distributions of the five morphogeological belts with the pericratonic and displaced terranes and the accreted superterrane. The Takla Group is located in the Intermontane Belt, which is entirely composed of accreted terranes. From Gabrielse, 1992.

A review of these belts is presented in Gabrielse et al. (1992). The Foreland Belt consists of folded and imbricated miogeoclinal and clastic wedge assemblages deposited on and adjacent to the craton. The Omineca Belt is an uplifted region which straddles the boundary between ancestral cratonic North America and the accreted terranes. It is largely composed of deformed metamorphic and plutonic rock. The Intermontane Belt consists mostly of sedimentary and volcanic rocks that attain greenschist facies metamorphic grade. The Coast Belt is predominantly composed of granitic and metamorphic rocks ranging from the greenschist to the upper amphibolite facies. The Insular Belt, which forms the modern Pacific margin, consists of volcanic arc and clastic wedge assemblages.

According to Monger et al. (1982), the morphology of the Cordilleran belts is related to the accretion of two large superterranes, labeled I and II. Superterrane I is composed of the Quesnel, Cache Creek, Stikine, Slide Mountain and Kootenay terranes (Fig. 1.1). It had amalgamated by early Jurassic time and at present lies largely in the Intermontane Belt. Superterrane II presently lies mainly in the Insular Belt and was formed by the amalgamation of the Wrangel and Alexander terranes by late Jurassic time (Fig. 1.1).

Physiographically, the Cordillera consists of two rugged plutonic and metamorphic belts (the Omineca and Coast Belts) bordered by topographically lower volcano-sedimentary dominated assemblages (the Foreland, Intermontane and Insular Belts). According to Monger et al. (1982), the deformation of the Omineca and Coast belts reflects tectonic overlap and compressional thickening of the crust during the accretion of the superterranes. Evidence supporting this theory is (1) the position of the Omineca Belt between ancestral North America and superterrane I, (2) the position of the Coast Belt between superterranes I and II, (3) the

ages of structural and metamorphic features present in the belts and (4) the timing of detrital sedimentation from the belts onto the adjacent superterrane.

1.5 Location and Physiography of Study Area

The Takla Group lies in the eastern half of the McConnell Creek map area (Fig. 1.4) which is bounded by latitudes 56°N, 57°N and longitudes 126°W, 127°W and is located approximately 360 km northwest of Prince George. This thesis concentrates on the Takla Group of the Stikine Terrane which is west of the Pinchi Fault. Relief is up to 1300 m and elevation reaches a maximum of 2500 m at Sustut Peak. According to Monger (1977), the Takla Group units consist of blocks of rugged mountains separated by north-north-westerly trending valleys up to 8 km wide.

1.6 Previous Work

The Takla Group was originally mapped by Lord (1948) who divided it into a lower division of Upper Triassic age and an upper division of Upper Triassic to Upper Jurassic age. Church (1973, 1974) mapped much of the area close to Sustut Peak, in light of the discovery of extensive copper showings at the Sustut Copper property (Plate 1.1). In 1976, Monger and Church revised the stratigraphy of the Takla Group and redefined Lord's divisions. They defined the Takla Group as consisting only of Upper Triassic-aged formations and renamed the Upper-Triassic to Upper-Jurassic formations as the Hazelton Group. In Stikinia, Monger and Church (1976) divided the newly-defined Takla Group into three formations called the Dewar, Savage Mountain and Moosevale. The Quesnellian Takla Group remains undivided.

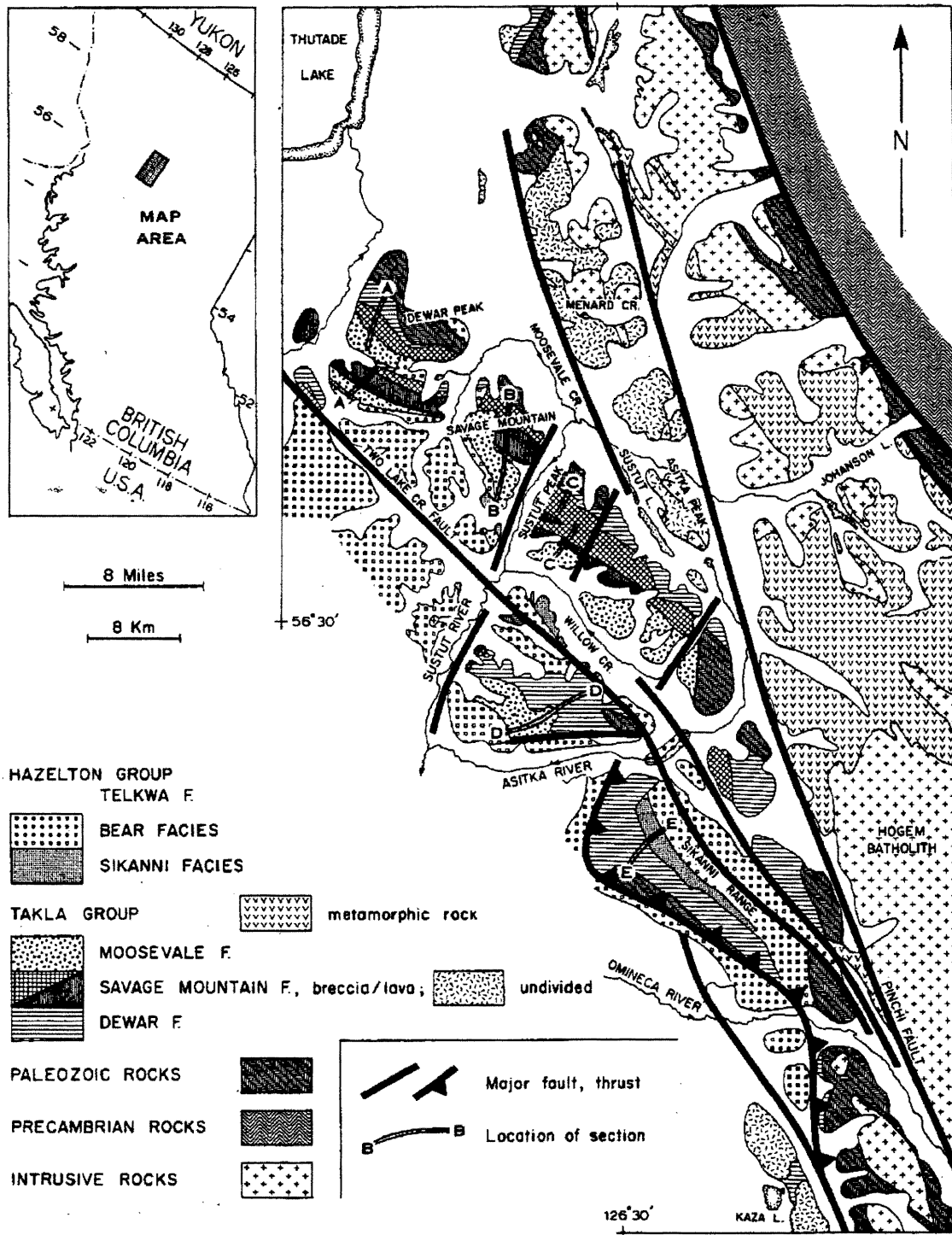


Figure 1.4 Distribution of Takla Group rocks in the McConnell Creek area. Pinchi Fault marks terrane boundary of Stikinia (west) and Quesnellia (east). Also shown are stratigraphic section locations. Takla Group samples used in this study are taken from section labelled C (Monger and Church, 1976).

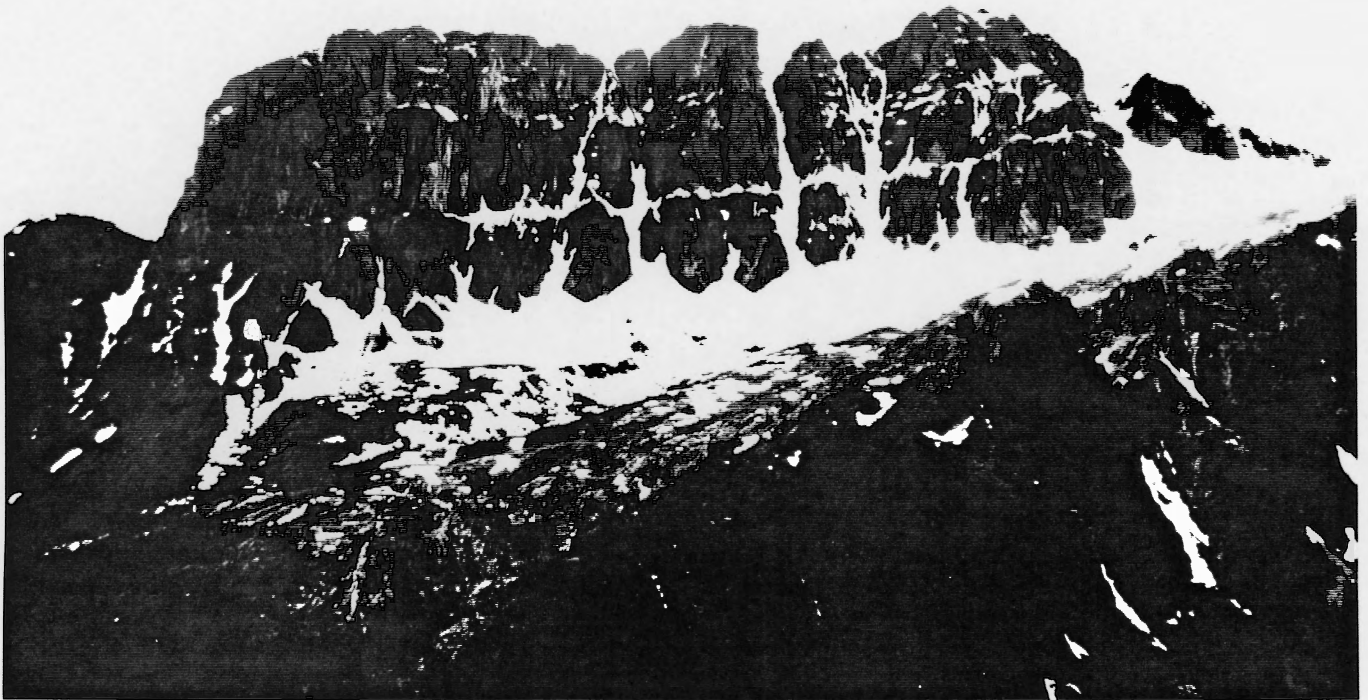


Plate 1.1 Sustut copper area. Panoramic view of north cliff area showing gently dipping units of the Moosevale Formation at the south ramparts of Mount Savage.

Monger (1977) described the stratigraphy of the Takla Group of both terranes. In 1989, Minehan determined the paleotectonic setting of the Takla Group of Quesnellia and suggested a paleotectonic setting for the Stikinian Takla Group, as mentioned above.

1.7 Geology of the Study Area

The three formations of the Takla Group of Stikinia are shown in Figure 1.5. The Dewar Formation consists of up to 1500 m of dark gray to brown volcanic sandstone, tuff and argillite. This formation underlies and is the distal basinward equivalent of the Savage Mountain Formation, which consists of as much as 3000 m of dark gray green, locally red, pillow basalt, massive basalt, subaerial flows, breccia and tuff (Plate 1.2). Both formations are overlain by the Moosevale Formation which is composed of up to 1800 m of red and green or reddish gray marine and non-marine volcanoclastics with clasts similar to Savage Mountain lithologies. The following lithologic descriptions are based on observations by Monger (1977).

1.7.1 Contacts

The Takla Group of Quesnellia is in fault contact with the underlying Permo-Pennsylvanian Lay Range Assemblage while the Stikinian Takla Group is in fault contact with the underlying Cache Creek Group and disconformably overlies the Permian Asitka Group. Within the Takla Group of Stikinia, the contact between the Dewar and Savage Mountain formations is gradational. The contact between the Dewar and Savage Mountain Formations and the Moosevale Formation is conformable and locally gradational. The contact of both the

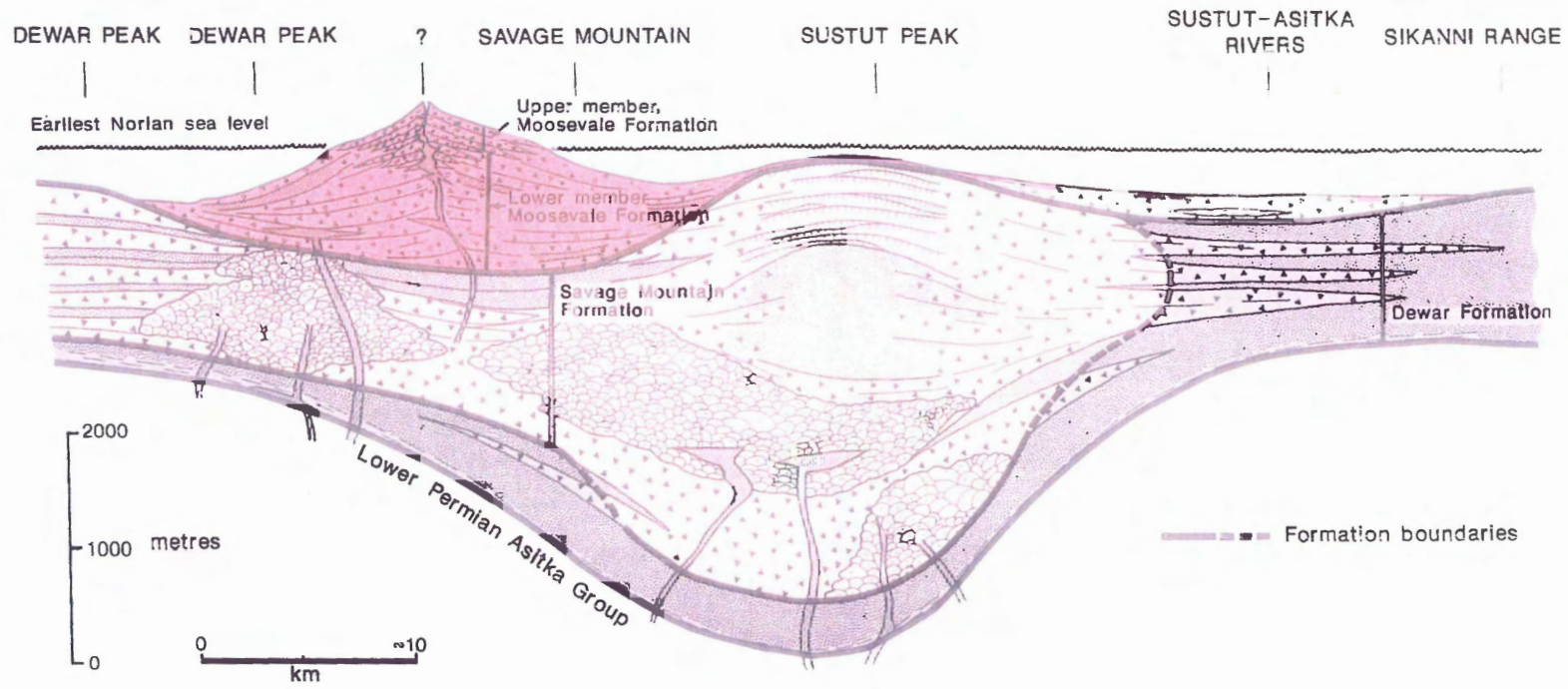


Figure 1.5 Stratigraphic relationships of the Takla Group of Stikinia in the McConnell Creek area (Monger, 1977).



Plate 1.2 View of Moosevale Formation shale and overlying volcanoclastic units resting on Savage Mountain Formation basaltic units.

Stikinian and Quesnellia Takla groups with the lower Jurassic Hazelton Group is thought to represent a regional unconformity (Lang et al., 1995).

1.7.2 Dewar Formation

This formation is composed of well bedded volcanogenic sandstone and argillite. Basal members consist of brown weathered, dark gray to black, locally graphitic and pyritic argillite with siltstone laminae and lenses of argillaceous limestone and cherty argillite. The central portion of the formation is composed of brown weathering, light gray to green gray, fine- to medium-grained sandstone or siltstone interbedded with dark gray argillite. Cross-bedding, grading and rip up clasts are present in these layers which range in thickness from mm-scale laminae up to 50 cm. The volcanogenic particles comprising the sandstone consist mainly of semi-opaque fragments of vesicular feldspar-augite porphyritic basalt, augite porphyritic basalt, pyroxene grains, plagioclase grains, opaque minerals and fragments of fine grained sedimentary rocks. The upper portion of this formation contains homogeneous, massive beds of volcanic breccia, between 10 and 25 m thick, which are characteristically similar to beds in the Savage Mountain Formation. Clasts within the breccia are subrounded to angular and are usually less than 10 cm in diameter but can be up to 50 cm. They are mainly composed of augite-feldspar porphyritic basalt and augite porphyritic basalt. According to Monger (1977), the nature of the lithic fragments and abundance of pyroxene grains in the Dewar Formation indicate that it was derived from the coeval Savage Mountain Formation. The deposition of the Dewar Formation is assigned to the upper Carnian and lower Norian according to the presence of Anatropites and Halobia respectively.

1.7.3 Savage Mountain Formation

This formation is up to 3000 m thick and consists of basaltic effusive and pyroclastic rocks. The massive and pillowed flows are mostly augite-feldspar basalts, augite porphyritic basalts, aphanitic basalts and occasional basalts with coarse platy feldspar. Pillows are commonly less than 1 m in length and form tubes as well as isolated pillows in a tuffaceous matrix (Plate 1.3). They are commonly interbedded with pillow breccia and range from black and glassy to more altered, red and green in colour. Amygdular massive flows are typically 10 m thick and are capped by flow top breccia.

Pyroclastic rocks of the Savage Mountain Formation range from coarse breccias to crystal lithic tuffs. Bedding varies from massive to graded and cross-bedded. Finer grained beds are lithologically similar to tuffs of the Dewar Formation but are not interbedded with argillite. Some beds contain marine fossils. Breccia clasts (generally up to 30 cm but locally up to 1 m) consist mostly of augite porphyritic basalt and augite-feldspar porphyritic basalts to andesites. Crystal lithic tuffs contain fine-grained augite-feldspar porphyritic basalt to andesite fragments, semi-opaque pumiceous fragments, rare augite or feldspar porphyritic basalt to andesite fragments, augite crystals and feldspar crystals.

1.7.4 Moosevale Formation

This formation varies in thickness from 900 to 1800 m and consists mainly of coarse-grained volcanoclastic layers. The volcanoclastic rocks range from green to reddish gray and contain feldspar porphyritic andesite fragments as well as fragments typical of older Takla Group rocks. At the type area, this formation is composed of two members, a lower mafic unit



Plate 1.3 Pillow basalt of the Savage Mountain Formation.

reflecting marine deposition and an upper non-marine intermediate unit.

The lower unit is composed of massive breccia with interbedded volcanogenic sandstone and fossiliferous mudstone. The breccia locally contains red argillaceous rip-up clasts as well as fragments of augite porphyritic basalt, augite-feldspar porphyritic basalt and abundant feldspar porphyritic basalt to andesite fragments (Fig. 1.4). A mudcracked mudstone with abundant bivalves is present in the upper part of this lower unit.

The upper unit consists of volcanic breccia, conglomerate, volcanogenic sandstone and mudstone. Bedding is well defined and layers contain cross-bedding and mudcracks. Clasts within this unit of the Moosevale Formation consist of fragments lithologically similar to Savage Mountain porphyritic rocks as well as a variety of other feldspar porphyritic basalts to andesites. Finer grained clastic deposits of this unit are composed largely of volcanic detritus.

The most diagnostic fossil of the Moosevale Formation (Mojsisovicsites kerri) indicates a lower Norian age. This fossil was also found below mafic pillow layers in the Savage Mountain Formation. According to Monger (1977), this implies that the periods of mafic and intermediate volcanism were close in age.

1.7.5 Metamorphism and Alteration

Low metamorphic grades, ranging from zeolite to prehnite-pumpellyite facies, are present throughout the Takla Group of Stikinia. In contrast, the metamorphic grade of the Quesnellian Takla Group ranges from prehnite-pumpellyite to lower greenschist facies.

Secondary alteration and metamorphic minerals of the Stikinian Takla Group include chlorite,



Plate 1.4 Moosevale Formation lahar with various blocks of augite porphyry lava (some amygdaloidal), bladed feldspar porphyry and fine-grained andesite. Located at Mount Savage.

calcite, epidote, talc, prehnite and pumpellyite. Zeolite (laumontite) mineralization is limited to the Moosevale Formation. Space-filling alteration and metamorphic minerals occur as veins and amygdules. Pervasively altered rock matrices are common.

1.7.6 Deformation

The Dewar Formation is highly deformed and contains areas of intense crumpling and folding. The Savage Mountain Formation is tilted and faulted, but is generally not folded. Likewise, the Moosevale Formation is tilted at moderate angles and is locally highly fractured and faulted, but is not folded. According to Monger (1977), these differences in deformational style reflect the competency contrast of the units.

1.7.7 Depositional History of the Stikinian Takla Group

The depositional history of the Stikinian Takla Group spans the late Carnian to early Norian. The oldest argillitic, limy and cherty beds of the Dewar Formation lower member and pillowed lavas and marine fossils of the Savage Mountain Formation indicate that these formations were deposited in a marine shale basin. Coarse-grained volcanoclastic rocks of the Savage Mountain Formation were derived through local volcanic activity, while the fine-grained volcanoclastic rocks of the Dewar Formation formed as a distal facies of this volcanism. Some Dewar Formation volcanoclastic layers were deposited as turbidites (Monger, 1977) (Plate 1.5).

Closely following Savage Mountain volcanism, the Moosevale Formation basalts to andesites were deposited conformably on both the Savage Mountain and Dewar formations.

The early turbiditic sandstones and later unsorted breccia and conglomerate units of the Moosevale Formation suggest that it records the transition from subaqueous to subaerial depositional conditions. The latest alluvial fan stream channel deposits further suggest that the Moosevale Formation, which was developing on the flanks of the Savage Mountain volcanic pile, had built above sea level.



Plate 1.5 Dewar Formation turbidite with abundant broken pyroxene and plagioclase crystals from the Savage Mountain Formation.

CHAPTER 2: PETROGRAPHY AND MINERAL CHEMISTRY

2.1 Introduction

Geochemistry plays an important role in the determination of paleotectonic setting. However, the analysis of other lithologic features, such as a rock's petrographic characteristics, is also beneficial. Microscopic examination of the textures and mineralogy of the Stikinian Takla Group effusive and pyroclastic samples is useful for preliminary classification and will subsequently aid in the interpretation of the geochemical analyses. Petrographic examination is also important because it reveals the source of many inconsistencies that appear in the geochemical analyses of the samples. For instance, pyroclastic rocks may contain allochthonous clasts and are also more susceptible to alteration than effusive rocks due to their increased permeability. Alteration assemblages in both pyroclastic and effusive rocks, as well as detrital particles in pyroclastic rocks, can be identified and sometimes attributed as the cause of geochemical anomalies. In effusive rocks, the occurrence of large percentages of phenocrysts may affect trace element behaviour, which varies according to distribution coefficients for certain mineral phases. The identification of effusive rocks that are rich in phenocryst phases or cumulus in nature explains certain irregular trace elements patterns. This chapter consists of a petrographic examination of the Stikinian Takla Group volcanic rocks. In Chapter 5 this analysis will be used in the comparison of the two outcrop belts of the Takla Group.

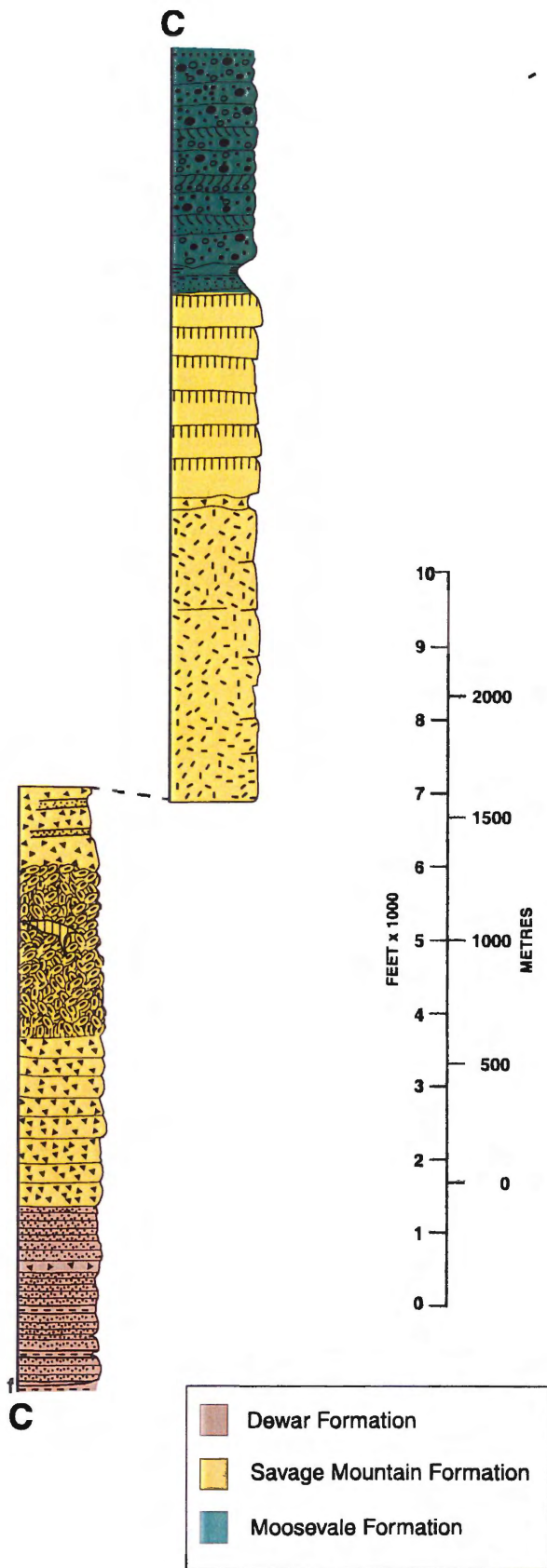
This chapter contains only brief petrographic descriptions of the volcanic rocks of the Stikinian Takla Group. Detailed petrographic descriptions of most samples used for

geochemical analysis are contained in Appendix A. Microprobe techniques and data, used in the determination of mineral chemistry, are presented in Appendix B.

Thin section and hand sample descriptions were made of effusive and pyroclastic rocks of the Savage Mountain and Moosevale Formations. The mainly sedimentary Dewar Formation is not used in geochemical analysis and as a result is not petrographically described. Samples labeled CS, W, S and WIL are taken from the stratigraphic column shown in Figure 2.1, while NW samples are from east of Moosevale creek, at the headwaters of Menard Creek (Fig. 1.4). CS samples, of the Savage Mountain Formation, consist mainly of augite porphyritic pillow lavas. W samples, also of this formation, are primarily augite porphyritic basalts with infrequent tuffaceous and volcanic breccias. S samples are composed of tuffs, lapilli tuffs and tuffaceous breccias of the Moosevale Formation. WIL samples, also of the Moosevale Formation, consist mainly of tuff breccias and rare volcanic breccias. NW samples, which consist of augite and plagioclase porphyritic basalts, are from the Savage Mountain Formation.

2.2 Effusive Rocks

In this thesis, the term effusive refers to volcanic deposits that are produced directly from the cooling of lava, in contrast to pyroclastic rocks, which are formed by the accumulation of explosively disrupted particles. Stikinian Takla Group effusive rocks are commonly amygdular (Plate 2.1c) and are normally porphyritic with rare aphanitic samples. Porphyritic varieties contain phenocrysts of clinopyroxene and plagioclase in hypocrySTALLINE to holocrySTALLINE matrices consisting of varying proportions of cryptocrySTALLINE glassy material



Stratification Characteristics

- Flows
- Pillows
- Cross-beds
- Massive; stratification not apparent or beds tens of metres thick
- Medium to thick bedded (>10 cm)
- Thin bedded (<1 cm)
- Laminated (<1 cm)

Termination of sections

- Stratigraphic contact
- f** - Fault
- Erosion surface
- End of measured section

Generalized Lithologies

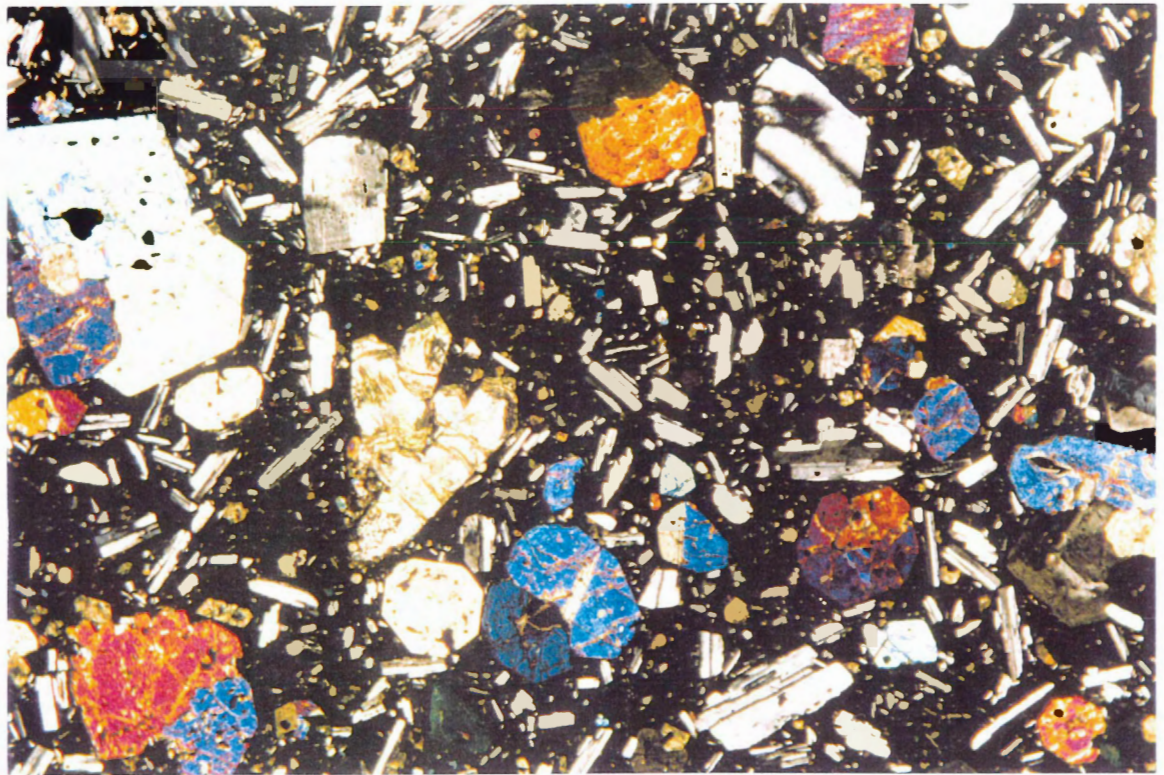
- Volcanic conglomerate and breccia; rounded and angular clasts; numerous clasts of intermediate composition in addition to lithologies below; colour predominantly red, red-grey
- Volcanic breccia, mainly angular, some rounded, clasts of the lithologies below together with intermediate volcanic clasts, fine-grained feldspar porphyry common; colour predominantly green, with variable amounts of red clasts
- Mafic, pyroxene bearing sills and dykes
- Aphanitic or non-porphyritic basalt
- Coarse bladed feldspar porphyry
- Augite, augite feldspar porphyry
- Volcanic breccia and lapilli tuff; mainly clasts of augite, augite feldspar porphyry, rare coarse bladed feldspar porphyry; colour predominantly grey-green
- Crystal lithic tuff, volcanic sandstone
- Carbonate
- Argillite, siltstone fine grained tuff
- Semischist, chlorite schist
- Phyllite, chlorite schist

Figure 2.1 Stratigraphic column C shown in Fig. 1.4. CS and W samples are from the Savage Mountain Formation. S and WIL samples are from the Moosevale Formation (Monger, 1976).

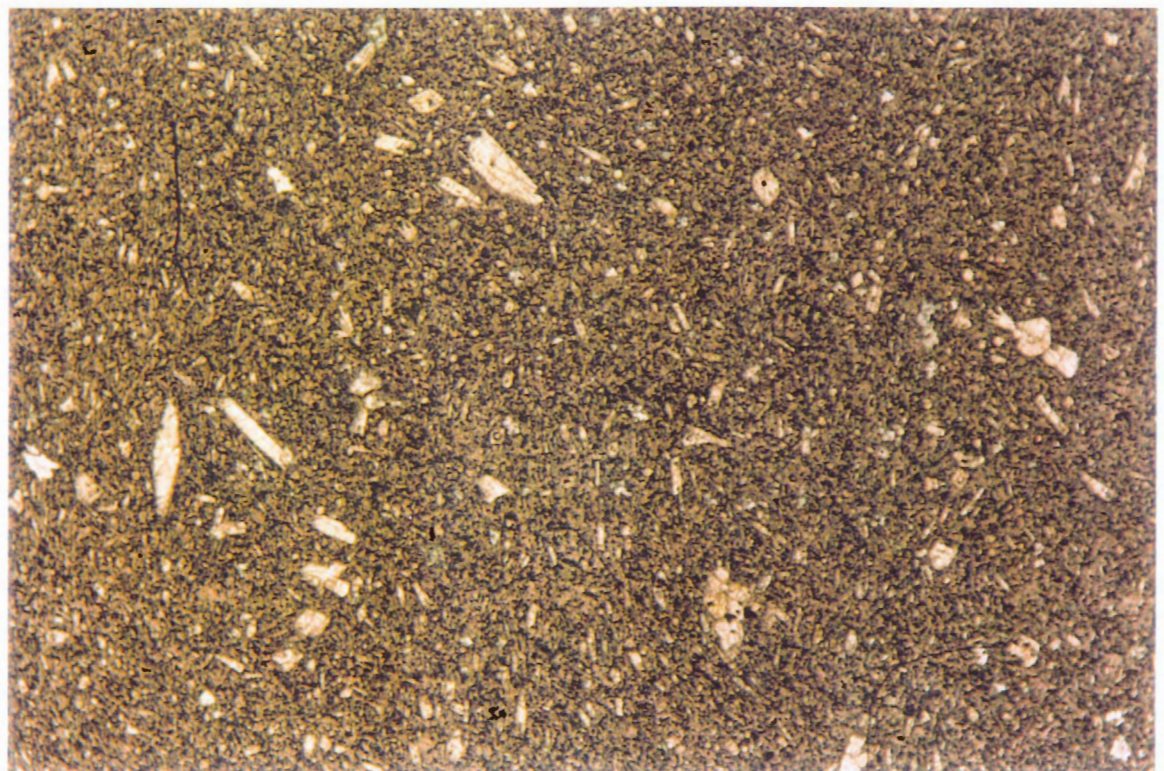
Plate 2.1 Effusive rock textures

- (a) Clinopyroxene-plagioclase porphyritic basalt. Clinopyroxene is frequently glomeroporphyritic. Note cluster of olivine pseudomorphs left of centre. Groundmasses are usually fine-grained and hypocrySTALLINE. Field of view is 1.6 cm in length. Photo is taken with polars crossed.
- (b) Aphanitic basalt often contains minor lath-shaped clinopyroxene microphenocrysts. Field of view is 1.9 cm. Photo taken in plane polarized light.
- (c) Some basalt samples are highly amygdular. Amygdules in this sample are composed of albite, chlorite and minor pumpellyite. Field of view is 3.2 cm. Photo taken in plane polarized light.
- (d) Weak alignment of plagioclase laths in clinopyroxene-plagioclase porphyritic basalt. Clinopyroxene and plagioclase seriate textures are common. Field of view is 1.2 cm in length. Photo is taken with polars crossed.

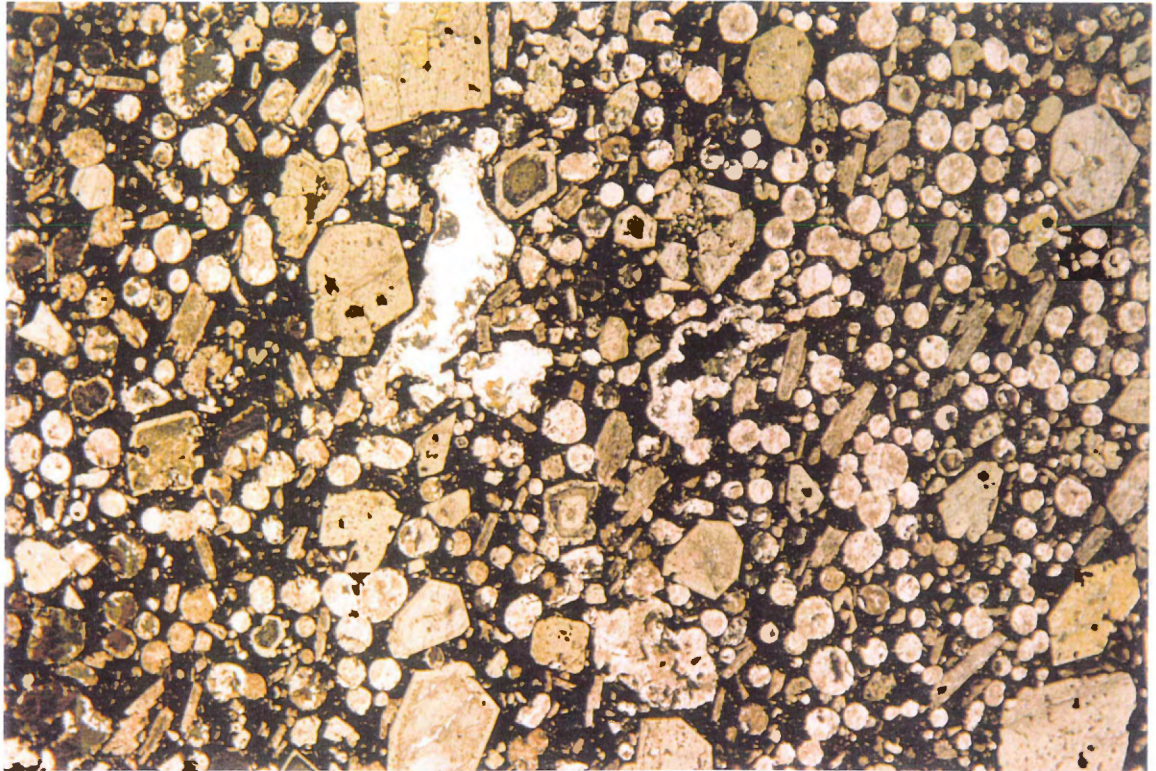
(a)



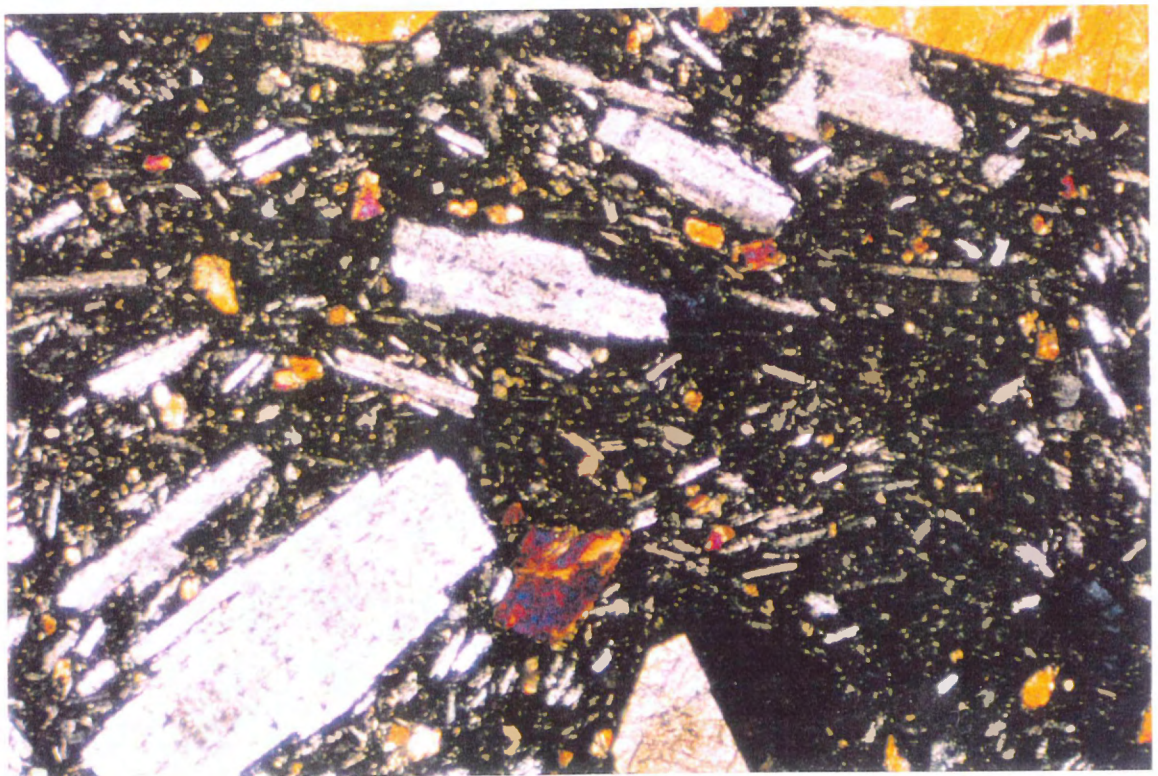
(b)



(c)



(d)



and microcrystalline clinopyroxene, plagioclase, magnetite and minor ilmenite (Plate 2.1a).

Effusive rock matrices commonly appear chloritized.

Pilotaxitic texture is present in some samples and is defined by the sub-parallel alignment of microcrystalline plagioclase laths (Plate 2.1d). Seriate textures are common in plagioclase and clinopyroxene crystals. Aphanitic phases are mineralogically and texturally similar to porphyritic phases, with rare phenocrysts (Plate 2.1b).

2.2.1 Phenocryst Mineralogy and Textures

2.2.1.1 Clinopyroxene

Generally unaltered, euhedral to subhedral clinopyroxene phenocrysts are typically 1.2 by 1.0 mm but can be as large 3 by 3 mm. They are present in all porphyritic effusive samples, composing on average ~32 modal %. Glomeroporphyritic texture is common in clinopyroxene phenocrysts (Plate 2.1a) and may be the result of synneusis during clinopyroxene crystallization which is effective only in magmas with low viscosities (Vance, 1969).

Based on colour differences, two types of clinopyroxene can be distinguished. The most common is light yellow-green and occurs as individual grains as well as rims in zoned clinopyroxene phenocrysts. The less abundant type, which composes ~10% of the total amount of clinopyroxene, is colourless and occurs as cores in zoned clinopyroxene phenocrysts as well as rare individual grains (Plate 2.2a). The occurrence of unzoned colourless clinopyroxene phenocrysts and colourless clinopyroxene as cores in zoned phenocrysts is mutually exclusive. However, light yellow-green pyroxenes occur as rims and as unzoned grains within the same samples.

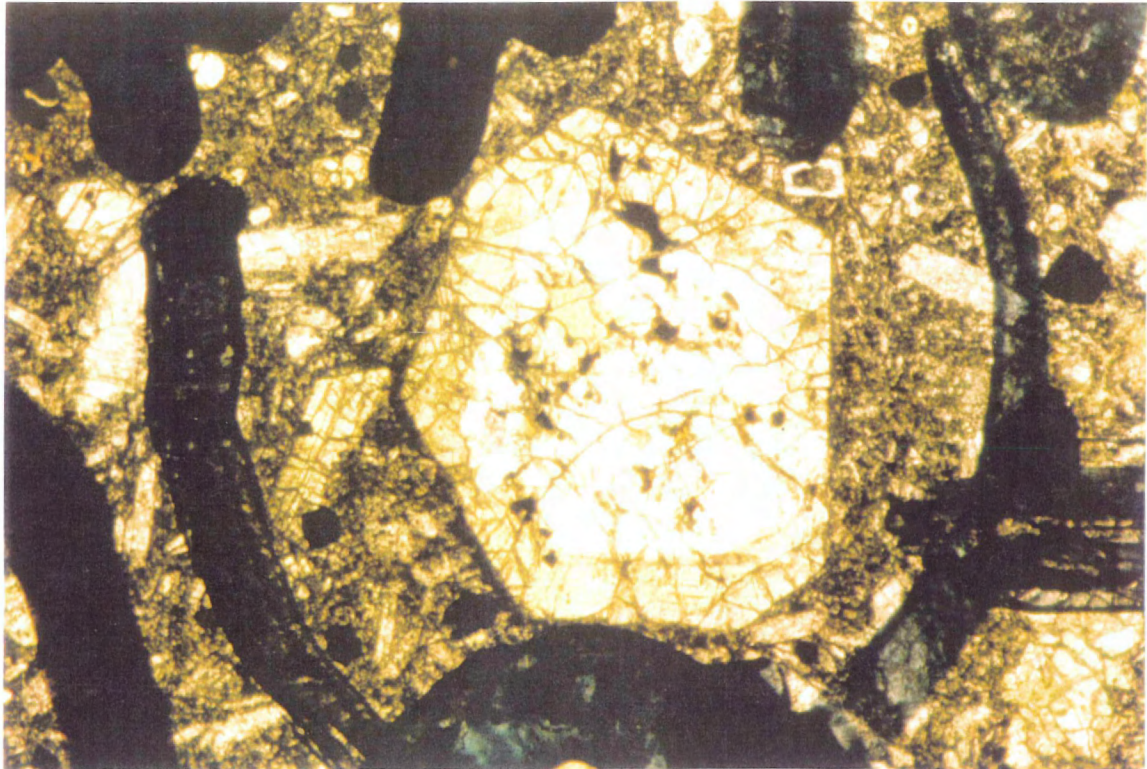


Plate 2.2 Zoned clinopyroxene phenocrysts are present in most porphyritic effusive samples. Colourless, often euhedral cores are rimmed by light yellow green pyroxene. Field of view is 10 mm in length. Photo is taken in plane polarized light

Zoned clinopyroxene phenocrysts are present in 10 of 13 clinopyroxene porphyritic effusive samples. Zoning occurs as simple non-oscillatory lamellar banding (Fig. 2.2).

Clinopyroxene core shape varies from euhedral and anhedral between samples.

Compositionally, colourless cores are enriched in Ca, Mg and Cr and depleted in Fe, Al and Ti relative to light yellow-green rims. Based on the presence of six oxygens in the pyroxene molecule, the En end member wt % varies from 38.7 to 50.9, the Fs end member from 4.9 to 18.0 and the Wo end member from 36.0 to 46.6. When plotted on a pyroxene quadrilateral diagram (Deer et al., 1985), core to rim compositional changes appear gradational (Fig. 2.3).

Zoning is chiefly produced through changes in melt composition, but is also influenced by changes in melt temperature and crystal growth rate. These factors affect the diffusion rate of chemical gradients at the crystal-melt interface (Downes, 1974). Complex and dramatic zonation patterns are thought to be the result of processes such as magma mixing and xenocryst introduction (Dobosi, 1989; Duda and Schmincke, 1985; Barton et al., 1982). In the case of the Takla Group clinopyroxene phenocrysts, the simple and gradual zonation sequence from more primitive to more evolved compositions is most likely a result of the compositional evolution of the melt. It has been suggested that the increase of Al and Ti concentrations in clinopyroxene rims is related to the degree of silica undersaturation in the melt (Downes, 1974). In melts of low Si content, Al^{+3} substitutes for Si^{+4} in the tetrahedral site. Ti cations enter the crystal structure to correct the charge deficiency produced by this substitution (McBirney, 1984). The lack of zoning of some of the more primitive colourless clinopyroxene phenocrysts, as well as the selective occurrence of zoning, could be indicative of magma chamber heterogeneity.

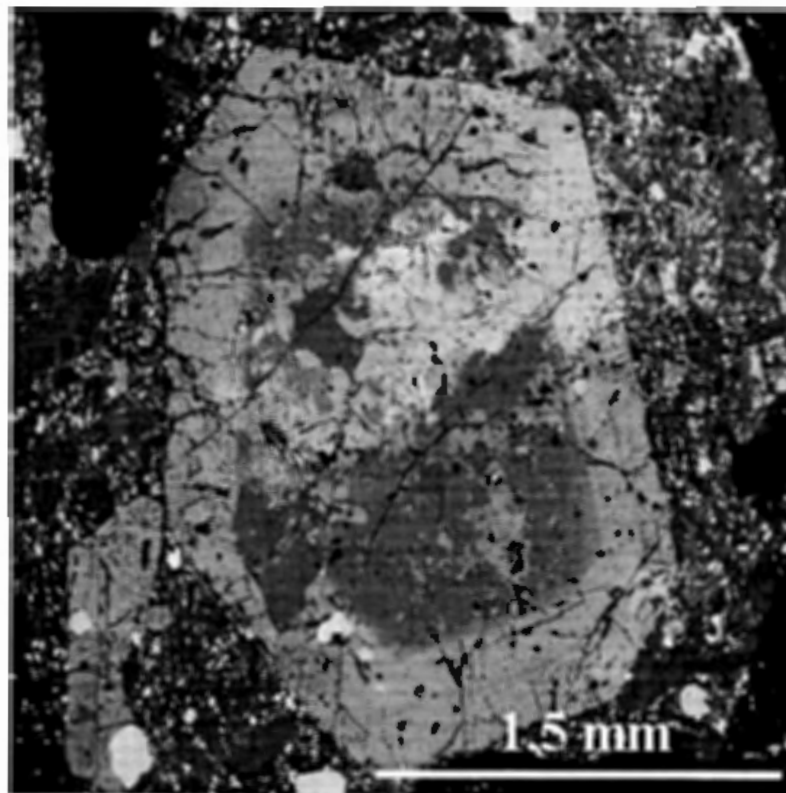


Figure 2.2 Electron microprobe backscatter images of zoned clinopyroxene phenocrysts. Dark, euhedral cores are colourless in plane polarized light, while rims are light yellow-green.

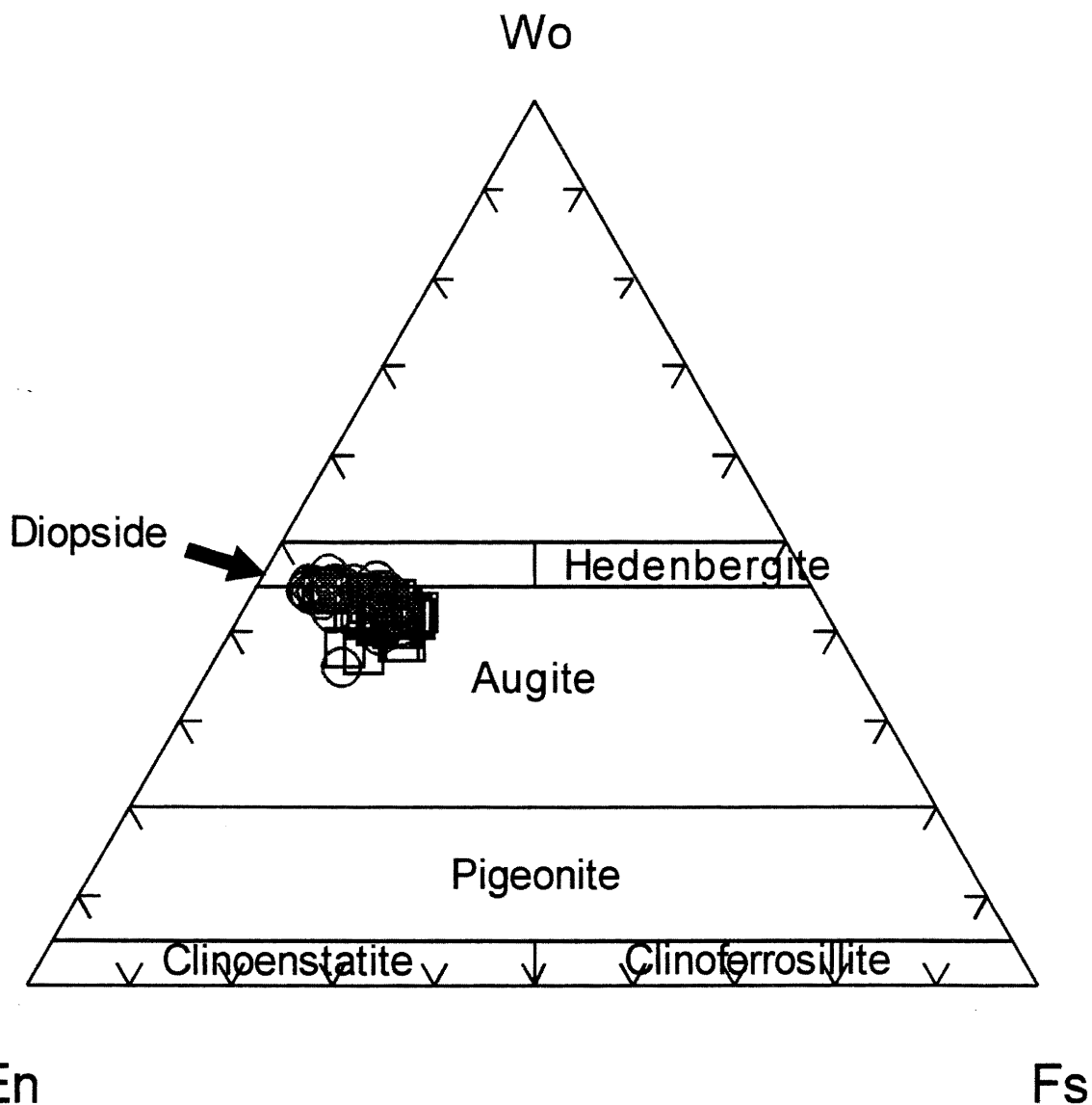


Figure 2.3 Core and rim clinopyroxene compositions plotted on the modified pyroxene quadrilateral (Wo-En-Fs) diagram of Deer et al. (1985). Clinopyroxene cores (gray circles) and rims (black squares) show gradual compositional variation from less to more evolved.

2.2.1.2 Plagioclase

Euhedral to subhedral, generally unzoned, plagioclase phenocrysts and microphenocrysts are typically 500 by 200 μm , but range up to 1.2 by 0.20 mm (Plate 2.3). Rarely, plagioclase ($\text{An}_{28}\text{-An}_{40}$) occurs as bladed phenocrysts up to 3 cm long (Monger, 1977). Composing on average ~12 modal %, plagioclase phenocrysts are not as predominant as clinopyroxene phenocrysts in porphyritic basalt samples. However, in effusive rocks of andesitic composition plagioclase forms the dominant phenocryst phase. Plagioclase anorthite content is as low as An_2 , but commonly ranges from An_{51} to An_{64} . The low An content and unrealistic primary sanidine component (Fig. 2.4) of some Stikinian Takla Group plagioclase phenocrysts and microphenocrysts suggests that secondary alkali alteration took place. Plagioclase crystals are partially pseudomorphed by sericite, saussurite and chlorite.

2.2.1.3 Olivine

Typically 2 by 1 mm pseudomorphs of olivine are present in 5 out of 15 porphyritic samples and normally constitute ~5 modal % of each sample, but may constitute up to ~15 modal % (Plate 2.4a,b). The pseudomorphs are recognized as olivine on the basis of (1) stubby bipyramidal prismatic pseudomorph shapes, (2) the preservation of distinctive curved fractures emphasized by opaque material, and (3) the presence of fresh clinopyroxene crystals in association with the pseudomorphs which implies that they are unlikely to be altered clinopyroxene. Olivine is pseudomorphed by at least one type of chlorite (possibly two), serpentine, talc, hematite, and in some cases, calcite. Fe-Ti oxides commonly occur in cracks

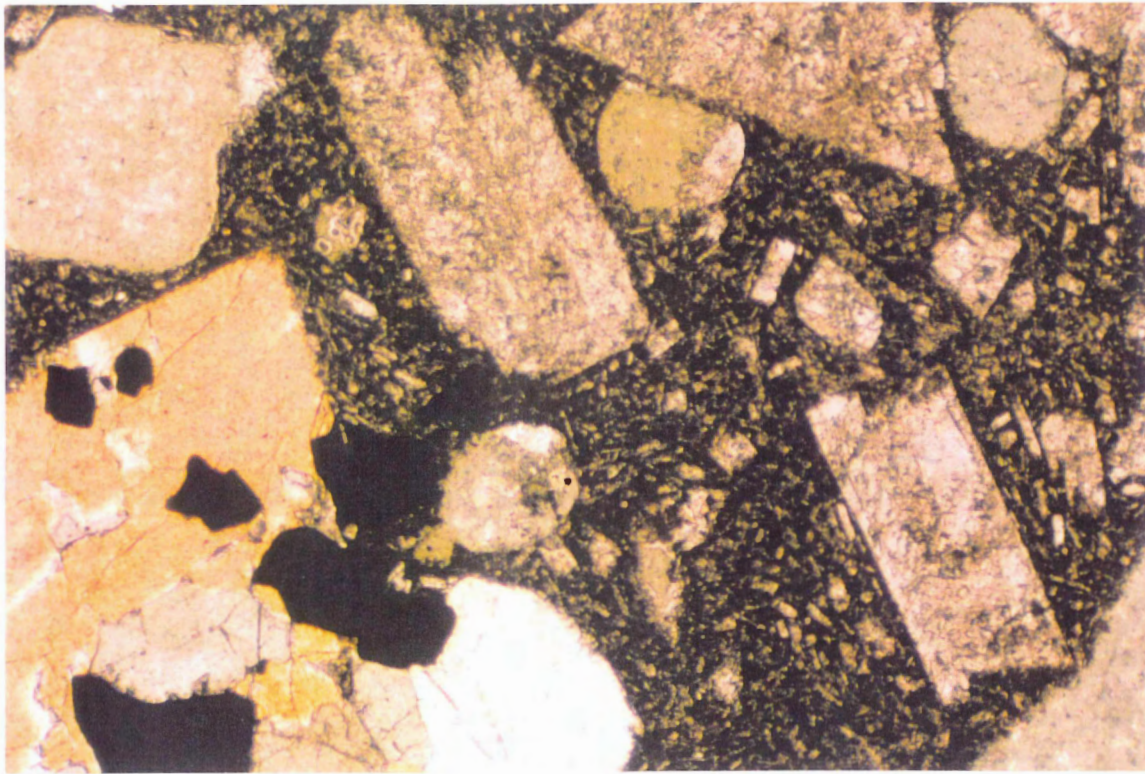


Plate 2.3 Subhedral to euhedral plagioclase phenocrysts are commonly strongly saussuritized and sericitized. Field of view is 1.2 cm in length. Photo taken in plane polarized light.

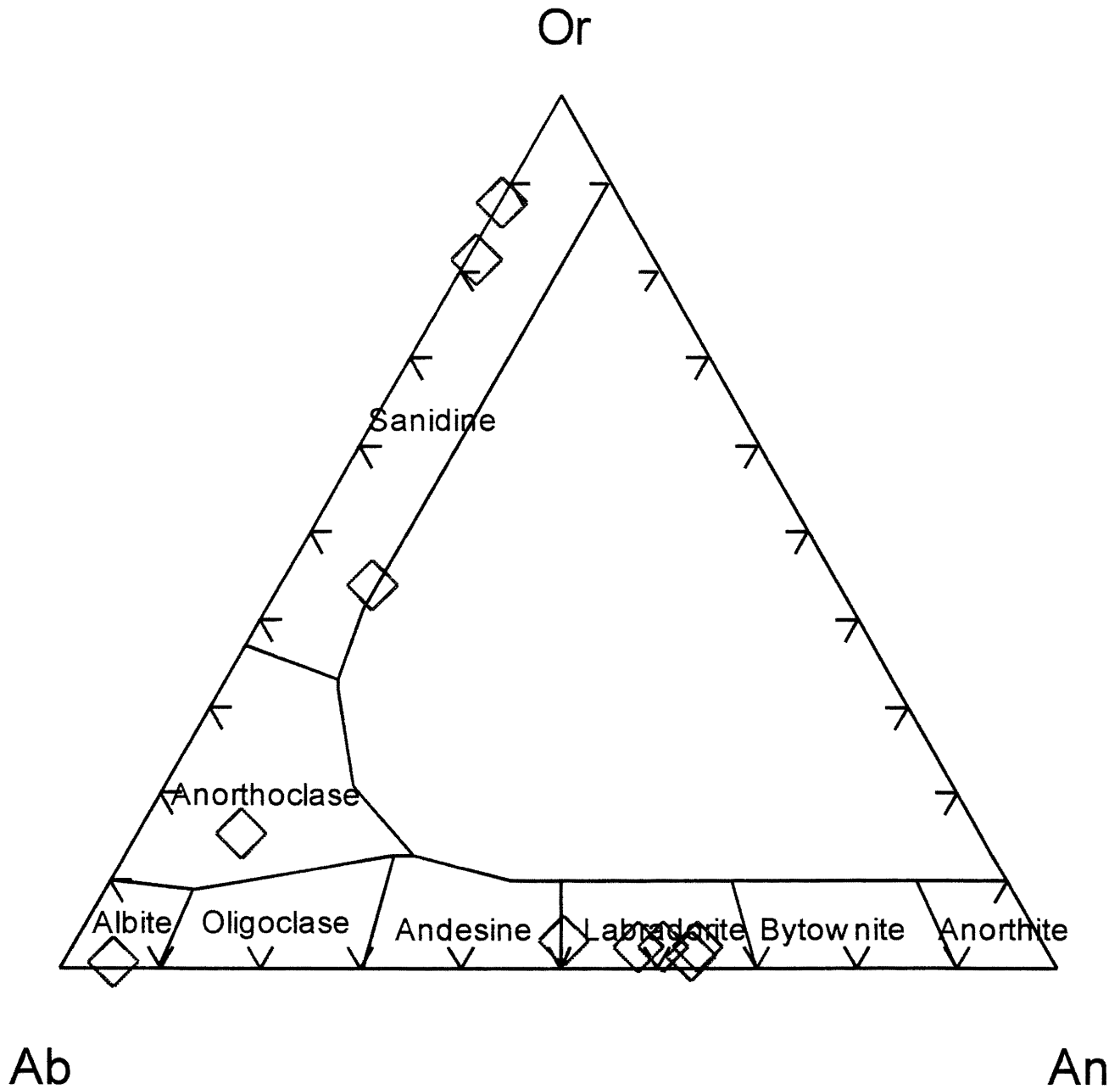


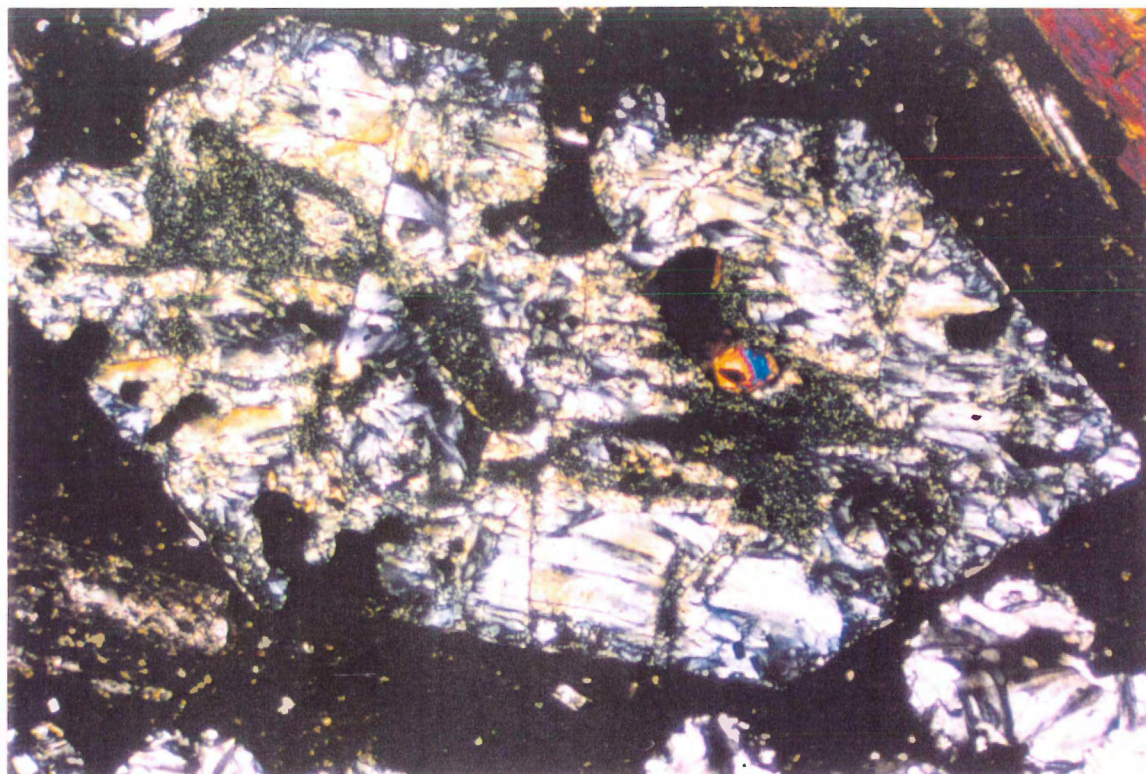
Figure 2.4 Feldspar phenocryst compositions plotted on the feldspar ternary (Or-Ab-An) diagram of Deer et al. (1985). Most feldspar phenocrysts plot as Labradorite. Some show unrealistically high sanidine components for rocks of basaltic to andesitic composition and most likely have been affected by alteration.

Plate 2.4 a, b Olivine textures

(a) Euhedral olivine pseudomorphs replaced by chlorite, albite and fine-grained pumpellyite. Field of view is 2 mm. Photo taken under crossed polars.

(b) Anhedral olivine pseudomorphs with curved cleavage emphasized by opaque minerals. Pseudomorphs are inclusions within a clinopyroxene phenocryst and are replaced by chlorite, hematite and an opaque mineral. Field of view is 500 μm .

(a)



(b)



and along rims. Intercumulus olivine (Fo_{80}) is preserved in an orthocumulus pyroxenite sample which is most likely hypabyssal and related to the augite porphyritic basalts.

2.3 Pyroclastic Rocks

According to the grain size classification of Easton and Johns (1986) (Fig. 2.5), the pyroclastic samples of the Stikinian Takla Group include crystal lithic tuffs, lapilli tuffs and volcanic breccias. They are heterolithic with angular to subangular clasts of exclusively volcanogenic material and are generally matrix-supported.

Recrystallized glass shards commonly occur in crystal lithic tuffs (Plate 2.5c). Lapilli tuffs contain fragments normally between 1.2 and 1 cm in hypocrySTALLINE to completely opaque matrices with abundant euhedral and sometimes broken plagioclase phenocrysts (Plate 2.5b). In the pyroclastic rocks of the Savage Mountain Formation, fragments chiefly consist of plagioclase-augite porphyritic basalt, while plagioclase ($\text{An}_2\text{-An}_{12}$) porphyritic basalt and andesite fragments, including rare fragments of bladed plagioclase porphyry (Plate 2.5a), predominate in the pyroclastic rocks of the Moosevale Formation. Volcanic breccias contain lithologically similar clasts normally up to 30 cm, but locally up to 1 m.

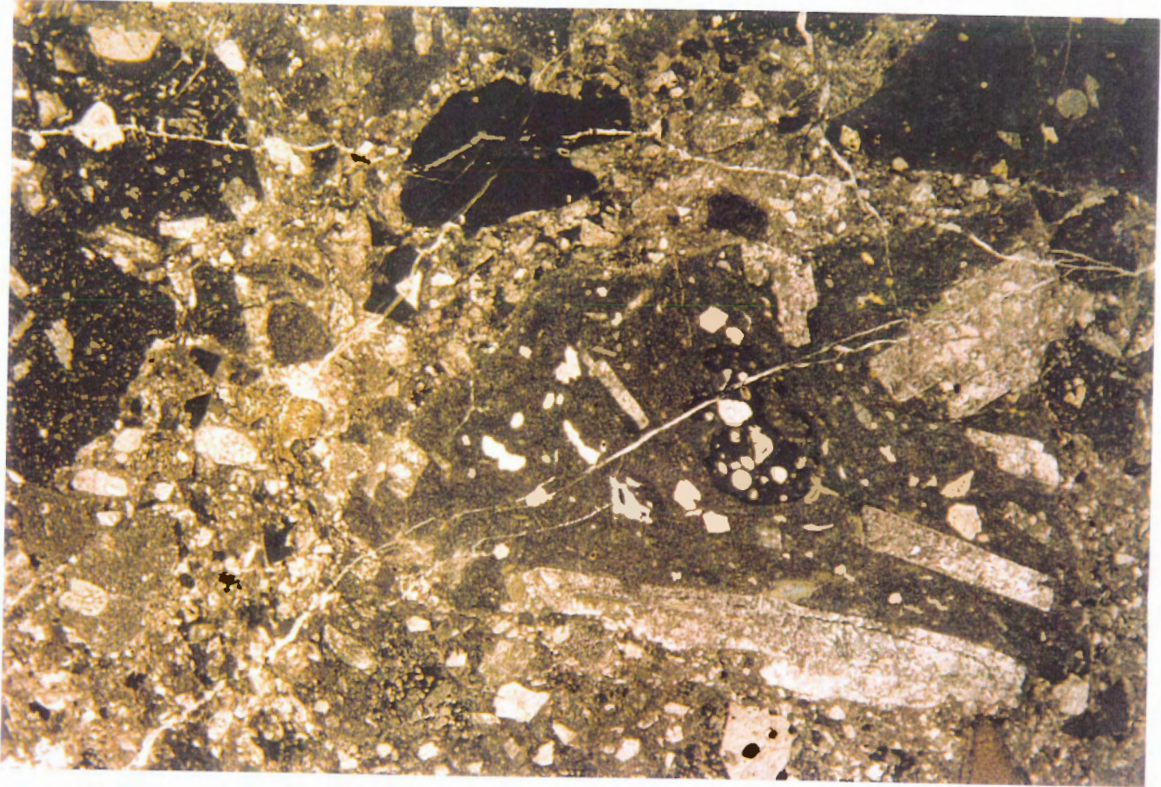
2.4 Alteration and Metamorphism

Space-filling alteration minerals compose between 2 and 40 modal % of the effusive and pyroclastic samples. A 22% increase in the average loss on ignition values of pyroclastic samples over effusive samples suggests that alteration is generally more intense in the pyroclastic rocks. Effusive sample vesicles are commonly filled by chlorite, calcite, albite, quartz, prehnite and pumpellyite. Amygdale mineral zonation (Plate 2.7a) may reflect changes

	unconsolidated deposits			consolidated deposits	
Size (mm)	epiclastic	pyroclastic			
256	boulder	coarse	blocks or bombs	breccia	
	cobble	fine			
64	pebble	lapilli		lapilli-tuff	
2	sand	coarse	ash	coarse	tuff
1/16	silt	fine		fine	
1/256	clay				

Figure 2.5 Classification scheme for volcanoclastic deposits of Easton and Johns (1986). Takla Group volcanoclastic rocks are mainly breccias and lapilli-tuffs.

(a)



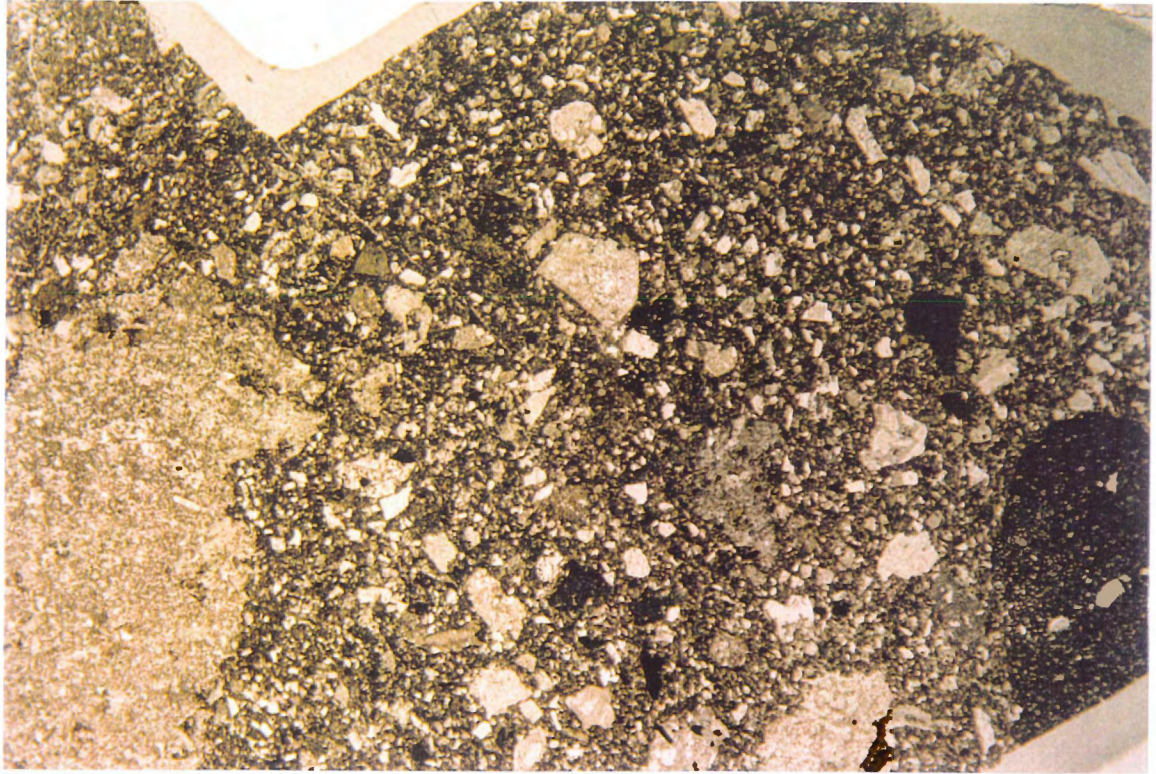
Plates 2.5 a-c Volcaniclastic rock textures

(a) Lapilli tuffs of the Takla Group normally contain angular, plagioclase porphyritic clasts. Field of view is 3.5 cm. Photo is taken in plane polarized light.

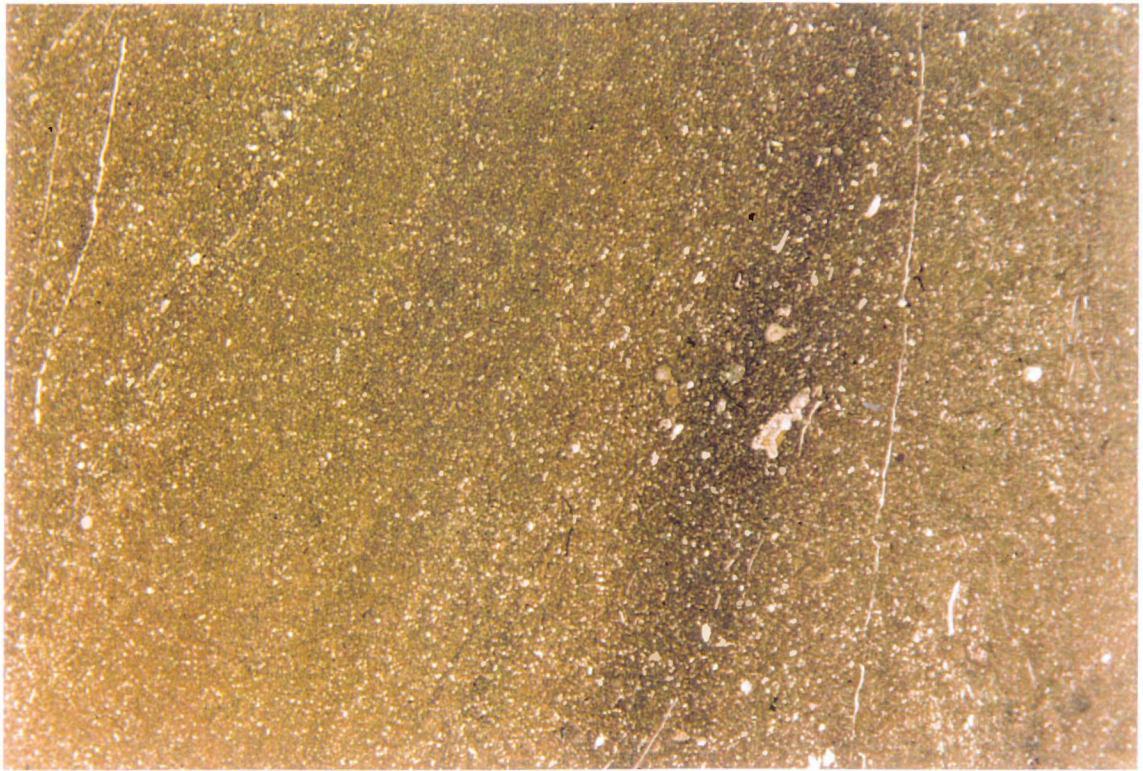
(b) The volcaniclastic rocks usually contain a number of fragment types such as the opaque-rich fragment at right and the feldspar-rich fragment at left. Volcaniclastic matrices contain abundant fragmented crystals in a grungy, brown groundmass. Field of view is 2.8 cm. Photo is taken in plane polarized light.

(c) Rare crystal tuffs are stratified and contain recrystallized glass shards. Field of view is 4 cm. Photo is taken in plane polarized light.

(b)



(c)



in the temperature and composition of the mineralizing fluid. Discontinuous and frequently irregular veinlets and cavities (Plate 2.6b) in effusive and pyroclastic samples contain calcite, chlorite, epidote, talc, prehnite, pumpellyite and minor quartz.

In samples of the Mount Savage Formation, prehnite and pumpellyite, which appear in textural equilibrium, are the dominant metamorphic minerals and occur in irregular cavities, veinlets and vesicles (photos 2.7b). The metamorphic grade of the Moosevale Formation is constrained by the abundance of zeolites, mainly of laumontite composition (Monger, 1977).

2.5 Petrographic Classification

The mineralogy and textures of the Stikinian Takla Group volcanic rocks can be used to determine their composition. The colour and abundance of ferromagnesian minerals suggest that they are predominantly mafic. Accordingly, modal classification (QAP) indicates that they range in composition from basaltic to andesitic (Barker, 1978). Some of the more differentiated Takla Group effusive samples display weak pilotaxitic texture which is common in volcanic rocks of andesitic composition.

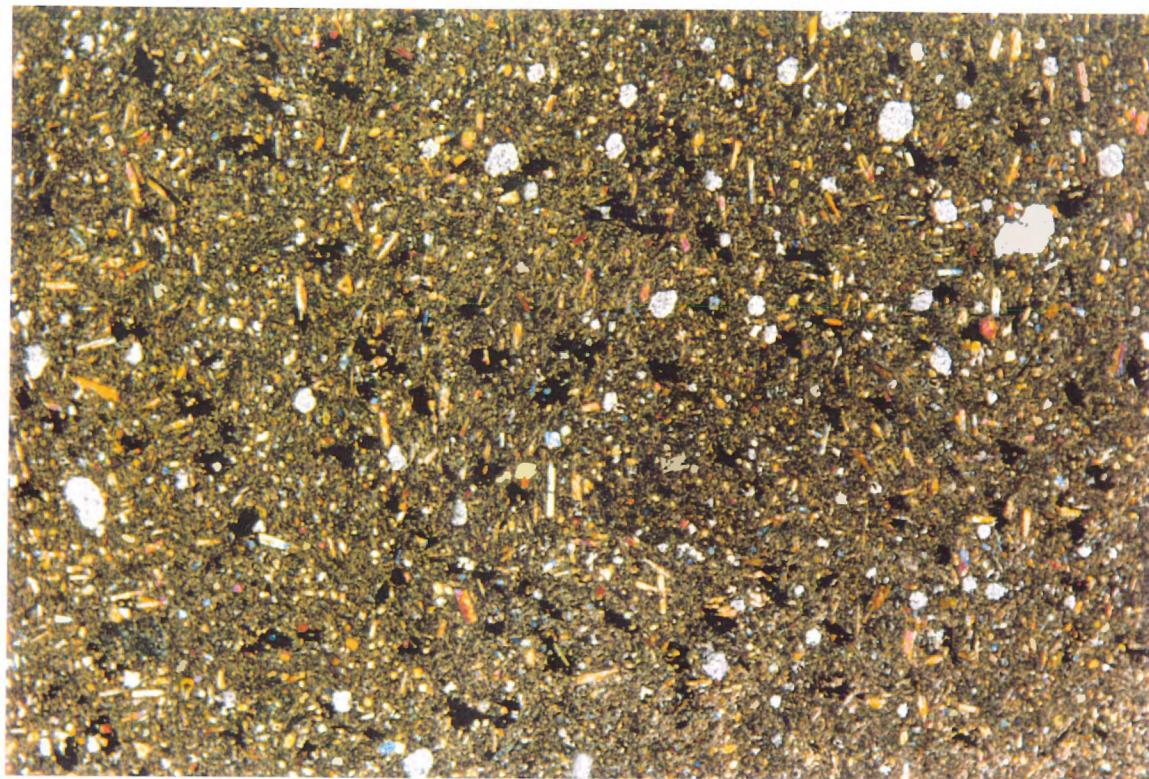
McBirney's (1984) criteria were used to assess the alkalinity of the samples. Nepheline normative basalts contain groundmass olivine while tholeiites contain olivine solely as pseudomorphs that tend to be rounded and show reaction with the groundmass. The apparent absence of groundmass olivine in the Takla Group volcanic rocks and the presence of wholly pseudomorphed olivine phenocrysts suggest a tholeiitic composition. The presence of hypersthene or pigeonite would confirm a subalkaline composition, however, these minerals are not present in the samples.

Plate 2.6 a, b Alteration mineralogy and style

(a) Irregular, space-filling pods of feathery chlorite occur in most sample matrices. Field of view is 2.5 cm in length. Photo is taken under crossed polars.

(b) Discontinuous, irregular veinlets occur in several samples. This 2 mm wide veinlet is filled by quartz and prehnite. Photo is taken under crossed polars.

(a)



(b)

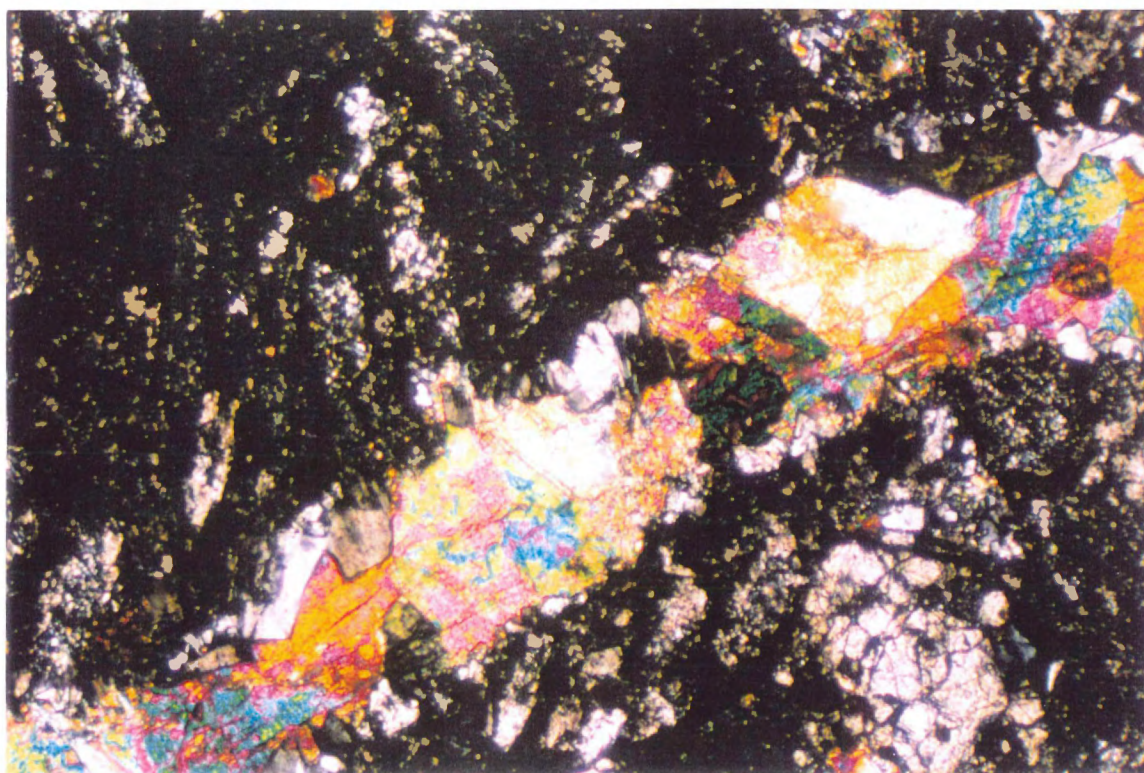
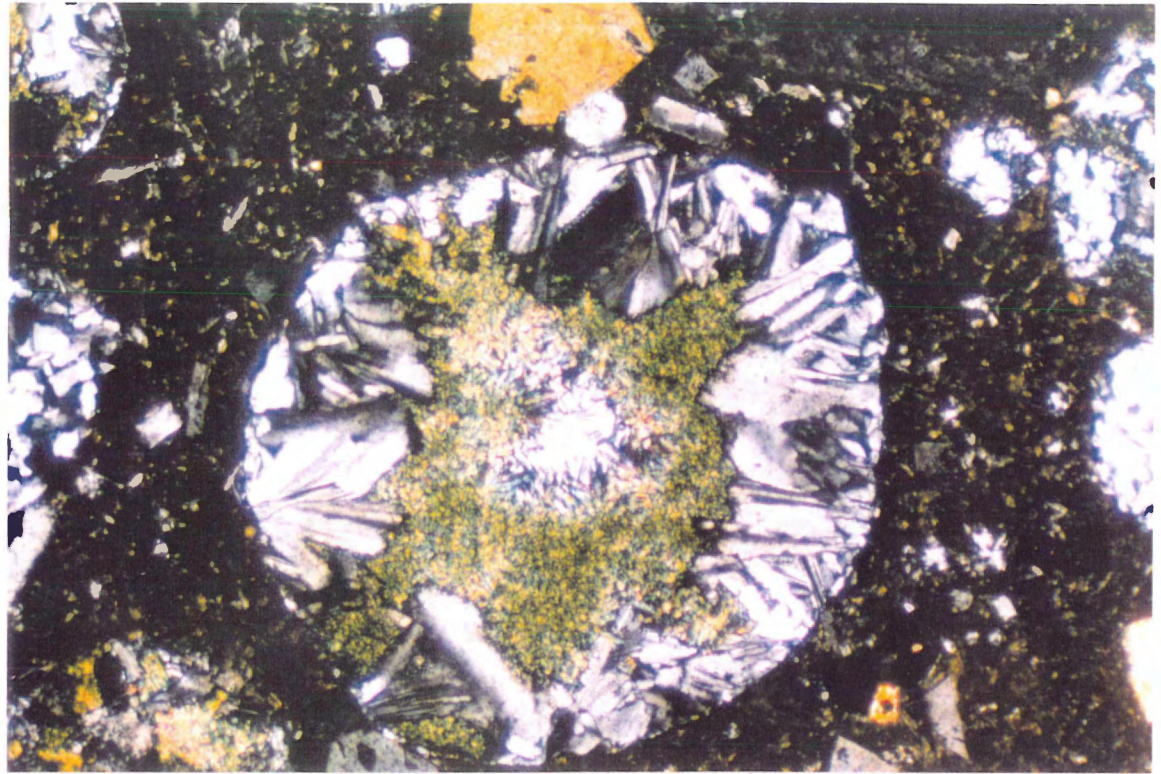


Plate 2.7 a, b Metamorphic minerals

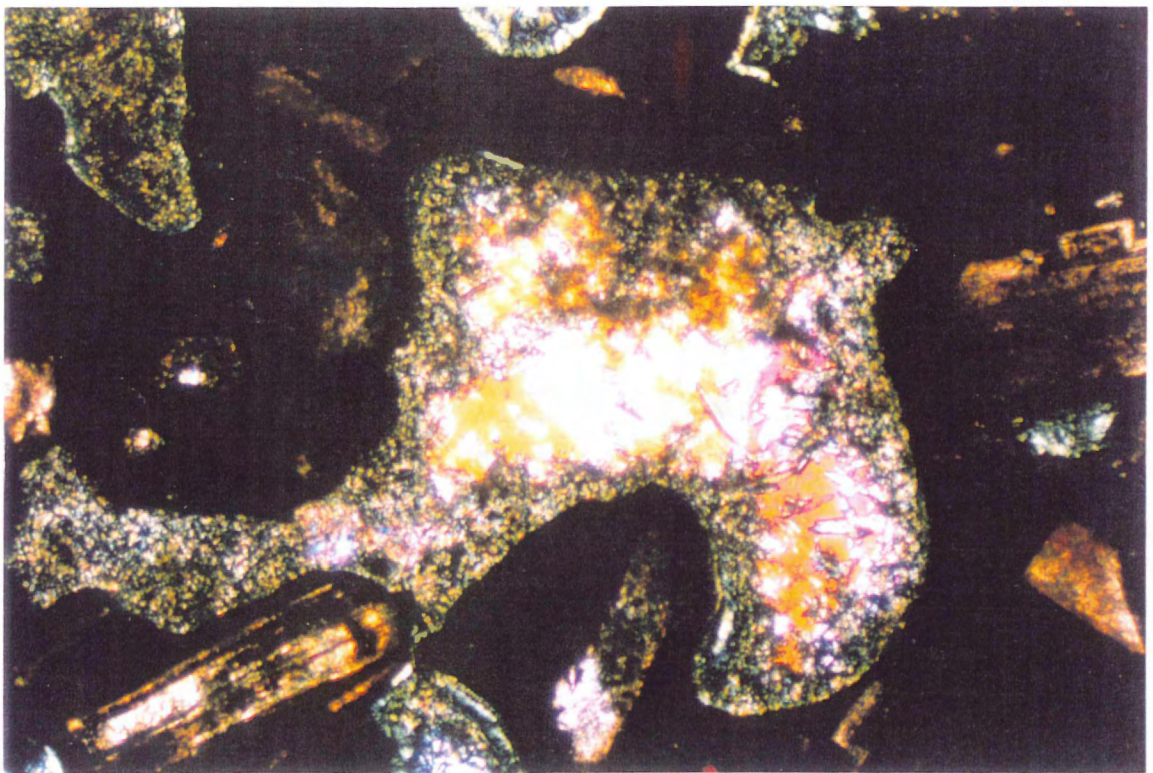
(a) Some amygdules show mineral zonation. This amygdale, which is 2.5 mm in diameter, contains lath-shaped albite and fine-grained to bladed pumpellyite. Photo taken under crossed polars.

(b) Prehnite and pumpellyite usually occur in association, as in this irregular, space-filling pod of fine-grained and acicular rim pumpellyite with prehnite in centre. Field of view is 5 mm. Photo taken under crossed polars.

(a)



(b)



2.6 Summary

The volcanic rocks of the Stikinian Takla Group consist of basaltic to andesitic effusive and pyroclastic rocks with varying proportions of clinopyroxene, plagioclase and olivine phenocrysts. Clinopyroxene zoning reflects normal melt evolutionary trends while plagioclase phenocryst anorthite content implies that alkali alteration has occurred. The mineralogy of the volcanic rocks suggests that they are of subalkaline composition.

CHAPTER 3: GEOCHEMICAL CLASSIFICATION

3.1 Introduction

As it was not possible to conclusively classify the Takla Group volcanic rocks of the Stikine Terrane by petrographic examination, geochemical analysis was necessary in order to define rock type. Because geochemical classification is based on element abundances, only those elements that behave in a relatively immobile fashion during post-magmatic processes can be used to derive meaningful results. In a volcanic suite like the Takla Group, which has undergone alteration and low grade metamorphism, it is important to determine which elements are reliable representatives of the initial rock composition. Following a discussion on element mobility, Chapter 3 continues with a geochemical classification of the Stikinian Takla Group volcanic rocks using relatively immobile elements. The use of elements that are not significantly mobilized during alteration and metamorphism is also critical in the application of the sample chemistry to the tectonomagmatic discrimination diagrams presented in Chapter 4.

3.2 Experimental Methods

Sixty-two Stikinian Takla Group samples were analyzed at the Regional X-ray Fluorescence (XRF) Laboratory at Saint Mary's University for 11 major elements and 17 trace elements on a Philips PW 1400 sequential XRF spectrometer using a Rh-anode X-ray tube and LiF 220 analyzing crystal. In this technique, primary X-rays bombard powdered and fused rock samples, producing secondary X-rays from individual elements in the sample

which are diffracted according to Bragg's Law (Ragland, 1989). Passage through an analyzing crystal isolates X-rays of selected elements which are then counted by a detector.

REE (La, Ce, Pr, Nd, Sm, Eu, Gd, Tb, Dy, Ho, Er, Tm, Yb and Lu) and 15 trace elements (Li, Rb, Sr, Y, Zr, Nb, Mo, Cs, Ba, Hf, Ta, Tl, Pb, Bi, Th and U) were measured on 14 Takla Group samples by inductively coupled plasma mass spectrometry (ICP-MS) at Memorial University. This highly sensitive method involves the dissolution of rock powders and the conversion of the solution into a plasma in which atoms ionize and molecules dissociate. The ions are then passed through a mass spectrometer where they are separated according to mass and counted at a detector. A review of plasma mass spectrometry is presented in Jarvis and Jarvis (1992). Major and trace element analysis results are presented in Appendix C. The accuracy and precision of XRF and ICP-MS analyses are also included in this appendix. Values of Zr obtained by ICP-MS are consistently low due to ineffective dissolution and are substituted with XRF-derived values.

3.3 Element mobility

Post-magmatic element mobility is tested by plotting selected elements against Zr. Because Zr is a high field strength element, it is not easily mobilized in aqueous fluid unless in the presence of certain complexing agents (Pearce and Norry, 1979). For this reason, it remains relatively immobile during alteration and low grade metamorphism. Furthermore, as a highly incompatible element, Zr behaves in a predictable manner during melt evolution. Correlation of an element with Zr implies that during post-magmatic fluid alteration, the

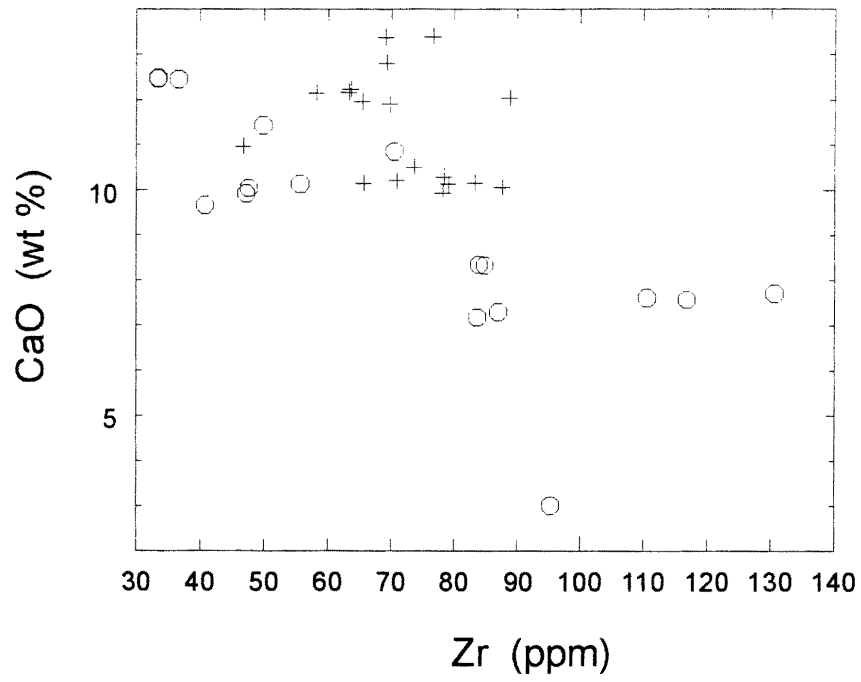
selected element behaved in a relatively immobile fashion. If this is true, then the abundance of the element reflects magmatic processes only.

According to petrographic observation and mineral chemistry, it is likely that Ca contained in plagioclase was mobilized and replaced by Na and K. The presence of calcite in veins and amygdules is a further indication of Ca mobility. A plot of CaO against Zr shows considerable scatter, confirming that Ca abundances are not uniquely influenced by magmatic processes. Other major elements (with the exception of Si, Ti and Al) show similar scatter when plotted against Zr. The FeO*/MgO ratio (where FeO* equals total iron) shows good correlation, suggesting that FeO* and MgO behaved similarly with respect to each other. Figure 3.1 demonstrates examples of relatively mobile and immobile element behaviour by plotting CaO and Ti against Zr.

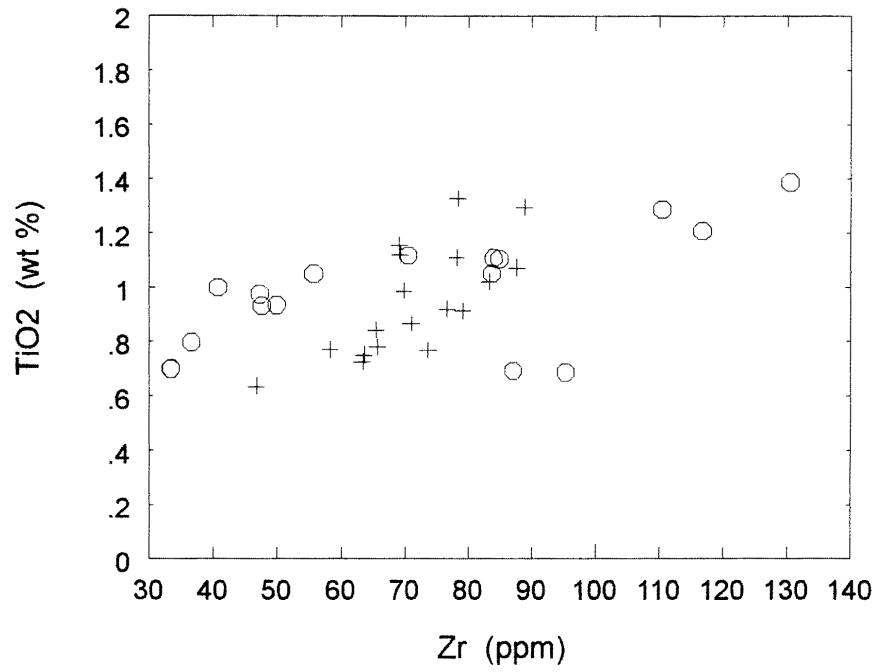
Alteration and metamorphism are generally thought to have no significant effect on rare earth element (REE) patterns. According to Nyström (1984), the REE can be significantly mobilized in highly vesicular volcanic rocks, but do not change in concentration with respect to each other. Similarly, Dostal and Strong (1983) state that REE in basaltic magmas metamorphosed to prehnite-pumpellyite grade are not significantly mobilized, only diluted. According to Hajash (1984), local redistribution of REE may occur with a minimal net effect. Cases do exist of significant REE mobility (Hellmen et al., 1979), especially of the light REE (Wilson, 1995). However, under normal conditions of moderate alteration and low grade metamorphism, as in the case of the Stikinian Takla Group, it is likely that the relative abundances of the REE have not changed significantly.

Figure 3.1 a, b Oxide trends with respect to the relatively immobile trace element Zr. Element mobility during post-magmatic processes is reflected in a plot of CaO vs. Zr which shows considerable scatter. The tighter correlation of TiO₂ represents magmatic trends indicative of restricted element mobility. Two sample groups are shown. O = NW samples; + = W samples.

(a)



(b)



Other trace elements such as Ni, Cr, V, Nb and Hf are generally considered to be immobile (Wilson, 1995), as are Ti and Y (Smith and Smith, 1976). These trace elements, along with the REE, correlate strongly with Zr. Ta abundance is not reliable due to sample contamination during crushing with tungsten carbide, which contains significant quantities of Ta. To summarize, elements that can be confidently used for geochemical analysis of the samples are Si, Ti, Al, Nb, Hf, Zr, Y, Th and the REE (La, Ce, Pr, Nd, Sm, Eu, Gd, Tb, Dy, Ho, Er, Tm, Yb and Lu), as well as the FeO*/MgO ratio.

3.4 Normative Calculation

CIPW normative analysis was performed on the Takla Group samples to determine magma type. All chemical analyses used for interpretation in Chapter 3 are of non-cumulus samples with oxide wt % values suggesting that extensive alteration has not taken place. For the normative calculation, the ferrous to ferric iron ratio was set at $\text{FeO}/(\text{FeO}+\text{Fe}_2\text{O}_3)=0.90$ (after Ragland, 1989). According to the analysis, 29 of 62 samples are nepheline normative, although no modal nepheline was observed. This result implies that almost half of the samples are alkaline. However, the average silica content of all basaltic samples on a volatile-free basis is 50.72 wt %, which exceeds the maximum defined silica content of alkaline basalts of 48 wt % (McBirney, 1984). Those samples that are nepheline normative show a 10 % increase in alkali element wt % over non-nepheline normative samples and also have unusually high $\text{Na}_2\text{O}/\text{K}_2\text{O}$ ratios. Such a result could be caused by secondary alteration, in which case Ca would have been removed from plagioclase and replaced by alkali elements (mainly Na). This interpretation is in agreement with plagioclase An contents as low as 1.8 wt %. In general, the

results suggest that normative calculation is not a reliable indicator of silica saturation for the Takla Group samples due to the effects of post-magmatic alteration.

3.5 Major and Trace Element Classification

3.5.1 Alkalinity and Degree of Differentiation

In the case of the Takla Group samples, major element plots traditionally used to determine alkalinity, such as the $(\text{Na}_2\text{O} + \text{K}_2\text{O})$ vs. SiO_2 plot of Irvine and Baragar (1971), are unreliable due to the mobility of the alkali elements. As a result, plots of relatively immobile elements must instead be used, such as the SiO_2 vs. Zr/TiO_2 and Zr/TiO_2 vs. Nb/Y plots of Winchester and Floyd (1977), in order to assess the degree of alkalinity and differentiation in volcanic rocks.

With progressive differentiation, the Zr/TiO_2 ratio increases due to the decline of TiO_2 in the melt phase and the increase in concentration of the incompatible element Zr. The rate of increase of the Zr/TiO_2 ratio with respect to SiO_2 is higher in magmas of alkaline composition. According to the SiO_2 vs. Zr/TiO_2 diagram (Fig. 3.2), the samples plot entirely in the subalkaline field and range from basaltic to andesitic compositions.

Nb/Y ratios are also a measure of alkalinity (Nb concentrations are higher in alkaline melts) but are not appreciably affected by differentiation (both elements are highly incompatible). A Zr/TiO_2 vs. Nb/Y plot (Fig. 3.3) confirms the subalkaline composition of the samples which have low Zr/TiO_2 and Nb/Y ratios. Pearce and Cann (1973) also use Y and Nb proportions to distinguish between alkaline and tholeiitic suites. An average Y/Nb ratio of 4.9 classifies the Takla Group as tholeiitic according to this method.

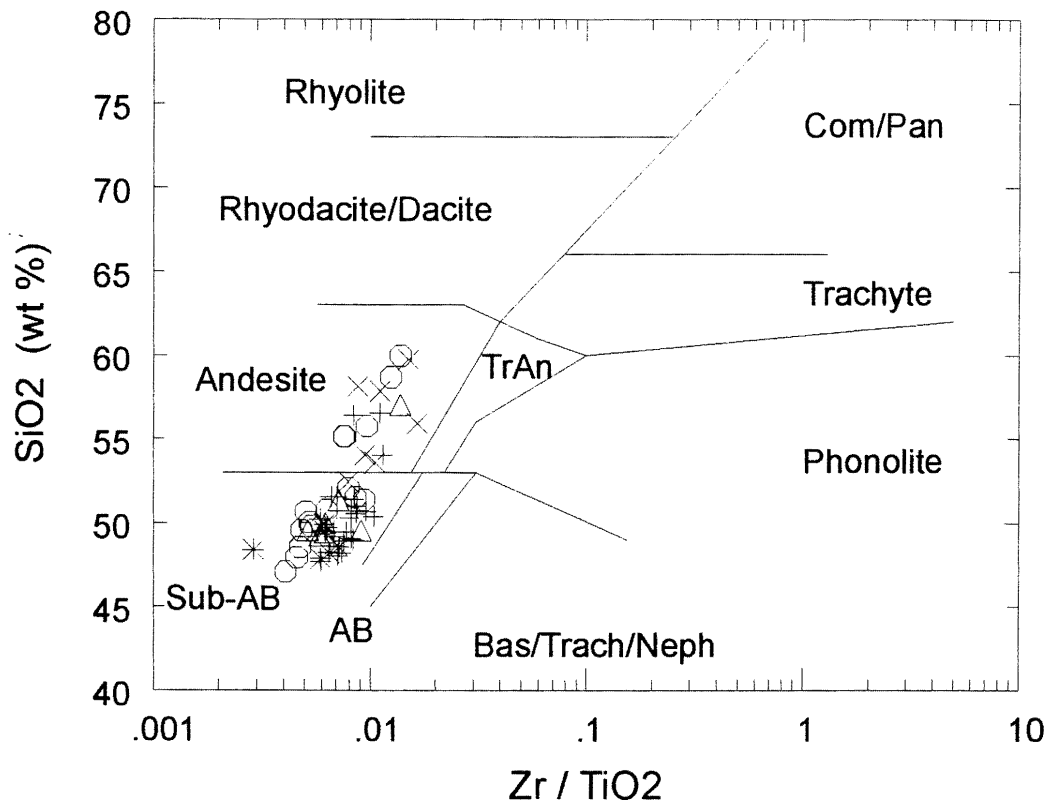


Figure 3.2 The SiO_2 vs. Zr/TiO_2 discrimination diagram of Winchester and Floyd (1977) indicates that the samples are subalkaline and range from basaltic to andesitic. Suitable effusive and pyroclastic samples are plotted. Δ = S samples; X = WIL samples; O = NW samples; + = W samples; * = CS samples. Abbreviations are as follows: Sub-AB = subalkaline basalt; AB = alkaline basalt; TrAn = trachyandesite; Com = comendite; Pan = pantellerite; Bas = basanite; Trach = trachyte; Neph = nephelinite.

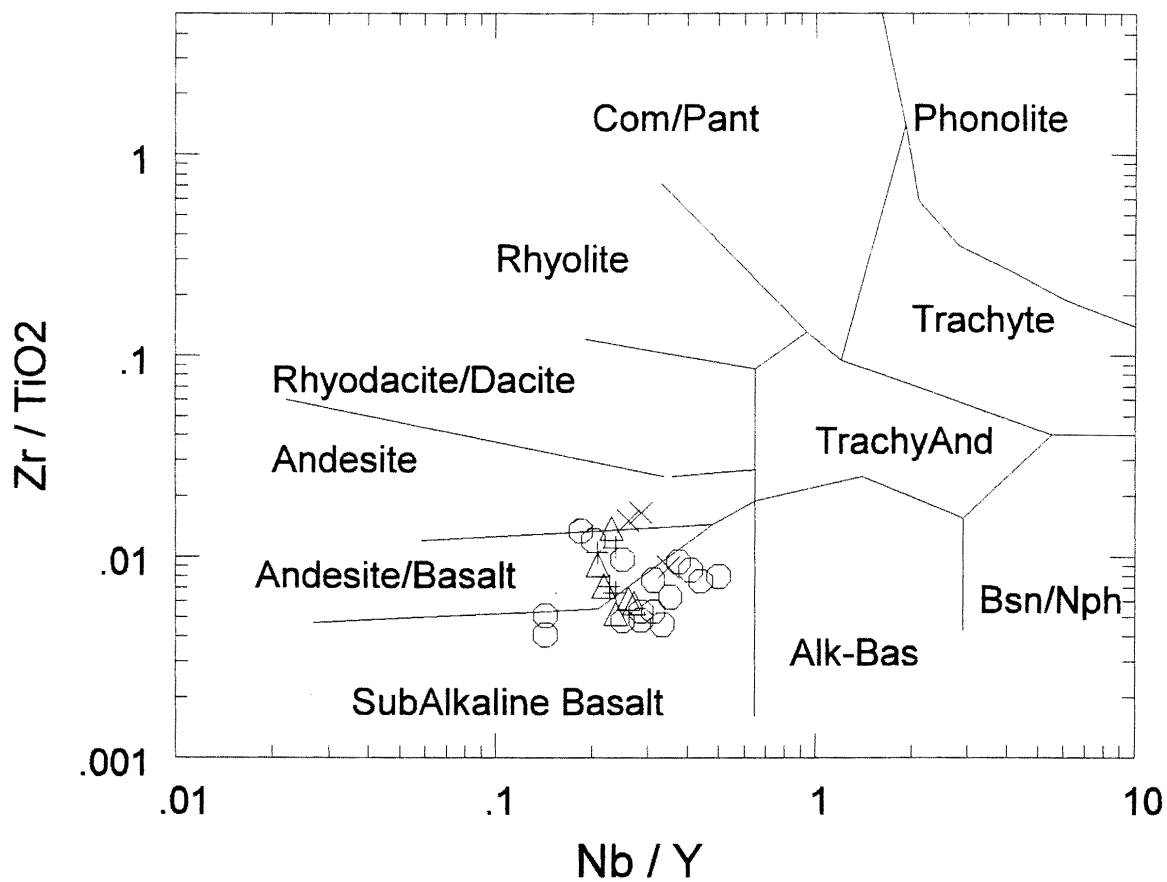


Figure 3.3 Low Zr/TiO_2 vs. Nb/Y ratios confirm the subalkaline composition of the samples according to this discrimination diagram of Winchester and Floyd (1977). Symbols and abbreviations as per Figure 3.2.

3.5.2 Tholeiitic and Calc-alkaline Associations

Traditionally, tholeiitic and calc-alkaline rock suites can be distinguished on the alkali-iron-magnesium (AFM) ternary diagram of Irvine and Baragar (1971). In this case, however, like the $(\text{Na}_2\text{O} + \text{K}_2\text{O})$ vs. SiO_2 plot, the AFM plot is unreliable due to the mobility of the alkali elements. On the other hand, Miyashiro (1974) distinguishes calc-alkaline from tholeiitic suites on the basis of (1) a higher rate of SiO_2 increase with fractionation (which is represented by the FeO^*/MgO ratio) and (2) lesser degrees of FeO^* and TiO_2 enrichment with fractionation. In magmas of basaltic composition, FeO^* content is strongly influenced by Fe-Ti oxide crystallization, which is dependent on oxygen fugacity. Reducing tholeiitic magmas suppress the precipitation of magnetite and cause the FeO^* concentration of the magma to increase with differentiation while the converse is true of the more oxidizing calc-alkaline magmas. Ti, which readily substitutes into Fe-oxide crystal structures, behaves similarly to FeO^* . According to Figure 3.4, which plots SiO_2 vs. FeO^*/MgO , the samples possess a weak tholeiitic tendency of lesser SiO_2 enrichment with fractionation. Figure 3.5 plots TiO_2 vs. FeO^*/MgO and produces TiO_2 enrichment trends intermediate between tholeiitic and calc-alkaline for the Takla Group volcanic rocks. These plots suggest that the samples do possess a tholeiitic characteristic, but are transitional between tholeiitic and calc-alkaline rocks. According to Jakeš and Gill (1970), a complete spectrum of magmas may exist between these two magma types. The occurrence of such intermediate magmas has been attributed to variations in mantle source composition from more “oceanic” (incompatible element depleted) to more continentally-influenced (incompatible element enriched), as well as to variation in low pressure crystal fractionation conditions (Wilson, 1995).

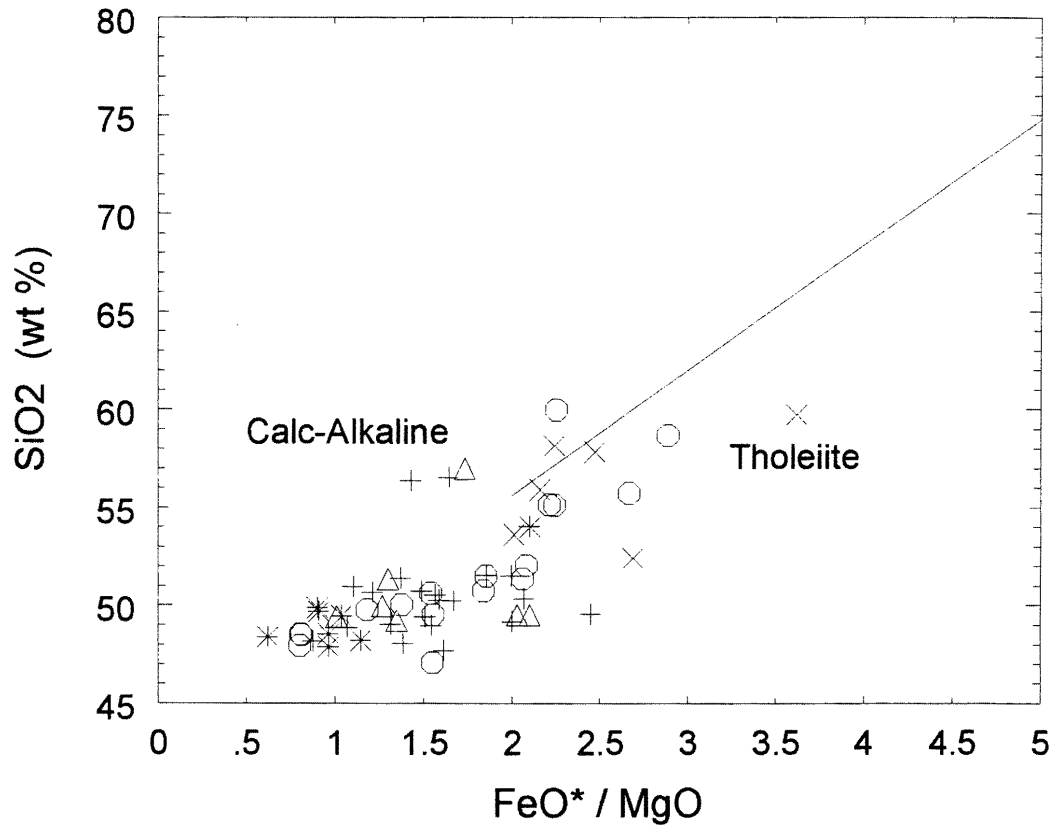


Figure 3.4 Minimal SiO₂ increase with differentiation (represented by FeO*/MgO) plots most of the Takla Group samples as tholeiitic according to this discrimination diagram of Miyashiro (1974). Symbols as per Figure 3.2.

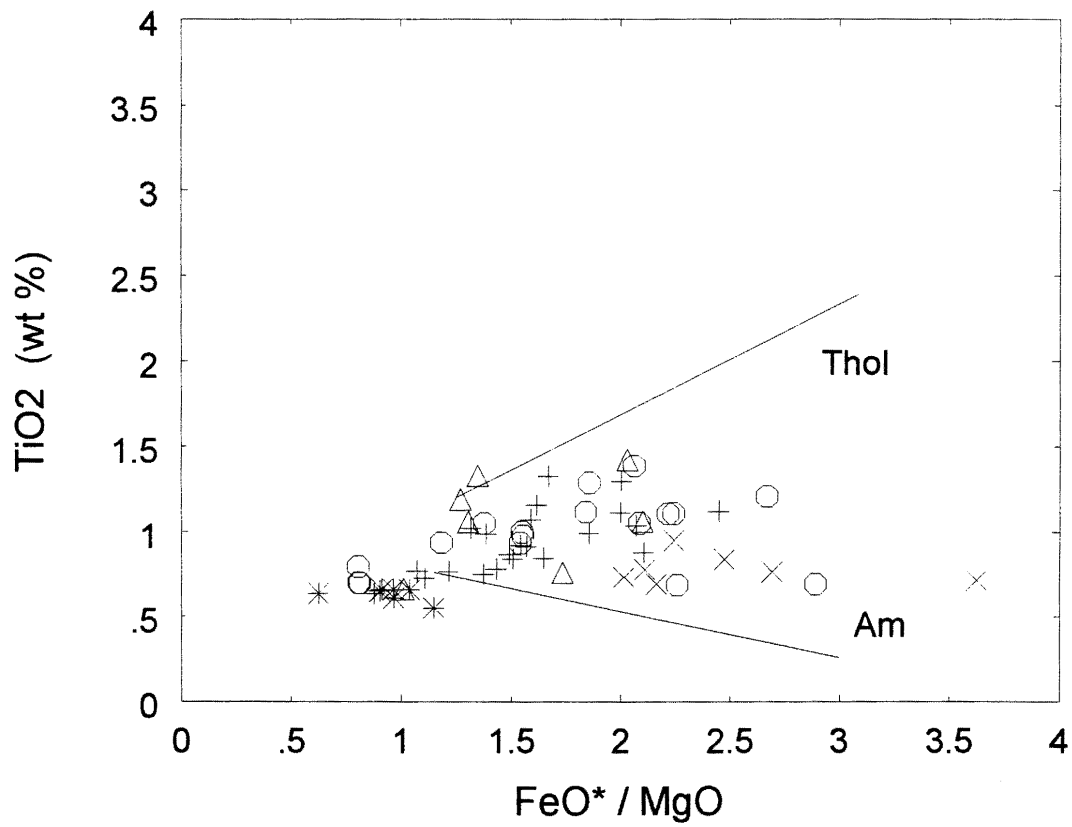


Figure 3.5 TiO₂ enrichment with differentiation is diagnostic of tholeiitic magmas while the converse is true of calc-alkaline magmas. The samples show an intermediate trend according to the discrimination diagram of Miyashiro (1974). Thol = tholeiite trend; Am = calc-alkaline trend. Symbols as per Figure 3.2.

3.5.3 Pyroclastic Composition

Relatively immobile element plots, such as Figures 3.2 and 3.3, demonstrate that pyroclastic and effusive samples are similar in alkalinity, but that pyroclastic samples are generally more SiO₂ enriched. This may reflect the greater tendency toward pyroclastic eruption in andesites. In terms of trace element composition, the pyroclastic and effusive samples are nearly identical (Fig. 3.6).

3.6 Petrogenesis and Melt Evolution

Certain REE patterns reflect melt source mineralogy (Philpotts, 1990). The generally flat pattern of chondrite-normalized heavy REE (Fig. 3.7) indicates that the source of the Takla Group magmas did not contain residual garnet, which has a high distribution coefficient for the heavy REE. Instead, the melt must have been produced in the spinel peridotite stability field of the mantle, at a depth of less than 60 km (White et al., 1992).

Using SiO₂ as an index of differentiation, binary variation diagrams were constructed to observe patterns in melt evolution (Fig. 3.8a-h). CaO and Al₂O₃ are used to determine the behaviour of feldspar. CaO declines steadily with differentiation while Al₂O₃ increases indicating that feldspar, which contains relatively more Al₂O₃ than CaO, did not fractionate from the melt until relatively late. CaO decrease can instead be attributed to the fractionation of clinopyroxene. Although Na has been disturbed, a strong Na₂O enrichment with differentiation confirms the delay of feldspar fractionation. Initially, the CaO/Al₂O₃ ratio decreases sharply with differentiation due to CaO decline in the melt. For NW samples, the trend flattens at a SiO₂ value of 51 wt %, possibly reflecting the onset of feldspar fractionation

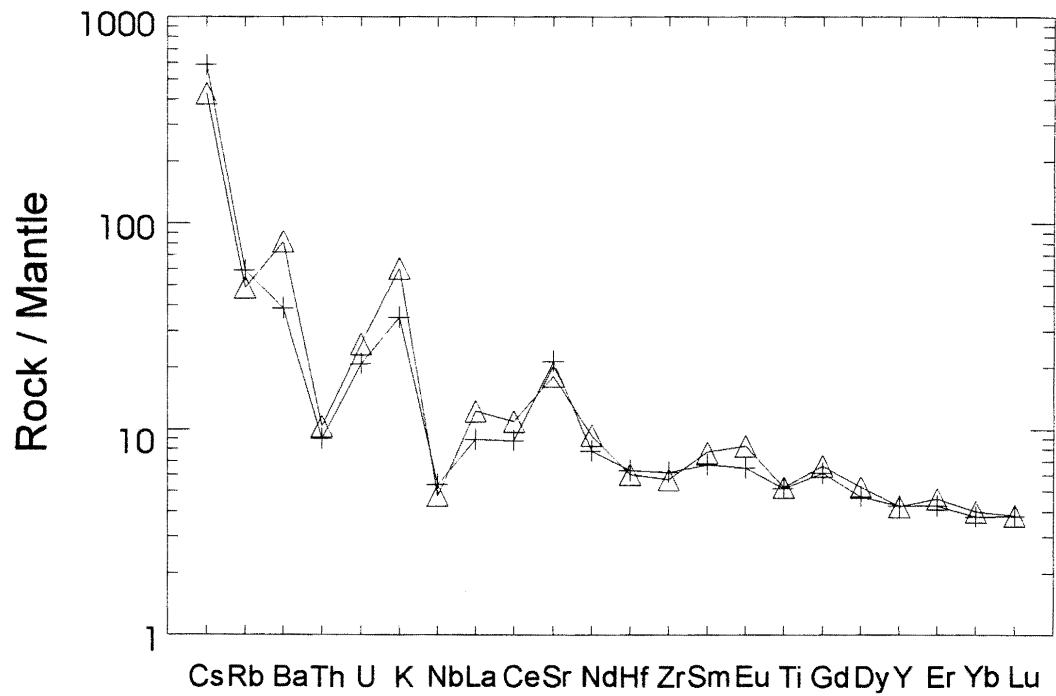


Figure 3.6 According to a mantle-normalized spider diagram, Takla Group volcanoclastic samples (represented by sample S-74, symbol Δ) are similar in trace element composition to effusive samples (represented by W-26, symbol +).

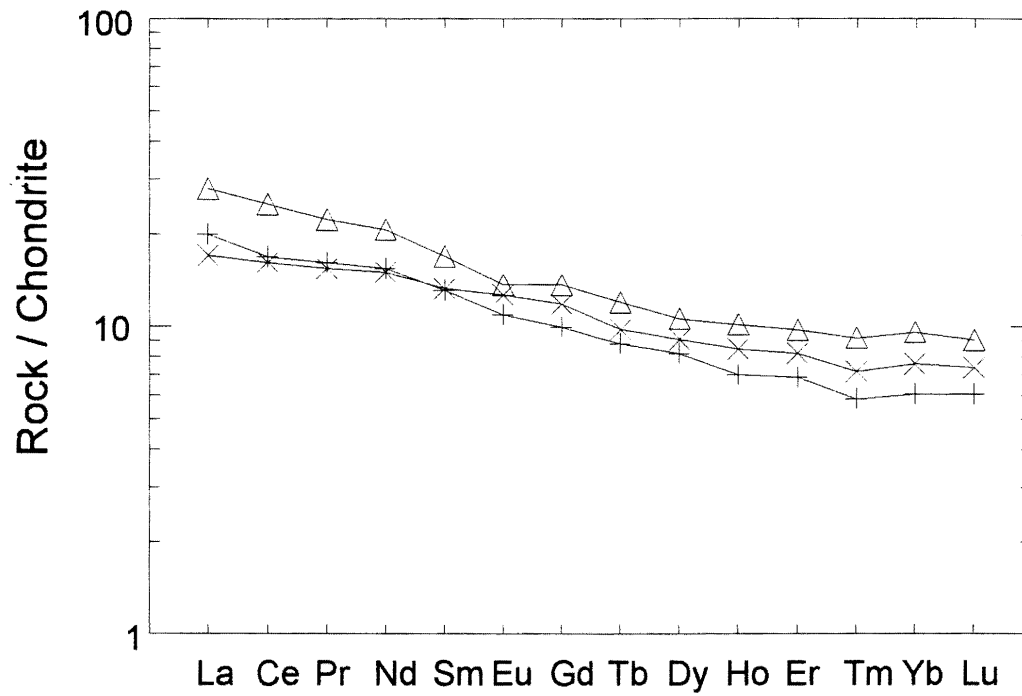


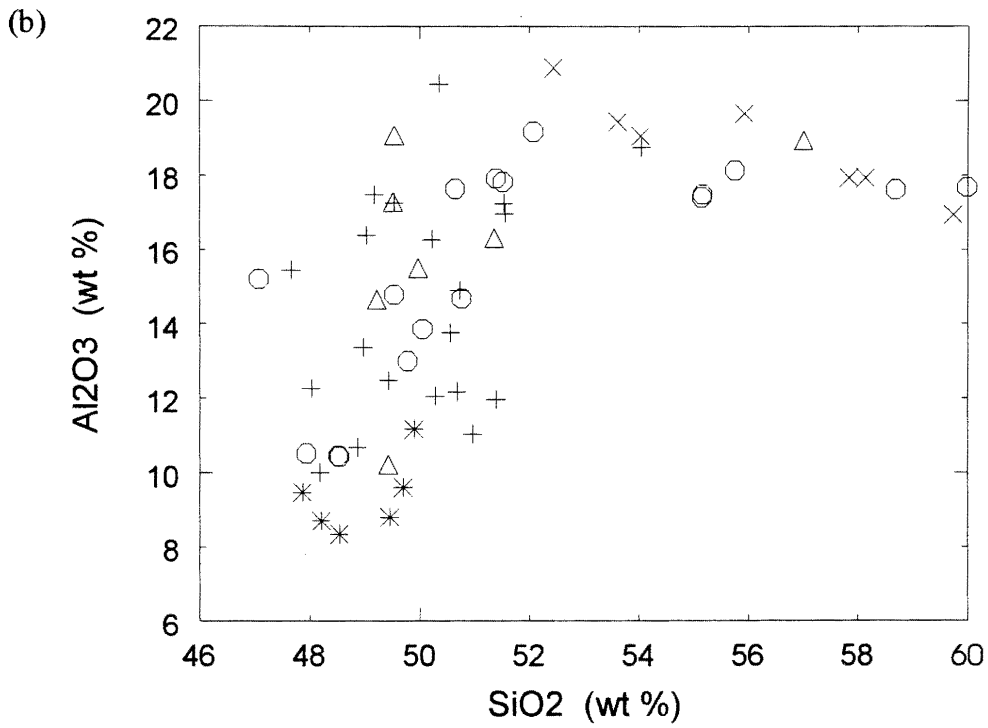
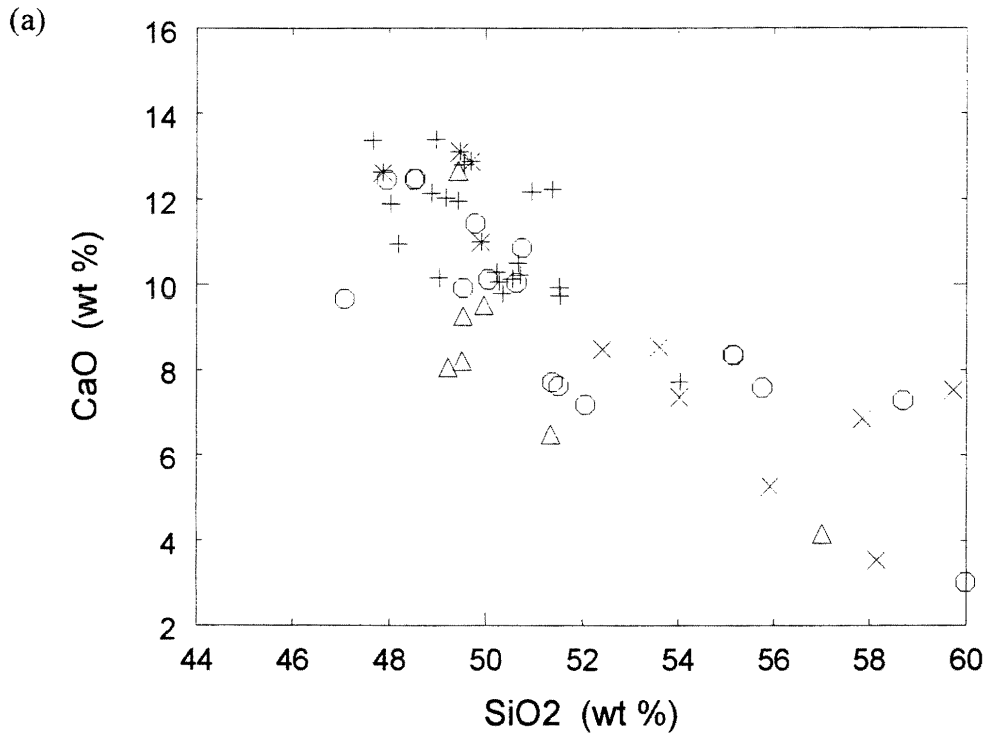
Figure 3.7 Generally flat heavy REE patterns for effusive samples W-31 (+) and W-26 (X) as well as volcaniclastic sample S-153 (Δ) suggest that garnet was not present as a residual source mineral.

through the removal of Al_2O_3 from the melt. However, it could also represent a cessation in clinopyroxene fractionation.

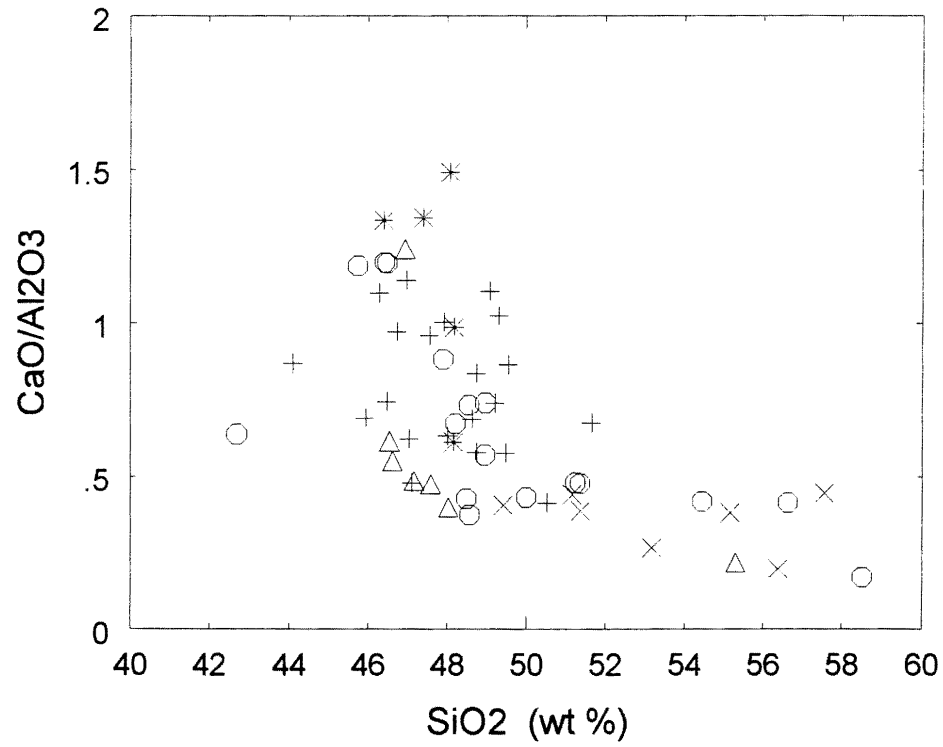
The trace elements Ni and Cr, which have high distribution coefficients for olivine and clinopyroxene, respectively, are relatively immobile, sensitive indicators of the behaviour of these phases. Ni and Cr decline sharply over a SiO_2 range of 47 to 52 wt %, suggesting early, rapid fractionation of olivine and clinopyroxene. This result is supported by the decline in CaO in the melt in response to clinopyroxene fractionation. The Cr/Ni ratio declines over a SiO_2 range of 48 to 52 wt %, then flattens dramatically. This suggests that clinopyroxene fractionated out of the melt at a faster rate than olivine over the 48 to 52 wt % SiO_2 range. Subsequent olivine and clinopyroxene behaviour is similar, possibly reflecting a switch to plagioclase-dominated fractionation.

P_2O_5 and TiO_2 were plotted to determine the role of apatite and the Ti-oxides during melt evolution. Generally, P_2O_5 content increases at a high rate over a SiO_2 range of 47 to 51 wt %, after which it continues to increase at a lower rate. This reflects a suppression followed by an onset of apatite fractionation. A separate P_2O_5 behavioural trend, which shows minor increase over a SiO_2 range of 52 to 60 wt %, is produced by the more differentiated WIL pyroclastic samples of the Moosevale formation. Similarly, TiO_2 shows a general trend of rapid increase over a SiO_2 range of 48 to 52 wt % and a separate WIL sample trend of minor TiO_2 increase over a SiO_2 range of 52 to 60 wt %. The WIL sample trends appear unconnected to the other Takla Group samples and could indicate heterogeneities in the source magma or the existence of multiple magma sources. Separate variation trends for the WIL samples could also form as a result of clastic contamination.

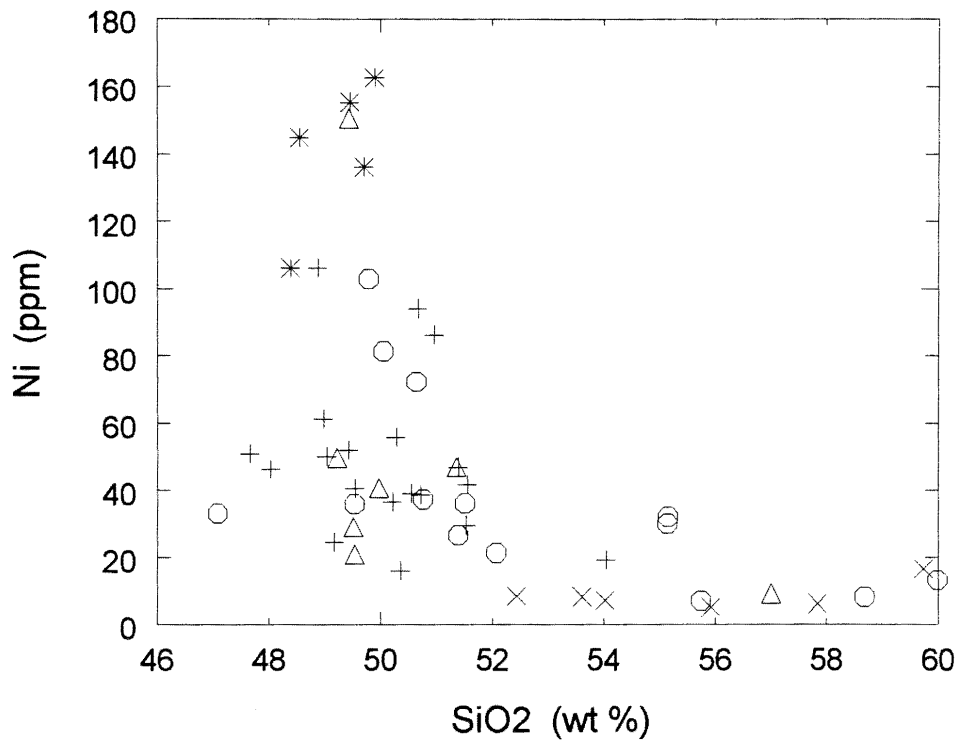
Figure 3.8 a-h Binary variation diagrams using SiO_2 as an index of differentiation. All five sample groups are shown. Δ = S samples; + = W samples; X = WIL samples; O = NW samples; * = CS samples. NW samples generally show the most complete trends. WIL trends are often distinct from other Takla Group sample trends and may reflect magma heterogeneity, multiple magma sources or clastic contamination.



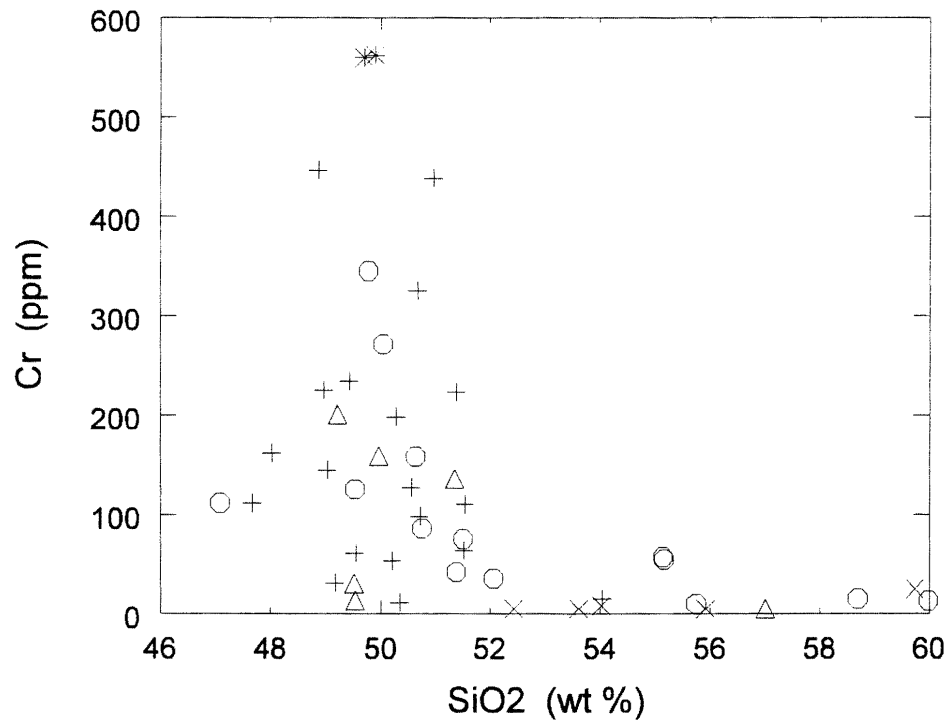
(c)



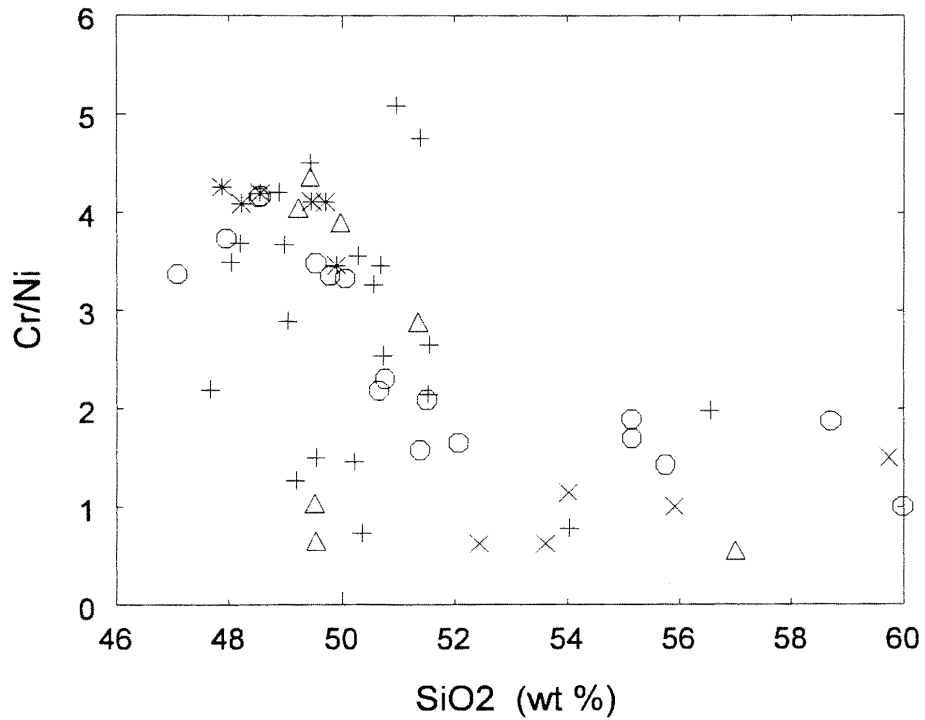
(d)

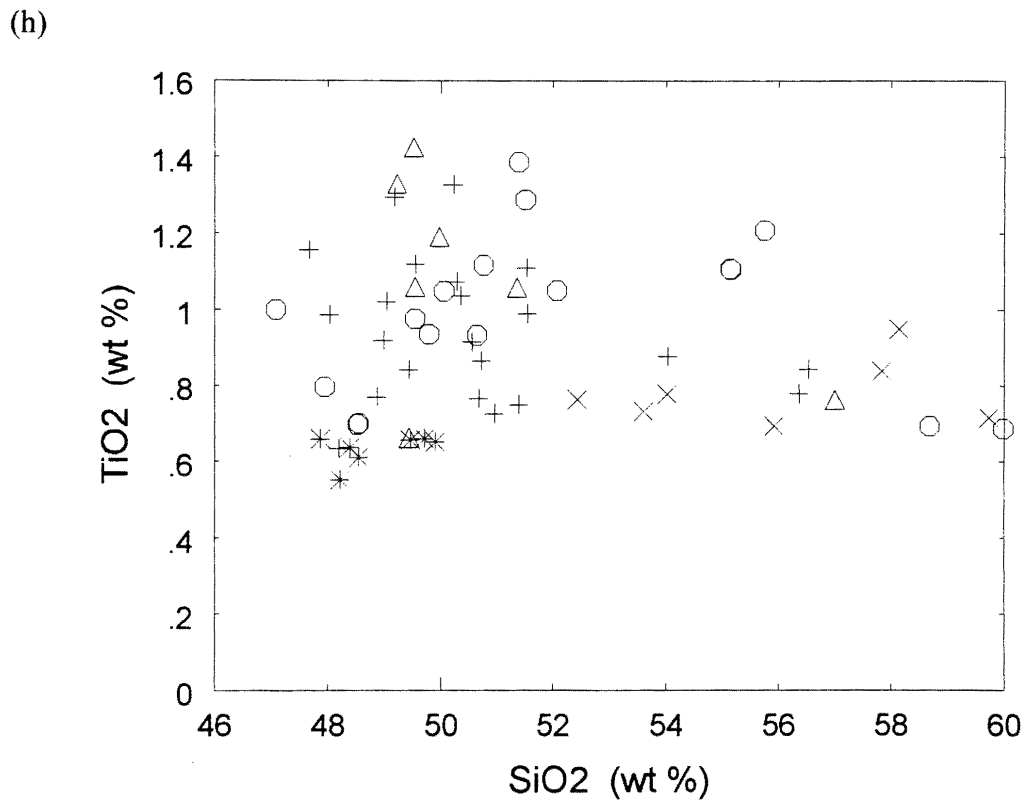
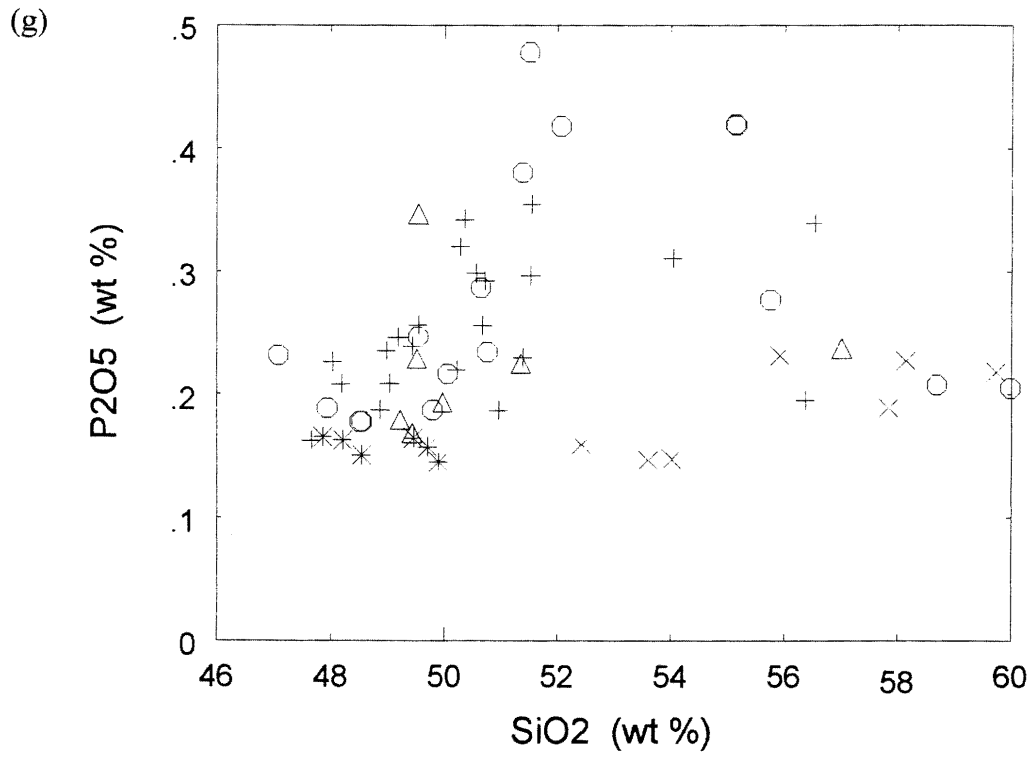


(e)



(f)





3.7 Summary

Once the effects of alkali element enrichment have been considered, geochemical analysis of the Stikinian Takla Group rocks indicates that they are sub-alkaline basalts to andesites. Magma trends do not conclusively classify the Takla Group magmas as tholeiitic or calc-alkaline, but rather suggest an intermediate composition. According to REE patterns and variation diagrams, the Takla Group magmas were derived from a spinel-peridotite mantle source. The early crystallization sequence of the magma was dominated by clinopyroxene and, to a lesser extent, olivine fractionation. Later stages were controlled by the fractionation of plagioclase, apatite and Ti-oxide minerals.

Because subalkaline magmas occur in numerous tectonic settings, further constraints are necessary to determine the paleotectonic setting of the Stikinian Takla Group. Chapter 4 continues with an interpretation of this tectonic setting using the relatively immobile elements presented in this chapter.

CHAPTER 4: PALEOTECTONIC INTERPRETATION

4.1 Introduction

In their application to discrimination diagrams and trace element plots, the geochemical characteristics of igneous rocks are frequently used to determine their paleotectonic setting. The construction of tectonomagmatic discrimination diagrams is based on the regular and predictable distribution of major and trace elements during magmatic processes such as partial melting, fractionation, assimilation and crystallization. Discrimination diagrams were developed by empirical analysis of the geochemistry of fresh rock samples derived from known, present day tectonic settings. With the exception of igneous activity during the early Precambrian (Wilson, 1995), similar trace element patterns would have been produced in the past by tectonic processes equivalent to those occurring today. As a result, tectonomagmatic discrimination diagrams are a potentially powerful tool in the interpretation of the setting of ancient volcanic suites. However, they are not infallible (e.g. Wang and Glover, 1992) and must be used in conjunction with other criteria such as field relationships, depositional setting, and percentage and type of associated volcanoclastic deposits.

Like the diagrams used to characterize igneous rocks in Chapter 3, tectonic setting diagrams and trace element patterns depend on the abundances of elements that have not been altered by post-magmatic processes. Only those elements that were determined to be relatively immobile will be used in this chapter.

4.2 Sample Screening

Most tectonomagmatic discrimination diagrams were constructed for volcanic rocks of basaltic composition since these are the most sensitive indicators of environmental change (Wilson, 1995). As a result, Takla Group samples were passed through Manson's (1967) chemical basalt screen. Forty-three of the 62 samples analyzed by XRF and 7 of the 14 samples analyzed by ICP-MS passed the screen (Fig. 4.1a,b). Several samples classified as basaltic andesites according to Winchester and Floyd (1977) also passed the screen.

a. Savage Mountain Formation:

Sample	Lithology	Sample	Lithology
W-26	Cpx porphyritic basalt	W-79	Cpx porphyritic basalt
W-27	Cpx porphyritic basalt	NW-1C	Plag porphyritic basalt
W-28	Cpx porphyritic basalt	NW-14B	Cpx porphyritic basalt
W-29A	Cpx porphyritic basalt	NW-26	Basaltic tuff breccia
W-29B	Cpx porphyritic basalt	NW-29	Cpx porphyritic basalt
W-31	Cpx porphyritic basalt	NW-56	Cpx porphyritic basalt
W-32	Cpx porphyritic basalt	NW-69	Plag porphyritic basalt
W-33	Aphanitic basalt	NW-73	Plag porphyritic basalt
W-34	Cpx porphyritic basalt	NW-75	Cpx-plag porphyritic basalt
W-36	Aphanitic basalt	NW-76	Plag porphyritic basalt
W-37	Amygdular aphanitic basalt	NW-77	Plag porphyritic basalt
W-73B	Basaltic andesite breccia	NW-92	Aphanitic basaltic andesite
W-75	Cpx porphyritic basaltic andesite	NW-93	Cpx porphyritic basalt
W-77	Amygdular cpx porphyritic basalt	CS-2	Plag porphyritic basalt

b. Moosevale Formation:

Sample	Lithology	Sample	Lithology
W-41	Basaltic andesite tuff breccia	WIL-34	Basaltic andesite tuff breccia
W-42	Tuffaceous basaltic andesite	S-15	Tuffaceous basaltic breccia
W-43	Basaltic andesite tuff breccia	S-32	Basaltic andesite tuff
W-44	Basaltic andesite breccia	S-42	Basaltic tuff
WIL-32	Basaltic andesite tuff breccia	S-67	Basaltic tuff
WIL-33	Basaltic andesite tuff breccia	S-74	Basaltic andesite tuff

Figure 4.1a, b Table of samples used in chemical analysis. Detailed petrographic descriptions of most samples are presented in Appendix A. Cpx = clinopyroxene; Plag = plagioclase.

4.3 Tectonomagmatic Discrimination Diagrams

4.3.1 Major Element Discrimination

Pearce et al. (1977) distinguish tectonic environments based on variations in MgO, FeO* and Al₂O₃ content. The behaviour of these elements is most sensitive in magmas of basaltic andesite composition. As a result, the samples were further screened for basaltic composition (SiO₂ of 51 to 56 wt %) for application to this diagram. The MgO-FeO*-Al₂O₃ ternary diagram (Fig. 4.2) suggests that the Stikinian Takla Group samples were erupted in an orogenic environment, in other words, an island or continental arc.

4.3.2 Trace Element Discrimination

The ternary plot of Pearce and Cann (1973) is based on Ti, Zr and Y content. Ti, Zr and Y abundances are generally inherited from the melt source. The Takla Group basalts plot in the field labeled B, which simultaneously represents ocean floor basalts, low K tholeiites and calc-alkali basalts, but eliminates a within plate basalt origin (Fig. 4.3).

The Hf-Th-Nb discrimination diagram for ocean floor basalts of Wood et al. (1979) indicates that the samples were erupted at a destructive plate margin (Fig. 4.4). This classification suggests a subduction-related melt derivation, which would produce magmas depleted in Nb relative to the REE and Th. A Hf/Th ratio of less than three plots the samples as calc-alkaline according to this diagram.

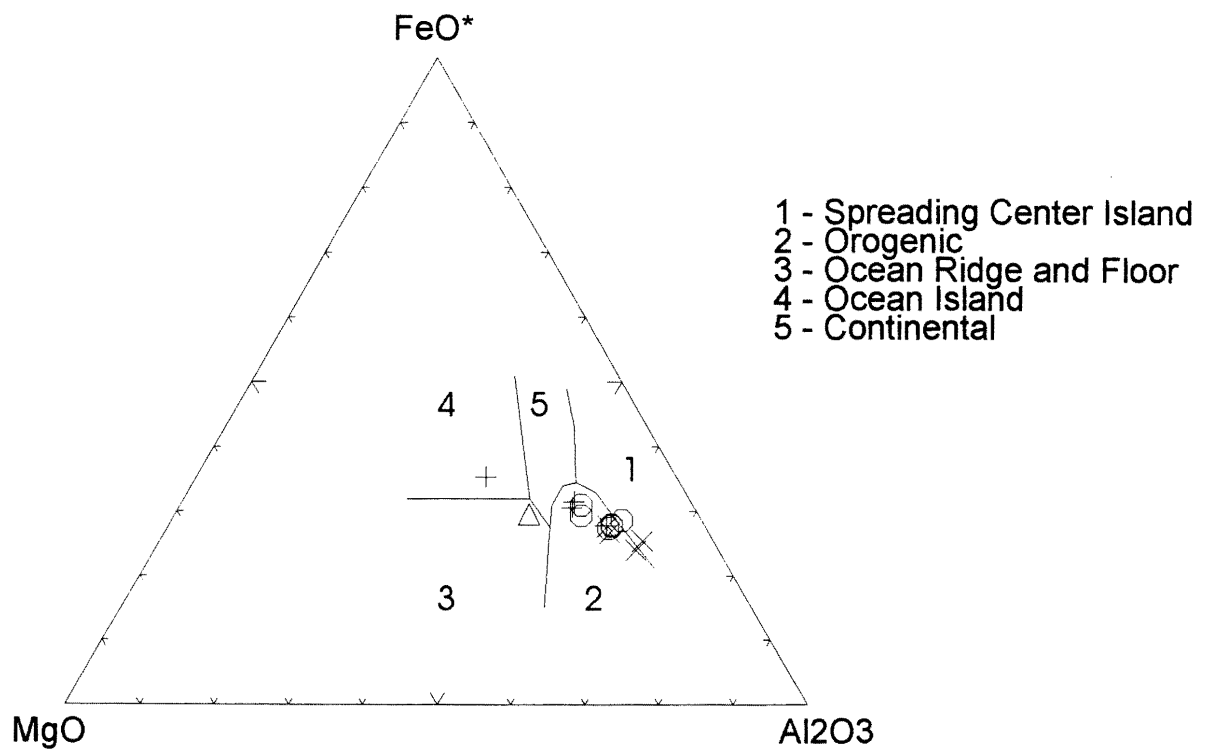


Figure 4.2 According to the major element FeO*-MgO-Al₂O₃ ternary discrimination diagram of Pearce et al. (1977), most Takla Group samples plot in the field labeled B, which suggests eruption in an orogenic setting. For this diagram, samples were screened for basaltic andesite composition (SiO₂ = 51-56 wt %). Δ = S samples; + = W samples; O = NW samples; X = WIL samples; * = CS samples.

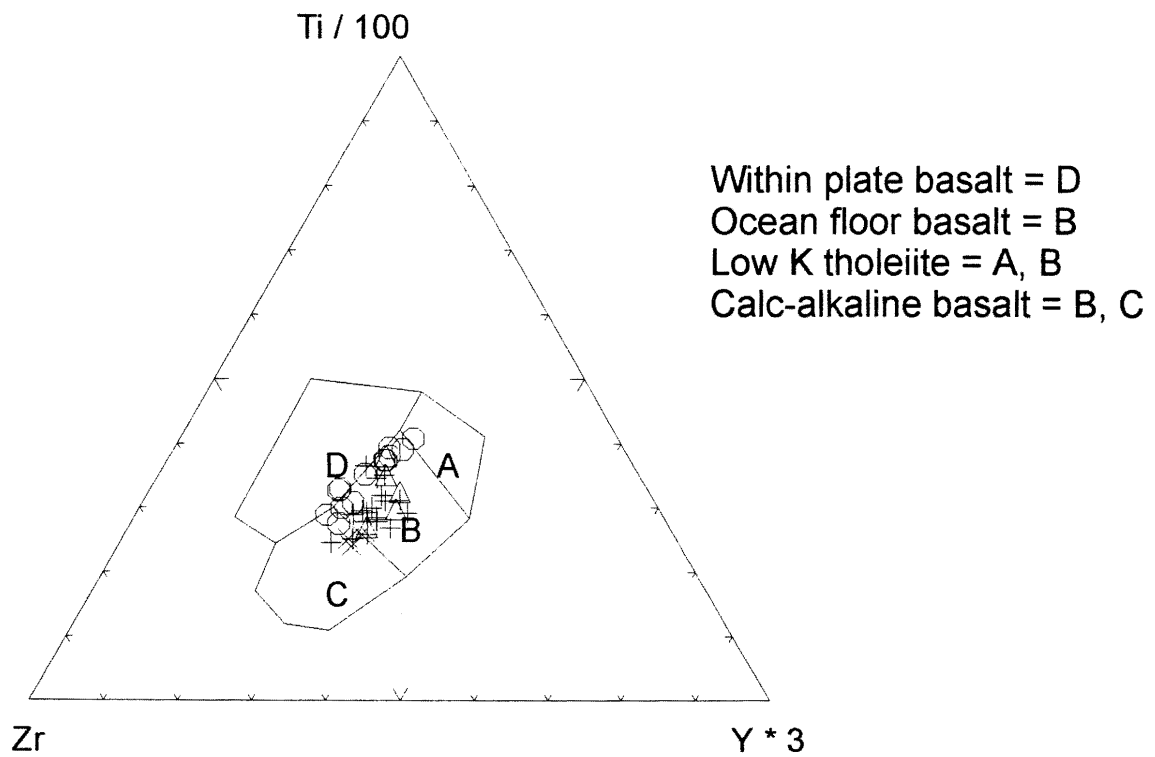


Figure 4.3 The samples cluster strongly in the field labeled B of the ternary discrimination diagram of Pearce and Cann (1973). This eliminates a within plate origin for the lavas. Symbols as per Figure 4.2.

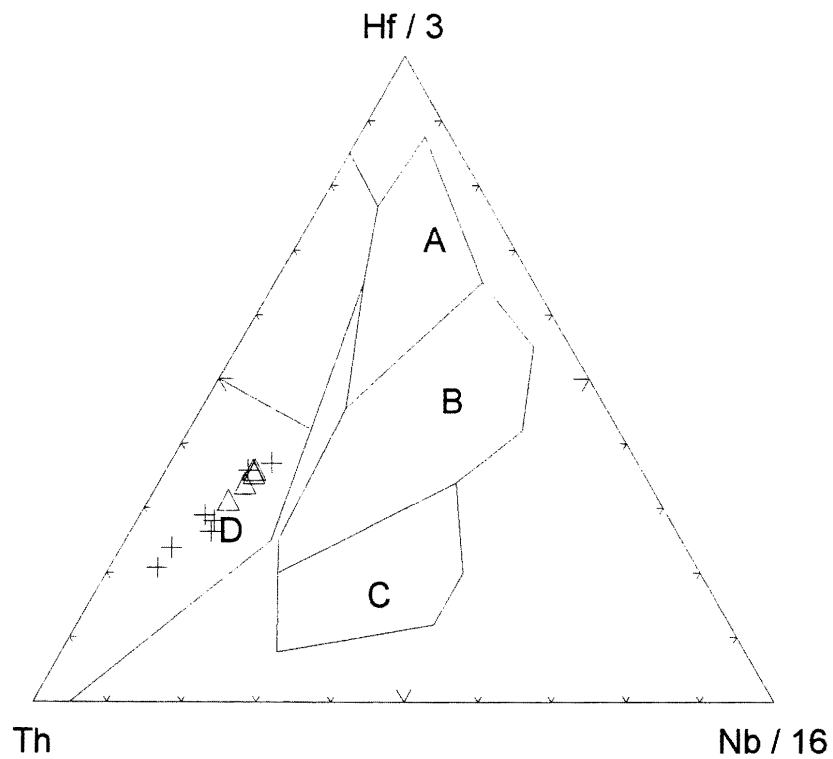


Figure 4.4 According to the Hf, Th and Nb discrimination diagram of Wood et al. (1979), the samples plot as lavas erupted at a destructive plate margin. Low Nb concentrations result from processes involved in subduction-related magmatism. This diagram suggests that the samples are calc-alkaline according to their low Hf/Th ratios. Fields are as follows: A = N-type MORB; B = E-type MORB; C = Alkaline within plate basalts and differentiates; D = Destructive plate margin basalts and differentiates.

4.4 Rare Earth Element Patterns

Rare earth elements (REE) are used in petrogenetic studies due to their incompatible and relatively immobile behaviour. The REE pattern of an igneous rock may reflect the conditions of melting, composition of the melt source, the degree of melting, and the effects of assimilation, metasomatism and differentiation (Hanson, 1980).

Generally smooth Takla Group REE patterns are slightly light REE enriched (Fig. 4.5) with REE pattern slopes that show a complete range of La/Yb ratios from 3.4 to 7.4. These are consistent with an arc-related style of magmatism. Arc basalts may show a variety of REE patterns, ranging from light REE depleted in immature island arcs to moderately light REE enriched in more mature island arcs or continental arcs (Murphy, 1988). The slightly enriched REE patterns of the samples suggest that magmatism occurred in a mature island arc or immature continental arc.

Figure 4.5 also shows the REE patterns of two typical arc-related volcanic rocks. JB-2 is an island-arc tholeiitic basalt from the O-Shima in Japan and AGV-1 is a calc-alkaline andesite from the Guano Valley, Oregon. Data for the samples are from Govindaraju (1994). The position of the Takla Group REE patterns in between those of the tholeiitic and calc-alkaline magma types again emphasizes its intermediate composition.

4.5 Spider Diagrams

Spider diagrams are plots of incompatible trace elements that, like the REE, reflect petrogenetic processes. Primitive mantle normalized spider diagrams of the samples reveal a distinct trough at Nb characteristic of subduction-derived magmas (Fig. 4.6). During the

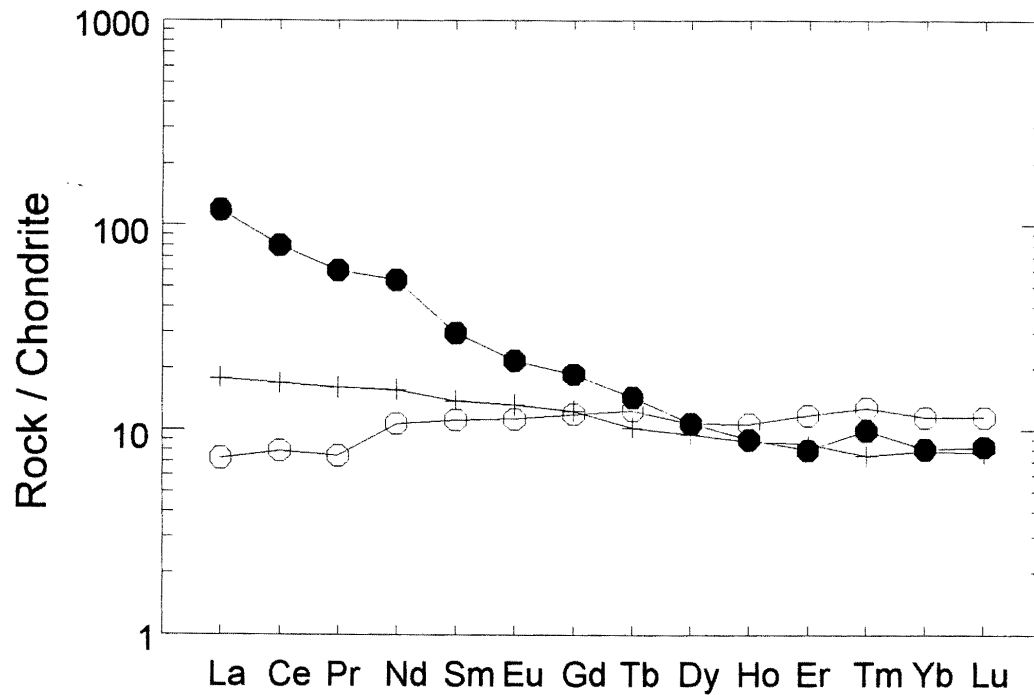


Figure 4.5 Clinopyroxene porphyritic basalt sample W-26 (+) displays a typical basalt REE pattern of the Takla Group samples. It is slightly light REE enriched, indicating that the source was not depleted in incompatible elements. Also shown are the REE patterns of samples JB-2 (O), a typical island arc tholeiite from the O-Shima volcano in Japan and AGV-1 (●), a typical calc-alkaline andesite from the Guano Valley, Oregon (data from Govindaraju, 1994). The W-26 REE pattern is intermediate between the tholeiitic and calc-alkaline samples. REE values are chondrite-normalized.

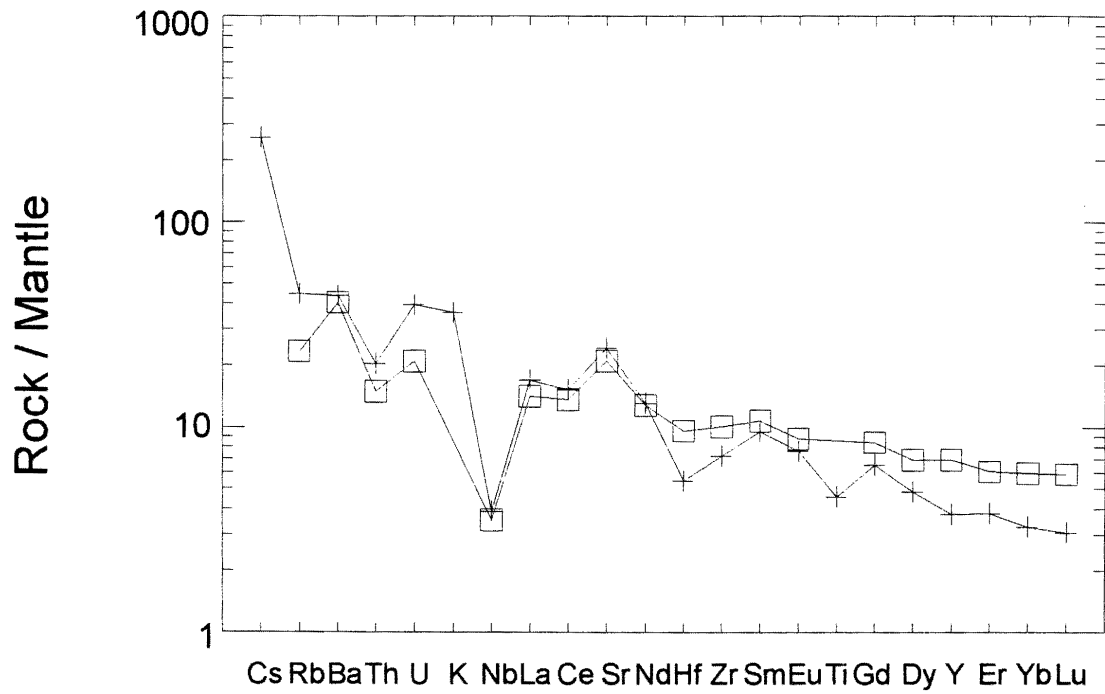


Figure 4.6 Mantle-normalized spider diagram plot of Takla Group amygdular aphanitic basalt sample W-37 (+) compared to JB-3, (□) a high-Al arc basalt from the Fuji volcano, Japan (data from Govindaraju, 1994). Both samples display pronounced Nb depletion and large ion lithophile enrichment characteristic of subduction-related magmas.

subduction of oceanic crust, dehydration reactions result in fluid release from the crust and overlying sediments. Not only do the released fluids decrease the solidus and initiate mantle melting, they also metasomatize the overlying mantle material. This process results in an enrichment of large ion lithophile elements such as Sr, K, Ba and Cs (also consistent with Takla Group samples) and a lack of enrichment of high field strength elements such as Nb and Ta. These high field strength elements are believed to be held in a mineral phase of the subducted slab that is insoluble during metasomatism. However, Ryerson and Watson (1987) suggest a number of other possibilities to account for high field strength element depletion, including depletion of the source region by a previous episode of melt extraction, zone refining and equilibration with a percolating melt.

In Figure 4.6, a Takla Group sample spider diagram pattern is compared with that of a typical high-Al basalt (JB-3) of the Fuji volcano in Japan. The samples have similar patterns (including negative Nb anomalies) and trace element abundances relative to the mantle.

4.6 Clinopyroxene Analysis

Letterier et al. (1982) constructed tectonic discrimination diagrams based on cationic abundances in clinopyroxene phenocrysts. This method is useful in the tectonic interpretation of rocks that have undergone alteration or low grade metamorphism because of the frequent preservation of clinopyroxene phenocrysts. It is based on the concept that cation abundances in clinopyroxene phenocrysts vary in proportion to the activity of those cations in the host magma. This relationship could be affected by (1) coupled substitution, (2) the timing of

clinopyroxene crystallization relative to other minerals (that may alter the composition of the melt), (3) the cooling rate of the melt, and (4) variations in temperature and pressure (which change element distribution coefficients). Despite these limitations, the clinopyroxene compositions show well defined relationships to host magma composition.

Alkali basalts are generally enriched in Ti, Ca and Al relative to sub-alkaline basalts. Figure 4.7a shows that Takla Group clinopyroxene phenocrysts are depleted in Ti, indicating that the basalts are not alkaline. Like Ti, Cr is low in orogenic basalts. Figure 4.7b shows that clinopyroxene phenocrysts are low in Cr and were therefore crystallized in an orogenic basalt as opposed to a basalt produced in a rift setting. Al contents are higher in island arc tholeiites as opposed to calc-alkaline basalts, while the reverse is true of Ti. Figure 4.7c does not show a clear distinction between tholeiitic and calc-alkaline orogenic basalts and again is consistent with an intermediate composition.

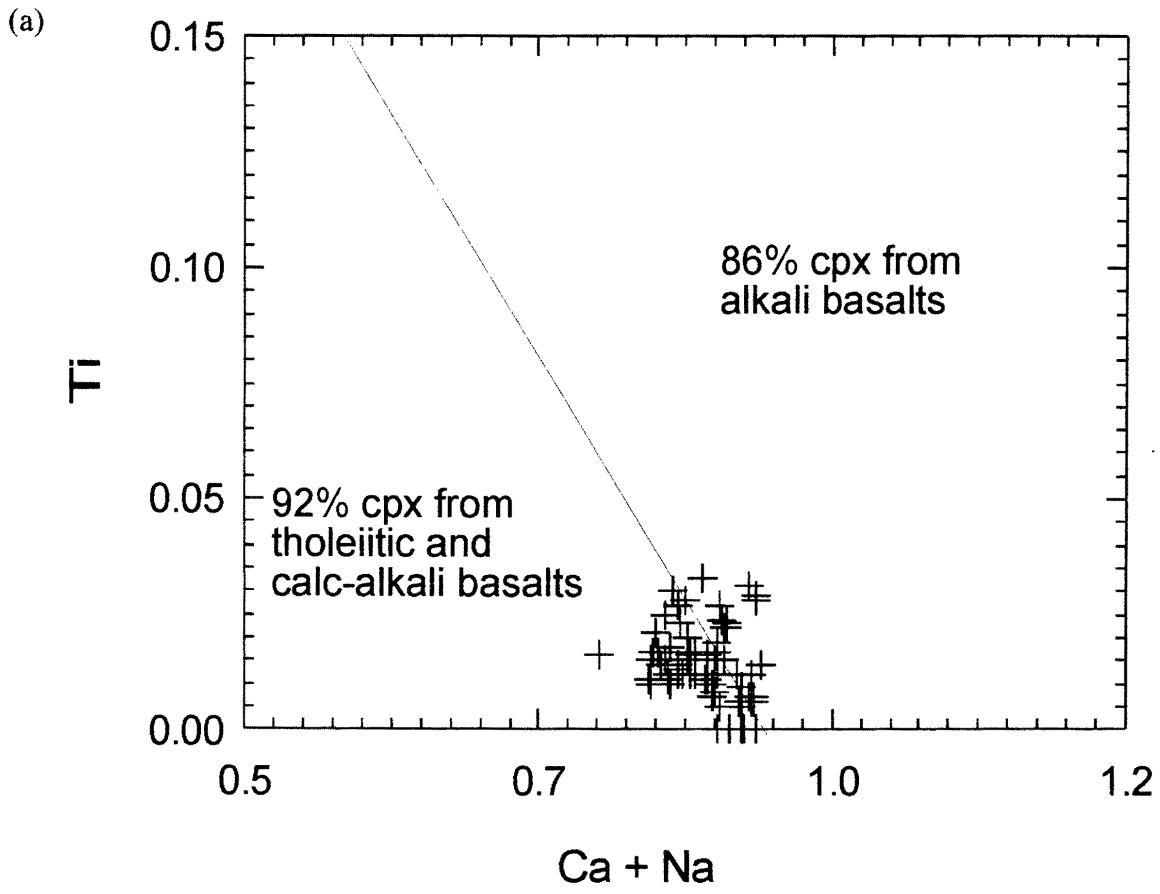
4.7 Discussion

As confirmation of the viability of the geochemical interpretation of tectonic setting, it is important to test that it concurs with the lithologic features of the Stikinian Takla Group. The basaltic to andesitic spectrum of differentiation products of the samples commonly occurs during arc volcanism. In contrast, lava produced at mid ocean ridges and oceanic islands is generally more uniform. The presence of abundant volcanoclastics is also common in present day arc settings and is less common in other environments.

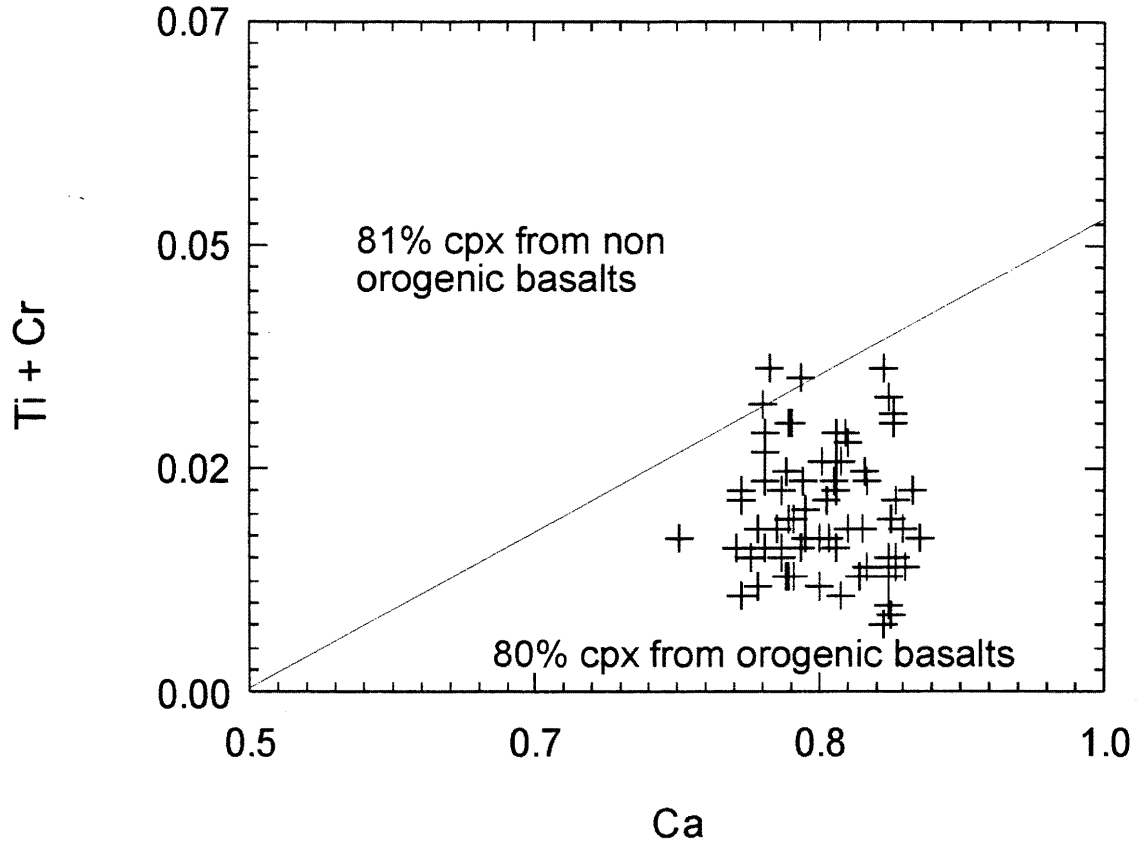
Given that magmatic processes in mature island arcs and immature continental arcs can be similar, lithologic features and field relations become important criteria in determining in

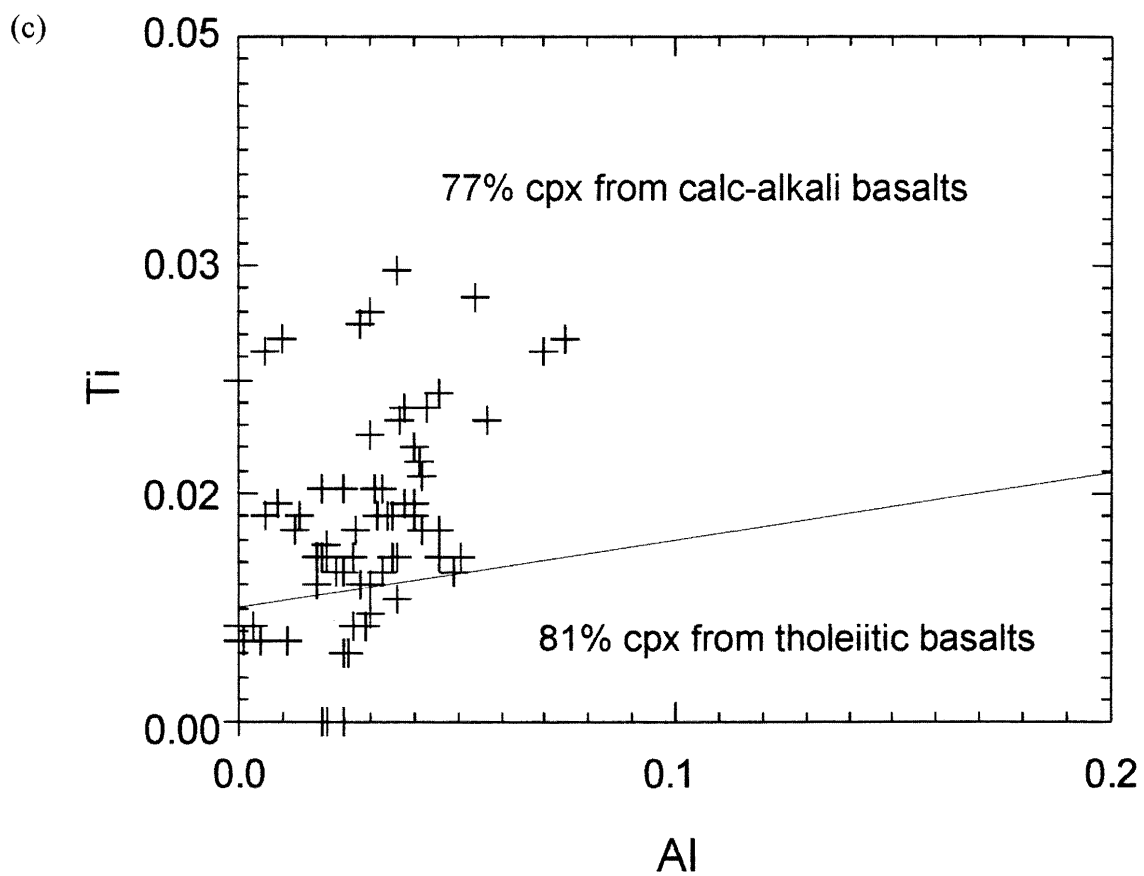
Figure 4.7 a-c Clinopyroxene tectonic discrimination diagrams of Leterrier et al. (1982).

- (a) The Ti vs. (Ca + Na) discrimination diagram indicates that the samples are not alkaline.
- (b) The (Ti + Cr) vs. Ca discrimination diagram indicates that the samples were erupted in an orogenic environment.
- (c) The Ti vs. Al discrimination diagram does not indicate whether the samples are calc-alkaline or tholeiitic, but is consistent with an intermediate compositional trend.



(b)





which environment magmatism occurred. The combination of (1) the large proportion of volcanic rocks of basaltic over andesitic composition, (2) the lack of continentally derived sediments, and (3) deposition in a shallow marine basin suggest that the lavas were erupted in a mature island arc setting. However, regional field relations show that Takla Group rocks are probably cored by a fragment of continental material (pers. com. F. Ferri, BC Mins. En. Min. Pet. Res., 1996). As an example, the presence of mature siliciclastics suggests that the Lay Range Assemblage (which underlies the Quesnellian Takla Group) was continentally influenced. These Mid-Proterozoic sedimentary rocks contain detrital zircons suggesting the existence of a nearby continental basement source, probably equivalent to the Yukon-Tanana Terrane, which is a possible fragment of the distal ancestral North American margin or of another continental land mass.

4.8 Summary

According to major and trace element tectonomagmatic discrimination diagrams, the volcanic rocks of the Stikinian Takla Group were erupted in a destructive, orogenic setting. Rare earth element patterns are typical of magmatism in the mature island arc or immature continental arc setting. Nb depletion and large ion lithophile enrichment shown in spider diagram patterns also imply magma genesis in a subduction-setting. These geochemical interpretations are consistent with the lithologic features of the volcano-sedimentary assemblage. Regional field associations suggest that the Takla Group was erupted in proximity to a continental land mass. This is in agreement with the transitional composition of the

samples between tholeiitic and calc-alkaline, reflective of a continentally influenced source region (Sect. 3.5.2).

CHAPTER 5: TECTONIC IMPLICATIONS

5.1 Introduction

The previously interpreted tectonic history of the McConnell Creek Map area is modified by the determination that the Stikinian Takla Group lavas were extruded in an arc setting. Formerly, the outcrop belts of the Takla Group to the east and west of the Pinchi fault were mapped as a single assemblage (Monger, 1977). In 1989, the Takla Group of Quesnellia was determined to be a product of mature island arc volcanism (Minehan, 1989). In the same study, the Takla Group of Stikinia was interpreted as a product of oceanic island volcanism (Minehan, 1989). However, Minehan's assessment of the Stikinian Takla Group paleotectonic setting was based on limited major element data from Monger (1977). Using a data set that includes trace elements, this thesis has determined that, as in the case of the Quesnellian Takla Group, the Stikinian Takla Group was erupted in an arc setting. Having determined that the two groups were produced in the same tectonic setting, it is reasonable to test for further common relations. This chapter begins with a broad lithologic comparison of the two groups and continues with a closer examination of the geochemical resemblances between them. Descriptions of the Quesnellian and Stikinian Takla Groups are taken from Minehan (1989) and Monger (1977), respectively.

5.2 General Comparison

5.2.1 Lithology

Effusive rocks of the Quesnellian Takla Group (QTG) range in composition from basaltic to dacitic while Stikinian Takla Group (STG) effusive rocks are limited to basaltic to andesitic compositions. Common phenocryst phases in the QTG consist of clinopyroxene ($\text{En}_{46}\text{Fs}_9\text{Wo}_{45}$) and plagioclase (An_{40}). Amphibole is also common, but only occurs in more evolved samples. In the STG, clinopyroxene ($\text{En}_{45}\text{Fs}_{12}\text{Wo}_{43}$) and plagioclase (An_{35}) also form the predominant phenocryst phases. Uncommon olivine (Fo_{80}) phenocrysts occur in the STG but are absent in the QTG. Effusive rocks of both groups possess porphyritic, glomeroporphyritic, seriate and pilotaxitic mineral textures.

Pyroclastic rocks in each group range in size from crystal tuffs to coarse breccias. Clasts of the QTG are composed of plagioclase-clinopyroxene porphyritic basalt to andesite and plagioclase porphyritic basalt to andesite, as in the case of the STG pyroclastic samples, but also include amphibole-plagioclase porphyritic clasts.

Sedimentary units in the QTG consist mainly of black siltstones that display dewatering structures, large- and small-scale ripple marks, cross-bedding and slump structures. Argillite, siltstone and volcanogenic sandstones compose the sedimentary units of the STG. Lamination, gradation, rip-up clasts and small-scale cross-beds are common features of the STG sedimentary rocks.

5.2.2 Stratigraphy and Contacts

Due to metamorphism and deformation, stratigraphic units cannot be distinguished within the QTG. In consequence, stratigraphic correlation between the two groups is not possible. However, the presence of Halobia in both groups dates them to the Upper Carnian to Lower Norian periods and indicates that they are time equivalent.

The Takla Groups are underlain by different assemblages. The STG overlies the Asitka Group, both disconformably and in fault contact, as well as the Cache Creek Group, also in fault contact. The exposed underlying unit in fault contact with the QTG is the Lay Range assemblage. Both groups are unconformably overlain by the Hazelton Formation.

The groups are separated by a branch of the Pinchi Fault (Fig. 1.4), which represents the collisional boundary of the Stikine and Quesnel terranes and has been in existence since the Middle Jurassic. Renewed strike-slip activity along the Pinchi Fault occurred during the Tertiary. Estimates of lateral displacement, based on the age of the youngest rocks involved in faulting, are in the order of 200 km (Gabrielse, 1992).

5.2.3 Post-Magmatic Processes

Faulting is the dominant style of deformation in both Takla Groups. An exception is the Dewar Formation of the STG which is characterized by dramatic folding due probably to its relative incompetence. The STG is metamorphosed to prehnite-pumpellyite and zeolite grades, whereas the QTG contains leucoxene and actinolite, indicating that it experienced lower greenschist grade metamorphic conditions. The QTG was heavily intruded by mafic,

intermediate and felsic sills as well as by one tonalite and several gabbroic intrusions. The STG has been intruded to a lesser degree, but still contains mafic sills and dikes.

5.3 Geochemical Comparison

Because the range of differentiation products from each group is different, geochemical comparison is limited to samples of basaltic to basaltic andesite composition with a SiO_2 range of 48 to 56 wt % . XRF data for the QTG are taken from Minehan (1989) and are presented in Appendix D. Trace element analyses are limited to Sr, K, Rb, Ba, Nb, Zr, Ti and Y. REE data for the QTG are unavailable.

5.3.1 Major and Trace Element Composition

The Zr/TiO_2 vs. Nb/Y plot of Winchester and Floyd (1977) shows that the two groups are similar in alkalinity (Fig. 5.1). This contrasts with the estimate of alkalinity obtained from the $(\text{Na}_2\text{O} + \text{K}_2\text{O})$ vs. SiO_2 diagram of Irvine and Baragar (1971) (Fig. 5.2). The discrepancy is most likely due to a relative enrichment of the very mobile alkali elements in the STG during alteration. The FeO^*/MgO vs. SiO_2 plot of Miyashiro (1974) shows that basaltic samples from both groups concentrate in the tholeiite field (Fig. 5.3).

The Ti-Y-Zr tectonic discrimination diagram of Pearce and Cann (1973) shows close overlap of the two sample groups in the field labeled B, which is consistent with an arc-related setting (Fig. 5.4). For magmas in which crystal fractionation has not been extensive, the relative abundance of these trace elements is largely a reflection of source composition.

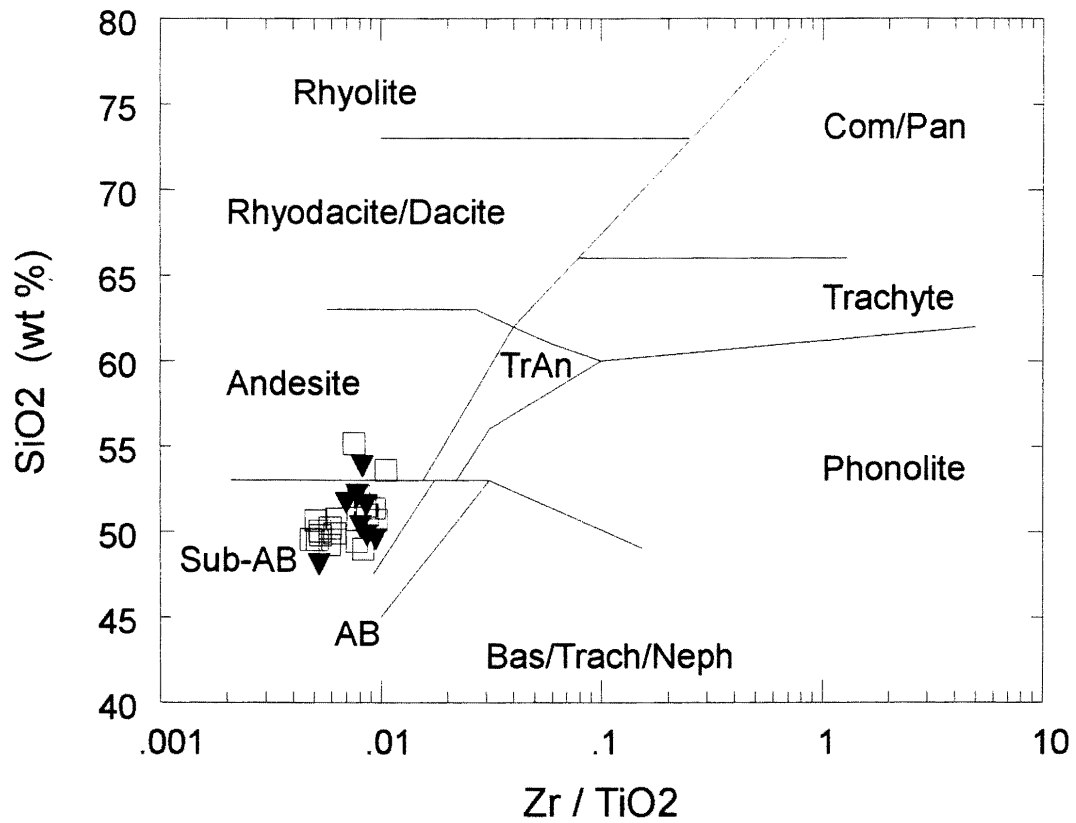


Figure 5.1 According to the discrimination diagram of Winchester and Floyd (1977), the STG (squares) and QTG (triangles) samples are similar in degree of alkalinity. For the purpose of comparison, samples were screened for SiO₂ content between 48 and 56 wt %.

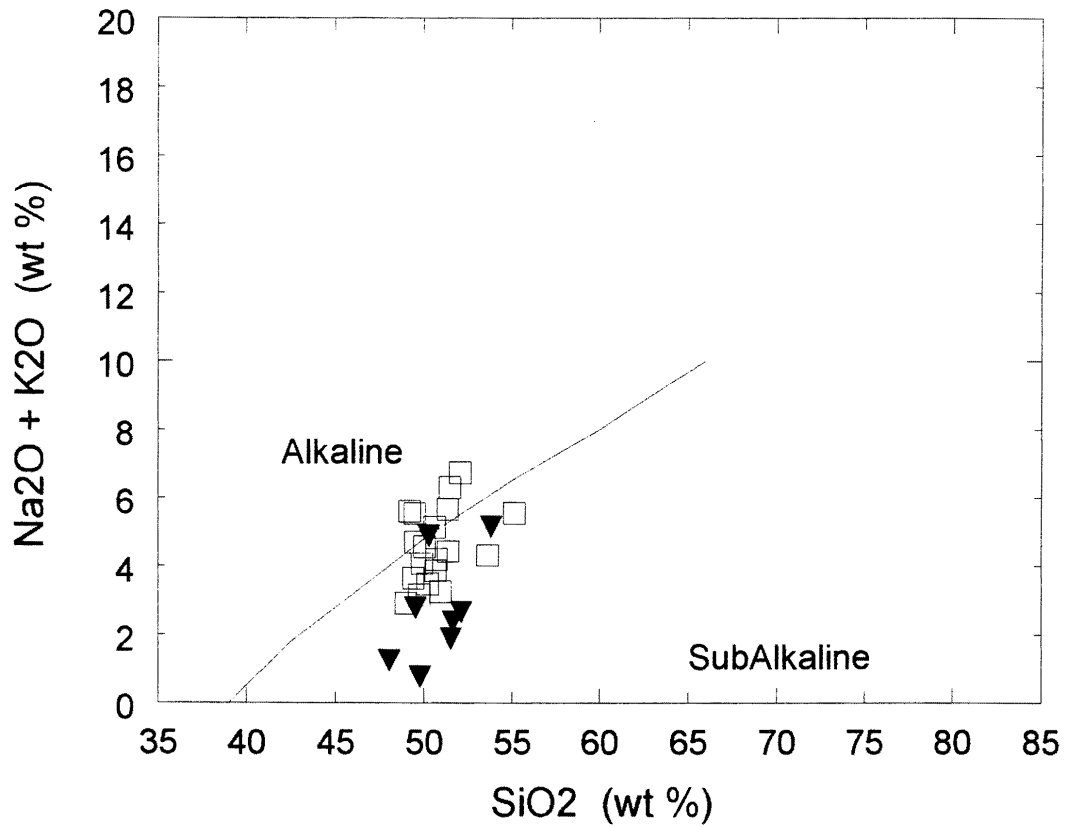


Figure 5.2 In contrast to the degree of alkalinity determined by the SiO_2 vs. Zr/TiO_2 discrimination diagram of Winchester and Floyd (1977), the $(\text{Na}_2\text{O} + \text{K}_2\text{O})$ vs. SiO_2 discrimination diagram of Irvine and Baragar (1971) indicates that the STG samples (squares) are generally higher in abundance of alkali elements than the QTG samples (triangles). This is most likely an effect of alkali element addition to the STG samples during alteration.

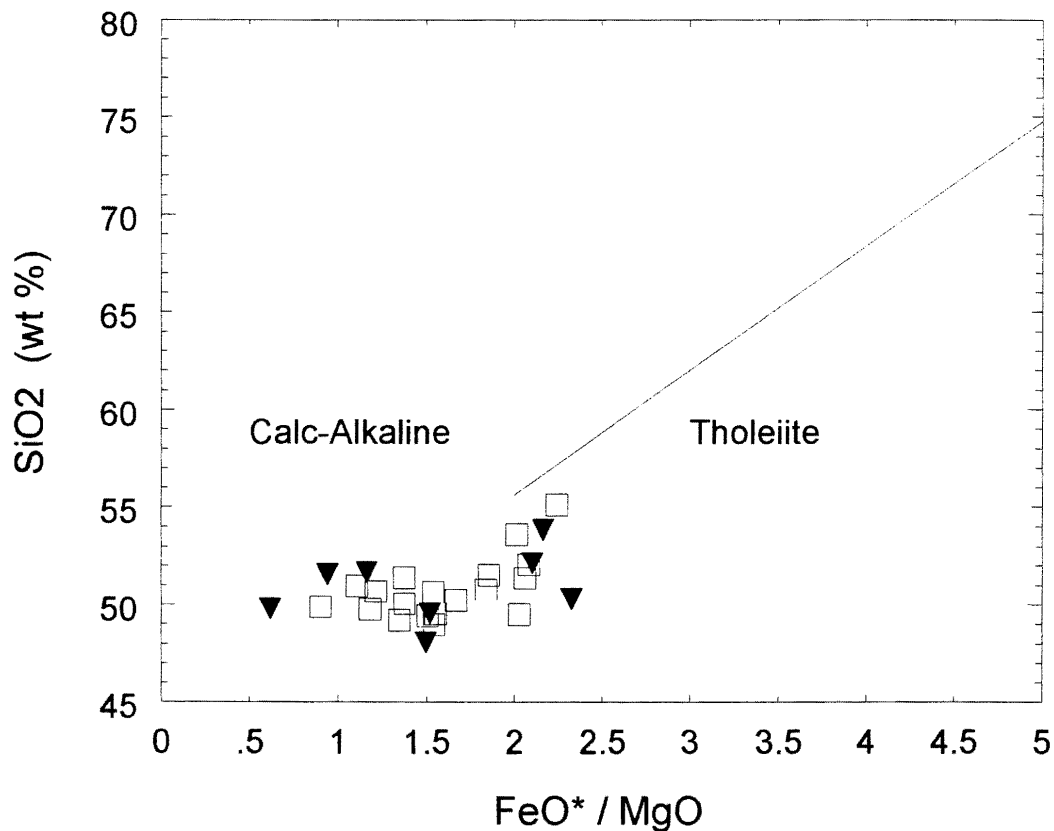


Figure 5.3 This plot of SiO₂ abundance with respect to differentiation suggests that the basalts to basaltic andesites of the STG (squares) and QTG (triangles) share a weak tholeiitic trend of slow SiO₂ enrichment with differentiation.

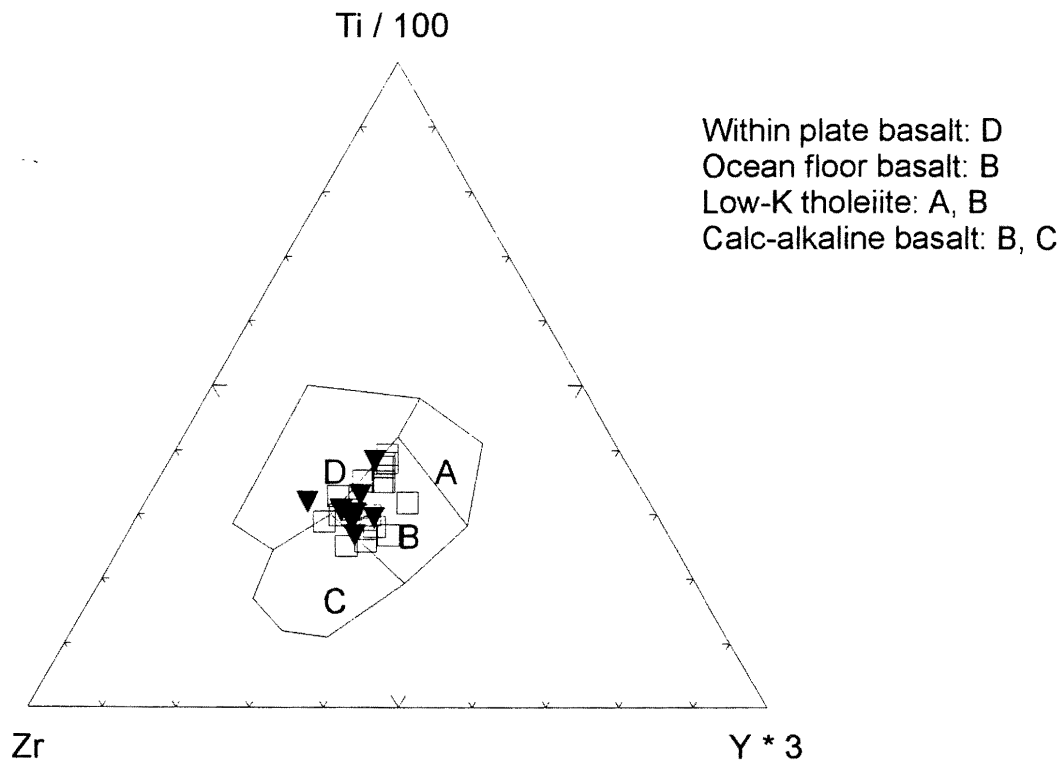


Figure 5.4 This ternary discrimination diagram of Pearce and Cann (1973) shows that the STG (squares) and QTG (triangles) samples are similar in terms of relative abundances of Ti, Zr and Y. According to this diagram, they plot in the field labeled B, which is consistent with arc magmatism.

5.3.2 Spider Diagrams

QTG and STQ trace element data are compared using a spider diagram in Figure 5.5.

There is a significant variation in large ion lithophile element abundance between the two groups, again reflecting enrichment of these elements in the STG during alteration.

Abundances of the more immobile trace elements of the two groups (Nb, Zr, Ti and Y) relative to mantle compositions are very similar, indicating potential similarity in the degree of partial melting and melt evolution of the two groups. The similar immobile trace element patterns of the two groups reflect compositional similarities inherited from the melt source.

5.4 Discussion

Although the Takla groups are remarkably similar in terms of lithology and age, they have been subject to different post-magmatic histories. The QTG has been more highly metamorphosed and intruded, while the STG appears more strongly altered. These factors, combined with the presence of different underlying units and separation of the groups by a major terrane boundary fault (which presupposes their location in two different terranes) precludes the possibility of a comagmatic relationship between them. However, this conclusion is contradicted by resemblances in trace element geochemistry that imply similar degrees of partial melting, melt evolution and source composition. This contradiction is most usefully examined with the current interpretations of Stikine and Quesnel terrane history in mind.

Stikinia and Quesnellia are two allochthonous, predominantly arc-related terranes separated by the mainly oceanic Cache Creek Terrane, which hosts an exotic Tethyan fauna (Fig. 5.6). In the McConnell Creek area, the Cache Creek Terrane is absent. Several models

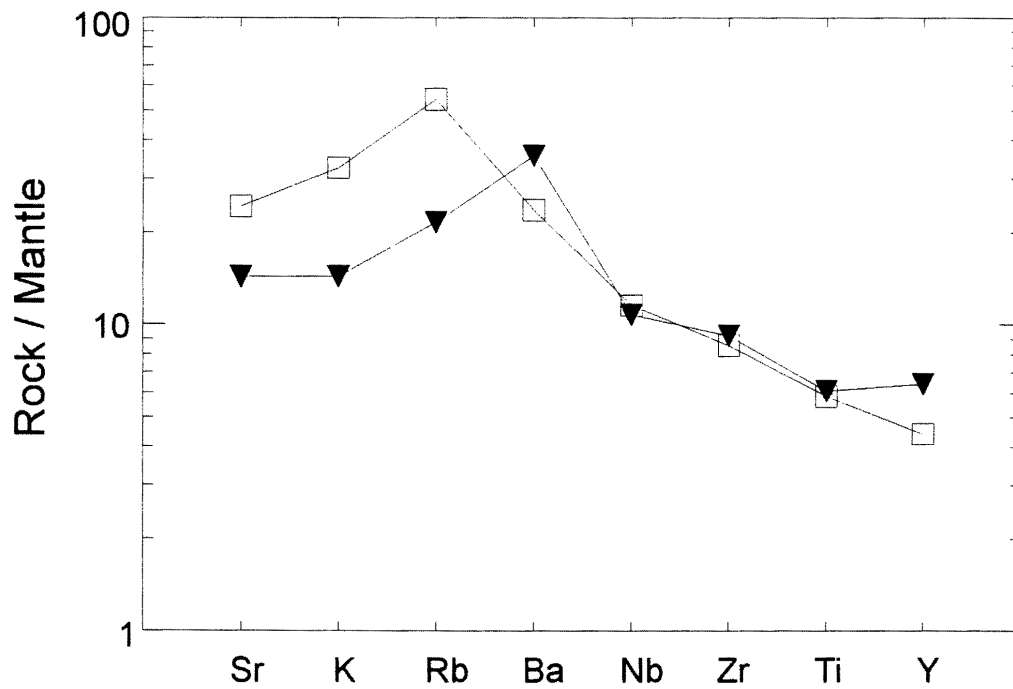


Figure 5.5 Mantle-normalized spider diagram of available trace elements. Abundances of large ion lithophile elements (Sr, K, Rb, Ba) of the STG sample (NW-77, squares) and QTG (KM-23, triangles) sample are dissimilar. However, the samples are generally similar in the more immobile trace elements Nb, Zr, Ti and Y in terms of abundance relative to mantle composition and pattern.

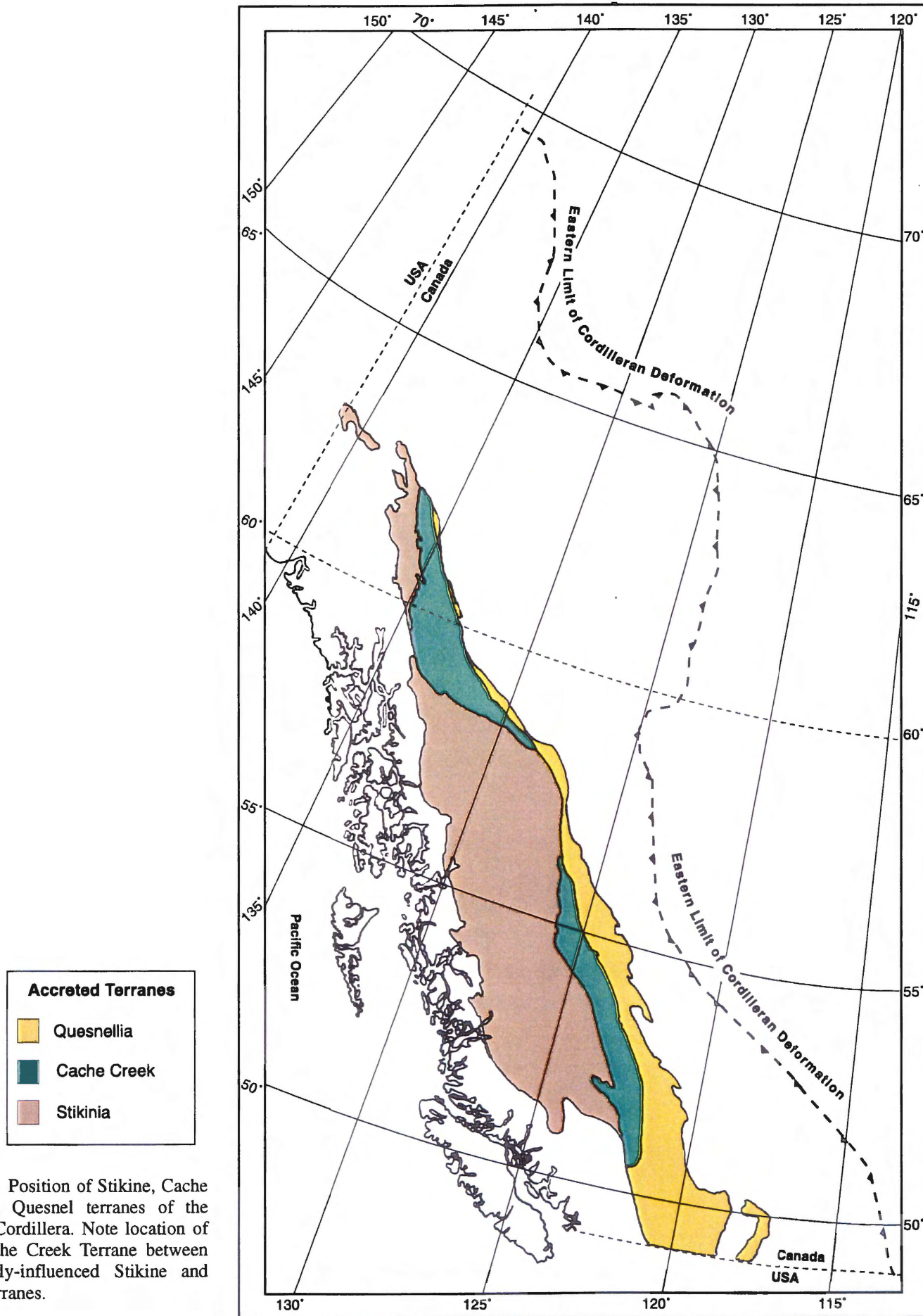


Figure 5.6 Position of Stikine, Cache Creek and Quesnel terranes of the Canadian Cordillera. Note location of exotic Cache Creek Terrane between continentally-influenced Stikine and Quesnel terranes.

exist to explain the amalgamation of the three terranes, among which is the currently accepted “oroclinal entrapment” model of Mihalynuk et al. (1994) (Fig. 5.7). This model is the most comprehensive to date, accounting for paleomagnetic rotation, paleobiogeography and time constraints. According to this model, Stikinia and Quesnellia were positioned as two adjacent arc systems, joined through their northern ends at an angle of 120° , during the Early Mesozoic. At this time they faced south toward the Cache Creek ocean. Late Triassic to Middle Jurassic counterclockwise rotation of Stikinia occurred in response to seafloor spreading behind the Stikine arc. This rotation caused the entrapment of Cache Creek oceanic crust and resulted in the collision of Stikinia with Quesnellia in the Middle Jurassic.

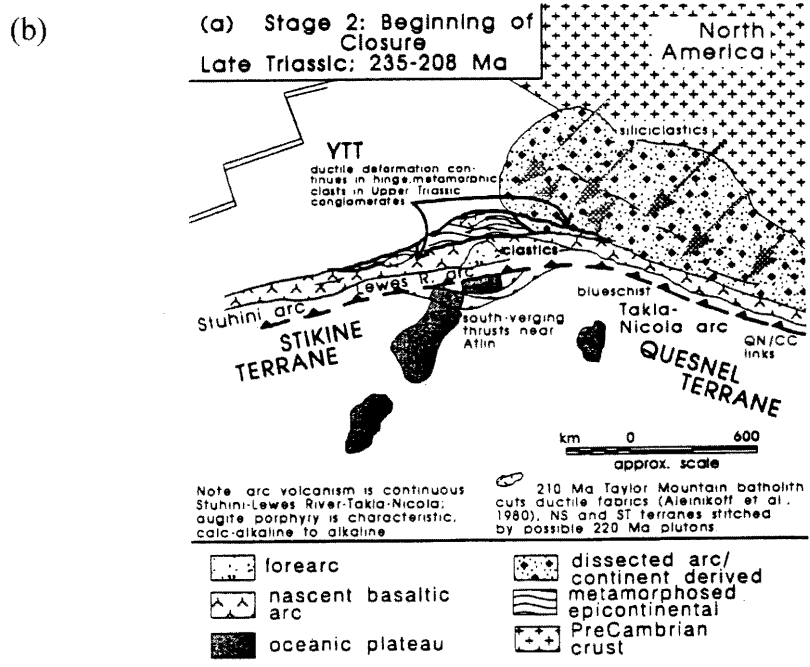
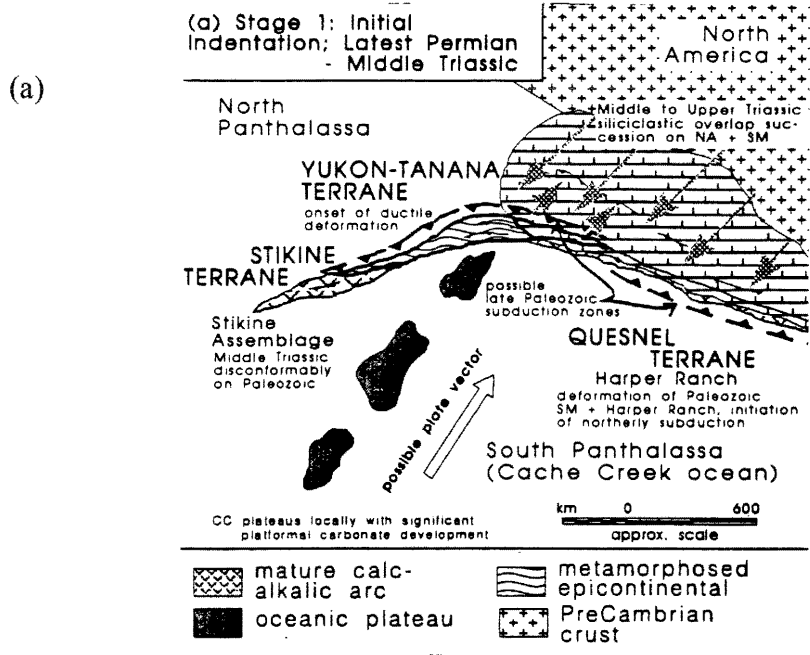
Temporal and lithologic similarity in the Early Mesozoic igneous rocks of Stikinia and Quesnellia has been noted in many regional studies of the North American Cordillera (Lang et al., 1995; Mihalynuk et al., 1994; Wernicke and Klepacki, 1988; Mortimer, 1986). In a gross sense, Mihalynuk et al. (1994) attribute this to the formation of two symmetrical subduction zones (beneath Stikinia and Quesnellia) that result from the consumption of Cache Creek oceanic crust during rotational closure of the Stikine and Quesnel arcs. Such a two-fold symmetry about Cache Creek would result in the occurrence of similar contemporaneous magmatic processes in each arc.

5.5 Summary

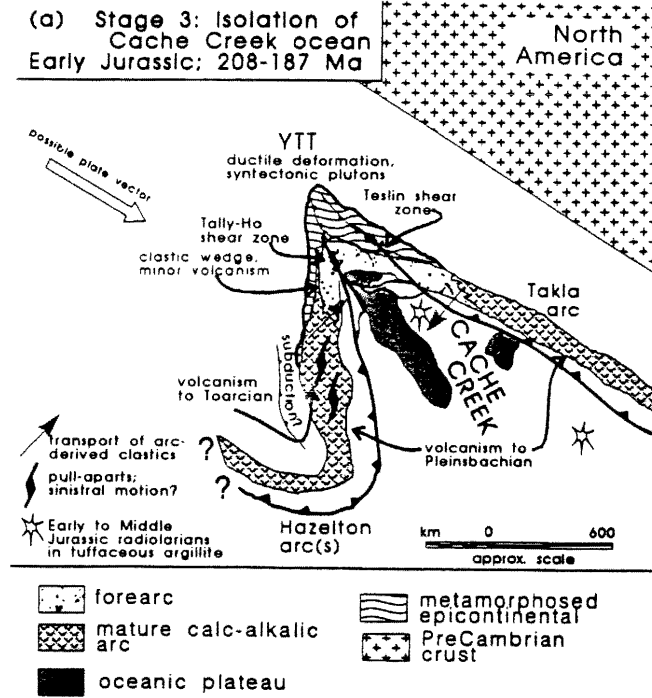
Comparison of the Stikinian and Quesnellian Takla groups reveals strong lithologic and temporal similarity. Furthermore, relatively immobile trace element patterns and abundances suggest similar source composition, degree of partial melting and melt evolution. Despite these

Figure 5.7 a-d Stages of Cache Creek terrane oroclinal entrapment according to Mihalyuk et al. (1994)

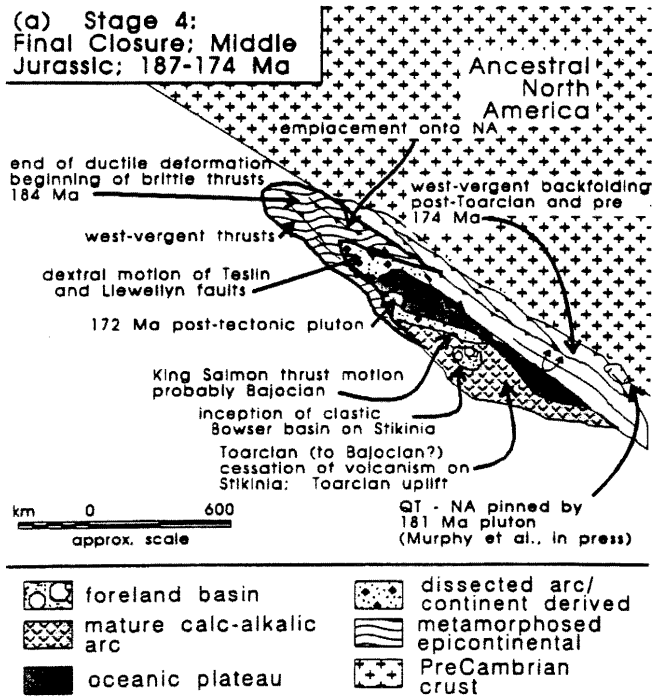
- (a) Latest Permian to Middle Triassic arrangement of tectonic elements predicted by the model.
- (b) Late Triassic configuration of tectonic elements predicted by the model.
- (c) Early Jurassic configuration of tectonic elements predicted by the model.
- (d) Middle Jurassic configuration of tectonic elements predicted by the model.



(c)



(d)



similarities, the groups have dissimilar post-magmatic histories, as well as underlying units and are located in two different terranes, implying that they are not genetically related. Rather, their similarity emphasizes the concept that Mesozoic magmatic processes in the Stikine and Quesnel arcs were remarkably alike.

CHAPTER 6: CONCLUSIONS

6.1 Results

In the case of the Stikinian Takla Group of the McConnell Creek area, major element mobility during alteration and metamorphism was sufficiently large to necessitate the use of relatively immobile trace elements to determine magma type and paleotectonic setting. Trace element analysis of these basaltic to andesitic effusive and pyroclastic rocks reveals that they are subalkaline and are intermediate between tholeiitic and calc-alkaline compositions. Such an intermediate composition is confirmed by REE patterns showing slight light REE enrichment. Tectonomagmatic discrimination diagrams consistently indicate that the Stikinian Takla Group lavas were erupted in an arc setting. Chemically, this interpretation is supported by spider diagram trace element patterns displaying pronounced Nb depletion and large ion lithophile enrichment. This interpretation is also supported by lithologic features of the assemblage, including an abundance of pyroclastic rocks and a compositional transition from basaltic to andesitic. The Stikinian Takla Group REE patterns further suggest that the eruption occurred in either a mature island arc or immature continental arc. On a regional scale, field relations indicate that Takla Group volcanics are cored by a fragment of continental crust, which suggest that magmatism occurred in proximity to the continental margin.

Comparison of the Stikinian and Quesnellian outcrop belts of the Takla Groups reveals strong lithologic and geochemical resemblances. Similarities in relatively immobile, incompatible trace element patterns and abundances suggests similar source compositions, degrees of partial melting and melt evolution for the two groups. However, local field relations

preclude a genetic association. As a result, the geochemical similarity of the two groups serves to emphasize larger-scale similarities between the Quesnel and Stikine terranes.

6.2 Recommendations

Chemical comparison of the Takla Group outcrop belts in the McConnell Creek area would be enhanced by a more complete trace element data set for the Quesnellian Takla Group. Furthermore, Nd and Pb isotopic analysis would serve to compare Takla Group magma source regions more rigorously. On a regional scale, further detailed geochemical comparison of lithologically similar Stikine and Quesnel Mesozoic igneous rocks should be performed to increase our understanding of the relationship between these two terranes.

References

- Barker, D.S. 1978. Igneous Rocks. Prentice-Hall, USA, pp. 86-123.
- Barton, M., Varekamp, J.C., Van Bergen, M.J. 1982. Complex zoning of clinopyroxenes in the lavas of Vulcini, Latium, Italy: evidence for magma mixing. *Journal of Volcanology and Geothermal Research*, **14**: 361-388.
- Church, B.N. 1973. Geology of the Sustut area. *In* Geology, Exploration and Mining in British Columbia, B.C. Department of Mines and Petroleum Resources, pp. 411-455.
- Church, B.N. 1974. Geology of the Sustut area; *in* Geology, Exploration and Mining in British Columbia, B.C. Department of Mines and Petroleum Resources, pp. 305-310.
- Deer, W.A., Howie, R.A., Zussman, J. 1985. An introduction to the rock-forming minerals. Longman Group Limited, Hong Kong, pp. 99-139.
- Dobosi, G. 1989. Clinopyroxene zoning patterns in the young alkali basalts of Hungary and their petrogenetic significance. *Contributions to Mineralogy and Petrology*, **101**: 112-121.
- Dostal, J. and Strong, D.F. 1983. Trace-element mobility during low-grade metamorphism and silicification of basaltic rocks from Saint John, New Brunswick. *Canadian Journal of Earth Sciences*, **20**: 431-435.
- Downes, M.J. 1974. Sector and oscillatory zoning in calcic augites from M.Etna, Sicily. *Contributions to Mineralogy and Petrology*, **47**:187-196.
- Duda, A. and Schmincke, H. 1985. Polybaric differentiation of alkali basaltic magmas: evidence from green-core clinopyroxenes (Eifel, FRG). *Contributions to Mineralogy and Petrology*, **91**: 340-353.
- Easton, R.M. and Johns, G.W. 1986. Volcanology and mineral exploration: the application of physical volcanology and facies studies. *In* Volcanology and Mineral Deposits. Edited by J. Wood and H. Wallace. Ontario Geological Survey Miscellaneous Paper 129, pp. 2-40.
- Gabrielse, H. 1992. Intermontane Belt. In Chapter 17, Part C of Geology of the Cordilleran Orogen in Canada. *Edited by* H. Gabrielse and C.J. Yorath. Geological Survey of Canada, Geology of Canada, no. 4, pp. 591-603.
- Gabrielse, H., Monger, J.W.H., Wheeler, J.O. and Yorath, C.J. 1992. Morphogeological belts, tectonic assemblages and terranes. *In* Chapter 2, Part A of Geology of the Cordilleran Orogen in Canada. *Edited by* H. Gabrielse and C.J. Yorath. Geological Survey of Canada, Geology of Canada, no. 4, pp.15-28.

- Govindaraju, K. 1994. Compilation of working values and sample description for 383 Geostandards. *Geostandards Newsletter*, **18**: 1-158.
- Hajash, A. Jr. 1984. Rare earth element abundances and distribution patterns in hydrothermally altered basalts: experimental results. *Contributions to Mineralogy and Petrology*, **85**: 409-412.
- Hanson, G.N. 1980. Rare earth elements in petrogenetic studies. *Annual Review Earth and Planetary Sciences*, **8**: 371-406.
- Hellman, P. L., Smith, R.E. and Henderson, P. 1979. The mobility of the rare earth elements: evidence and implications from selected terranes affected by burial metamorphism. *Contributions to Mineralogy and Petrology*, **71**: 23-44.
- Irvine, T.N. and Baragar, W.R.A. 1971. A guide to the chemical classification of the common volcanic rocks. *Canadian Journal of Earth Sciences*, **8**: 523-548.
- Jakeš, P. and Gill, J. 1970. Rare earth elements and the island arc tholeiitic series. *Earth and Planetary Science Letters*, **9**: 17-28.
- Jarvis, I. and Jarvis, K.E. 1992. Plasma spectrometry in the earth sciences: techniques, applications and future trends. *Chemical Geology*, **95**: 1-33.
- Lang, J.R., Lueck, B., Mortensen J.K., Russel, J.K., Stanley, C.R. and Thompson, J.F.H. 1995. Triassic-Jurassic silica-undersaturated and silica-saturated alkalic intrusions in the Cordillera of British Columbia: Implications for arc magmatism. *Geology*, **23**: 451-454.
- Letterier, J., Maury, R.C., Thonon, P., Girard, D. and Marchal, M. 1982. Clinopyroxene composition as a method of identification of the magmatic affinities of paleo-volcanic series. *Earth and Planetary Science Letters*, **59**: 139-154.
- Lord, C.S. 1948. McConnel Creek Map-area, Cassiar District, British Columbia. Geological Survey of Canada, Memoir 251, 72 p.
- Manson, V. 1967. Geochemistry of basaltic rocks: major elements. *In Basalts, the Poldervaart treatise on rocks of basaltic composition v. I. Edited by H.H. Hess and A. Poldervaart.* Interscience Publishers, New York, pp. 215-269.
- McBirney, A.R. 1984. *Igneous Petrology*. Jones and Bartlett, Boston, pp. 220-263.
- Mihalynuk, M.G., Nelson, J. and Diakow, L.J. 1994. Cache Creek terrane entrapment: Oroclinal paradox within the Canadian Cordillera. *Tectonics*, **13**: 575-595.
- Minehan, K. 1989. Paleotectonic Setting of Takla Group Volcano-Sedimentary Rocks Quesnellia, North Central British Columbia. Masters Thesis, McGill University, Montreal, Quebec.

- Miyashiro, A. 1974. Volcanic rock series in island arcs and active continental margins. *American Journal of Science*, **274**: 321-355.
- Monger, J.W.H. 1977. The Triassic Takla Group in McConnel Creek map area, north-central British Columbia. Geological Survey of Canada, Paper 76-29, pp. 1-45.
- Monger, J.W.H. 1989. Overview of Cordilleran Geology. *In* Western Canada Sedimentary Basin. *Edited by* B.D. Ricketts. Canadian Society of Petroleum Geologists, pp. 9-32.
- Monger, J.W.H., Price, R.A. and Templeman-Kluit, D.J. 1982. Tectonic accretion and the origin of the two major metamorphic and plutonic belts in the Canadian Cordillera. *Geology*, **10**: 70-75.
- Monger, J.W.H. and Church, B.N. 1976. Revised stratigraphy of the Takla Group, north-central British Columbia. *Canadian Journal of Earth Sciences*, **14**: 318-326.
- Mortimer, N. 1986. Late Triassic, arc-related, potassic igneous rocks in the North American Cordillera. *Geology*, **14**: 1035-1038.
- Murphy, J.B. 1988. Late Precambrian to Late Devonian mafic magmatism in the Antigonish Highlands of Nova Scotia: multistage melting of a hydrated mantle. *Canadian Journal of Earth Sciences*, **25**: 473-485.
- Nyström, J.O. 1984. Rare earth element mobility in vesicular lava during low-grade metamorphism. *Contributions to Mineralogy and Petrology*, **88**: 328-331.
- Pearce, J.A. and Cann, J.R. 1973. Tectonic setting of basic volcanic rocks determined using trace element analyses. *Earth and Planetary Science Letters*, **19**: 290-300.
- Pearce, J.A. and Norry, M.J. 1979. Petrogenetic implications of Ti, Zr, Y and Nb Variations in volcanic rocks. *Contributions to Mineralogy and Petrology*, **69**: 33-47.
- Pearce, T.H., Gorman, B.E. and Birkett, T.C. 1977. The relationship between major element chemistry and tectonic environment of basic and intermediate volcanic rocks. *Earth and Planetary Science Letters*, **36**: 121-132.
- Philpotts, A.R. 1990. *Principles of Igneous and Metamorphic Petrology*. Prentice Hall, USA, pp. 275-315.
- Ragland, P.C. 1989. *Basic Analytical Petrology*. Oxford University Press, New York, pp. 44-66.
- Ryerson, F.J. and Watson, E.B. 1987. Rutile saturation in magmas: implications for Ti-Nb-Ta depletion in island-arc basalts. *Earth and Planetary Science Letters*, **86**: 225-239.

- Smith, R.E. and Smith, S.E. 1976. Comments on the use of Ti, Zr, Y, Sr, K, P and Nb in classification of basaltic magmas. *Earth and Planetary Science Letters*, **32**: 114-120.
- Vance J.A. 1969. On Synneusis. *Contributions to Mineralogy and Petrology*, **24**: 7-29.
- Wang, P. and Glover, L.III. 1992. A tectonics test of the most commonly used geochemical discriminant diagrams and patterns. *Earth-Science Reviews*, **33**: 111-131.
- Wernicke, B. and Klepacki, D.W. 1988. Escape hypothesis for the Stikine block. *Geology*, **16**: 461-464.
- White, R.S., McKenzie, D. and O'Nions, R.K. 1992. Oceanic crustal thickness from seismic measurements and REE inversions. *Journal of Geophysical Research*, **97**: 19,683-19,715.
- Williams, H., Turner, F.J. and Gilbert, C.M. 1982. *Petrography: an introduction to the study of rocks in thin section*. W.H. Freeman and Company, San Francisco, pp. 36-93.
- Wilson, M. 1995. *Igneous Petrogenesis*. Chapman and Hall, Great Britain, pp. 3-190.
- Winchester, J.A. and Floyd, P.A. 1977. Geochemical discrimination of different magma series and their differentiation products using immobile elements. *Chemical Geology*, **20**: 325-343.
- Wood, D.A., Joron, J-L. and Treuil, M. 1979. A re-appraisal of the use of trace elements to classify and discriminate between magma series erupted in different tectonic settings. *Earth and Planetary Science Letters*, **45**: 326-336.

Appendix A: Petrographic Descriptions

A.1 Savage Mountain Formation**Sample:** W-26**Lithology:** Clinopyroxene porphyritic basalt**Location:** Near Sustut Peak**Textures:** Porphyritic, glomeroporphyritic clinopyroxene**Phenocryst Assemblage:**

clinopyroxene	20%	(1.5 by 1.2 mm, broken and anhedral to euhedral, unaltered, poikilitic, some grains intensely fractured)
plagioclase	35%	(1.2 by 0.4 mm, subhedral to euhedral, randomly oriented, strongly saussuritized and sericitized)
opaque minerals	10%	(subhedral)

Groundmass: 30%. Hypocrystalline, heterogeneous, grungy, green, red and black portions with fine-grained plagioclase, opaque grains and pyroxene.**Alteration:** 5%. Irregular, chlorite-filled cavities and prehnite veins (~0.5 mm).**Sample:** W-27**Lithology:** Clinopyroxene porphyritic basalt**Location:** Near Sustut Peak**Textures:** Porphyritic, weakly glomeroporphyritic clinopyroxene**Phenocryst Assemblage:**

clinopyroxene	32%	(2 by 2 mm, light greenish yellow, mainly euhedral, minor zoning)
plagioclase	24%	(1 mm by 0.3 mm, seriate, euhedral, fresh, randomly oriented, well developed polysynthetic twinning)
olivine pseudomorphs	6%	(0.2 by 0.1 mm, euhedral, stubby, prismatic, 6-sided, pseudomorphed by chlorite, serpentine, calcite, quartz)

Groundmass: 38%. Dark brown, hypocrystalline, with fine-grained pyroxene, opaque grains and acicular plagioclase laths.**Alteration:** weak, pervasive chloritization of groundmass.**Sample:** W-28**Lithology:** Clinopyroxene porphyritic basalt**Location:** Near Sustut Peak**Texture:** Porphyritic**Phenocryst Assemblage:**

clinopyroxene	19%	(2 by 1.8 mm, euhedral, minor zoning)
plagioclase microphenocrysts	13%	(0.1 by 0.1 mm, euhedral, cloudy, weak pumpellyite alteration)
olivine pseudomorphs	2%	(1.8 by 1.2 mm, euhedral, 6-sided, stubby, prismatic, pseudomorphed by chlorite and talc)

Groundmass: 23%. Brown, hypocrySTALLINE with minor acicular plagioclase and anhedral opaque grains.

Alteration: 43%. Albite-pumpellyite-epidote-filled amygdules. Pervasively chloritized groundmass.

Sample: W-29A

Lithology: Clinopyroxene porphyritic basalt

Location: Near Sustut Peak

Textures: Porphyritic, glomeroporphyritic clinopyroxene

Phenocryst Assemblage:

clinopyroxene	25%	(2 by 1.8 mm, transparent to light yellow green, subhedral to euhedral, strong composition- and inclusion-zoning)
plagioclase	15%	(1.2 by 0.2 mm, euhedral, strongly sericitized)
olivine pseudomorphs	4%	(1 by 0.8 mm, subhedral to anhedral, pseudomorphed by chlorite and opaque minerals)

Groundmass: 54%. Holocrystalline, composed of fine-grained plagioclase laths, pyroxene and opaque grains.

Alteration: 2%. Calcite, chlorite and talc-filled veinlets.

Sample: W-29B

Lithology: Clinopyroxene porphyritic basalt

Location: Near Sustut Peak

Texture: Porphyritic

Phenocryst Assemblage:

clinopyroxene	34%	(2 by 2 mm, light greenish yellow, minor zoning and lamellar twinning, ragged appearance)
plagioclase	6%	(1 by 0.3 mm, subhedral, moderately saussuritized)

Groundmass: 52%. Fine-grained, heterogeneous, ranging from holocrystalline with small grains of pyroxene, plagioclase and opaque minerals to hypocrySTALLINE with dark brown grungy material.

Alteration: 8%. Irregular, discontinuous veins and vesicles filled by two types of chlorite, epidote, calcite and prehnite.

Sample: W-31

Lithology: Clinopyroxene porphyritic basalt

Location: Near Sustut Peak

Textures: Porphyritic, glomeroporphyritic clinopyroxene, pilotaxitic plagioclase

Phenocryst Assemblage:

clinopyroxene	26%	(1.2 by 0.9 mm, euhedral to subhedral, light greenish yellow, zoned with greenish yellow rims, fractured, twinned)
plagioclase	14%	(0.8 by 0.2 mm, euhedral, weakly saussuritized)
olivine pseudomorphs	4%	(0.4 by 0.2 mm, stubby, 6-sided, prismatic, pseudomorphed by chlorite, epidote, calcite)

Groundmass: 48 %. Dark green holocrystalline to hypocrySTALLINE with plagioclase laths and equidimensional opaque grains (<<1 mm).

Alteration: 8%. Pervasive chloritization of groundmass; irregular chlorite, calcite and epidote-filled vesicles (0.4 by 0.6 mm) and discontinuous veins.

Sample: W-32

Lithology: Clinopyroxene porphyritic basalt

Location: Near Sustut Peak

Textures: Porphyritic, glomeroporphyritic clinopyroxene

Phenocryst Assemblage:

clinopyroxene	26%	(2 by 1.8 mm, euhedral, colourless to light greenish yellow, some compositional zoning)
plagioclase	12%	(1 by 0.2 mm, subhedral, cloudy, intensely sericitized)
olivine pseudomorphs	5%	(1.5 by 1 mm, subhedral, prismatic, pseudomorphed by chlorite and talc)

Groundmass: 52%. Holocrystalline with fine-grained tabular plagioclase, anhedral clinopyroxene and anhedral opaque grains.

Alteration: 5%. Irregular, chlorite-filled cavities (2.0 by 1.0 mm).

Sample: W-33

Lithology: Aphanitic basalt

Location: Near Sustut Peak

Textures: Microporphyritic

Microphenocryst Assemblage:

clinopyroxene	5%	(0.2 by 0.4 mm, euhedral, rare)
opaque minerals		accessory

Groundmass: 85%. Heterogeneous, mottled, hypocrySTALLINE, dark brown to light gray.

Alteration: 10%. Irregular, branching veinlets (~0.8 mm) of medium-grained elongate prehnite crystals or quartz and bladed pumpellyite. Small irregular quartz-pumpellyite-chlorite-filled vesicles.

Sample: W-34

Lithology: Clinopyroxene porphyritic basalt

Location: Near Sustut Peak

Textures: Porphyritic, glomeroporphyritic clinopyroxene, trachytic plagioclase

Phenocryst Assemblage:

clinopyroxene	15%	(2.4 by 2 mm, light yellow to light blue-green, euhedral, unaltered, zoned)
---------------	-----	-----------------------------------------------------------------------------

Groundmass: 65%. Hypocrystalline, homogeneous, dark brown with abundant aligned plagioclase laths, small clinopyroxene grains and minor opaque grains.

Alteration: 20%. Small, rounded to irregular pockets of chlorite abundant. Irregular, branching, discontinuous, zoned veins of (from rim to center) bladed pumpellyite, prehnite, chlorite, calcite.

Groundmass: 40%. Brown, hypocrySTALLINE with fine-grained pyroxene crystals, opaque grains and tabular plagioclase laths.

Alteration: 8%. Irregular pods and discontinuous veinlets of calcite, chlorite, talc and epidote. Moderate, pervasive chloritization of groundmass.

Sample: W-77

Lithology: Amygdular clinopyroxene porphyritic basalt

Location: Base of Mount Savage

Textures: Porphyritic, glomeroporphyritic clinopyroxene

Phenocryst Assemblage:

clinopyroxene 10% (2 by 1.6 mm, transparent to light greenish yellow, commonly zoned)

plagioclase 12% (1 by 0.2 mm, euhedral to subhedral, intensely saussuritized)

opaque minerals 5% (0.5 by 0.5 mm, subhedral)

Groundmass: 51%. Brown, hypocrySTALLINE, with weakly aligned, slender plagioclase laths and anhedral, rounded opaque grains.

Alteration: 22%. Quartz-chlorite-calcite microveining (2%) and irregular calcite-chlorite-epidote-pumpellyite amygdules compose (20%). Pervasive chloritization of groundmass.

Sample: W-79

Lithology: Clinopyroxene porphyritic basalt

Location: Base of Mount Savage

Texture: Porphyritic

Phenocryst Assemblage:

clinopyroxene 10% (0.6 by 0.4 mm, subhedral to anhedral, broken appearance)

plagioclase 35% (0.6 by 0.3 mm, intensely sericitized, euhedral to subhedral, some twinning recognizable)

opaque minerals 10% (0.5 by 0.5 mm, anhedral)

Groundmass: 30%. Brown, grungy, hypocrySTALLINE.

Alteration: 15%. Irregular, chlorite-filled cavities. Weak, pervasive chloritization of groundmass.

Sample: NW-26

Lithology: Basaltic tuff breccia

Location: East of Moosevale Creek, at headwaters of Menard Creek

Textures: Massive and fragmented

Clasts: 20%. Predominantly composed of plagioclase porphyritic, opaque-rich basalt. Angular clasts are typically 0.5 by 0.4 mm.

Matrix: 72%. HypocrySTALLINE, with subhedral, saussuritized plagioclase laths (1 by 0.4 mm), scattered opaque grains and fractured, subhedral clinopyroxene grains in a gray-brown, grungy groundmass.

Alteration: 8%. Abundant chlorite-filled pods and minor prehnite-filled pods.

Sample: NW-29

Lithology: Clinopyroxene porphyritic basalt

Location: East of Moosevale Creek, at headwaters of Menard Creek

Textures: Porphyritic, glomeroporphyritic clinopyroxene

Phenocryst Assemblage:

Clinopyroxene	32%	(3 by 3 mm, euhedral, strongly zoned, poikilitic)
Olivine pseudomorphs	15%	(1.2 by 1 mm, subangular, high relief, with curved cleavage, pseudomorphed by opaque minerals and fine-grained chlorite)
Plagioclase	8%	(1 by 0.4 mm, subangular, weakly saussuritized)

Groundmass: 42%. Holocrystalline, composed of plagioclase laths, small subhedral opaque grains and fine-grained pyroxene.

Alteration: 3%. Minor, fine-grained, feathery chlorite pods throughout groundmass.

Sample: NW-75

Lithology: clinopyroxene-plagioclase porphyritic basalt

Location: East of Moosevale Creek, at headwaters of Menard Creek

Texture: Porphyritic

Phenocryst Assemblage:

Clinopyroxene	20%	(1.5 by 1.2 mm, subhedral, fractured, some zonation, with abundant opaque inclusions, some hematite staining along fractures)
Plagioclase	38%	(1.5 by 0.4 mm, subhedral to euhedral, very cloudy, weakly saussuritized)
Olivine pseudomorphs	3%	(1.4 by 0.8 mm, subhedral to euhedral, 6-sided stubby prismatic, replaced by chlorite, opaque minerals and calcite)

Groundmass: 25%. Hypocrystalline with small, anhedral clinopyroxene grains, subhedral to euhedral opaque grains and minor plagioclase laths in a grungy, green-brown matrix.

Alteration: 14%. Irregular chlorite-filled pods abundant throughout matrix.

Sample: NW-92

Lithology: Aphanitic basaltic andesite

Location: East of Moosevale Creek, at headwaters of Menard Creek

Texture: Fine-grained

Phenocryst Assemblage:

Plagioclase	8%	(1 by 0.6 mm, rare, anhedral, very cloudy, strongly sericitized)
-------------	----	------------------------------------------------------------------

Groundmass: 90%. Hypocrystalline, predominantly composed of roughly aligned, fine-grained plagioclase laths, with subhedral, equant opaque grains in grungy, green, fine grained material.

Alteration: 2%. Minor, irregular chlorite-filled cavities. Moderate, pervasive groundmass chloritization.

Alteration: 2%. Chlorite throughout matrix in small irregular pods.

Sample: WIL-32

Lithology: Basaltic andesite tuff breccia

Location: Near Sustut Peak

Texture: Massive

Clasts: 35%. Predominantly composed of subangular fragments of plagioclase porphyritic basaltic andesite. Clast plagioclase phenocrysts (1.2 by 0.4 mm) moderately saussuritized. Minor glomeroporphyritic, subangular clinopyroxene phenocrysts and olivine pseudomorphs, replaced by talc, hematite and chlorite. Small, subangular, opaque-rich clasts also common.

Matrix: 57%. Hypocrystalline, light brown-green with subhedral, weakly sericitized plagioclase phenocrysts, anhedral clinopyroxene and anhedral opaque grains.

Alteration: 8%. Matrix contains abundant, irregular chlorite filled pods, hematite staining common, some clasts contain chlorite filled vesicles.

Sample: WIL-33

Lithology: Basaltic andesite tuff breccia

Location: Near Sustut Peak

Textures: Massive, fragmented

Clasts: 32%. Predominantly composed of plagioclase porphyritic andesite. Subangular clasts typically 1 cm by 0.8 mm. Clast plagioclase (0.5 by 0.2 mm) is euhedral, lath-shaped, sometimes fragmented, weakly sericitized. Clasts also contain minor subhedral clinopyroxene.

Matrix: 60%. Hypocrystalline, with fragmented plagioclase, clinopyroxene and opaque crystals in a heterogeneous groundmass of grungy brown-green material.

Alteration: 8%. Irregular chlorite-filled pods abundant throughout matrix. Hematite staining common.

Sample: WIL-34

Lithology: Basaltic andesite tuff breccia

Location: Near Sustut Peak

Texture: Massive, fragmented

Clasts: 25%. Predominant clast type is fine grained, plagioclase porphyritic (1 by 0.4 mm) andesite with minor subhedral, fractured clinopyroxene crystals and anhedral opaque grains. Clast plagioclase is weakly sericitized. Angular clasts typically 1.2 by 0.8 mm. Amygdular, opaque-rich clasts also abundant.

Matrix: 67%. Hypocrystalline, with sometimes fragmented, subhedral plagioclase and clinopyroxene crystals in a grungy, green-brown matrix.

Alteration: 8%. Abundant, irregular chlorite-filled pods. Hematite staining common.

Sample: S-15

Lithology: Tuffaceous basaltic breccia

Location: Mount Savage

Textures: Massive, fragmented

Clasts: 30%. Predominantly plagioclase porphyritic (0.9 by 0.2 mm) basalt, subangular, typically 0.8 by 0.5 mm.

Matrix: 65%. Hypocrystalline, heterogeneous, with abundant strongly saussuritized subhedral, cloudy plagioclase crystals, fractured, subhedral clinopyroxene and abundant small, subhedral, opaque grains.

Alteration: 5%. Irregular chlorite-filled pods common. Minor small prehnite-filled pods.

Samples W-43, NW-1C, NW-14B, NW-56, NW-69, NW-73, NW-76, NW-77, NW-93, S-32, S-42, S-67 and S-74 were unavailable for petrographic examination.

Appendix B: Microprobe Techniques and Data

B.1 Analytical Techniques

Microprobe data for mineral compositions were obtained at Dalhousie University using the JEOL 733 electron microprobe equipped with four wavelength dispersive spectrometers and an Oxford Link eXL energy dispersive system. Appropriate grains for microprobe analysis were located and circled on polished sections. Probe spot size was approximately 1 μm . All data were collected using energy dispersive spectra. The resolution of the energy dispersive detector was given as 137 eV at 5.9 keV. Each spectrum was acquired for 40 seconds with an accelerating voltage of 15 kV and a beam current of 15 nA. Instrument calibration was performed on cobalt metal. The raw data were corrected using Link's ZAF matrix correction program. Minpet 20.2 was used in the conversion of oxide weight percents into element abundances and in the calculation of mineral formulas.

Sample	CS3-4	CS3-7	NW24A-11A	NW24A-4	NW24A-7	NW24A-8	NW29-13	NW29-2A	NW29-2B	NW29-3
SiO ₂	51.73	51.39	54.62	51.5	54.77	55.16	53.72	50.13	51.56	51.96
TiO ₂	0.28	0.39	-	0.36	-	-	0.32	0.5	0.47	0.67
Al ₂ O ₃	2.77	3	1.3	3.21	0.96	0.91	1.92	4.559	3.36	2.37
FeO	6.58	6.83	3.75	6.6	3.2	3.28	4.9	7.4	7.56	9.85
Fe ₂ O ₃	-	-	-	-	-	-	-	-	-	-
Cr ₂ O ₃	-	0.001	0.54	0.46	0.68	0.76	0.46	0.31	-	-
MnO	-	0.001	-	-	-	-	-	-	0.18	0.33
NiO	-	-	-	-	-	-	-	-	-	-
MgO	15.56	15.7	17.82	16.3	18.51	18.56	17.01	14.68	15.78	16.27
CaO	22.2	22.8	22.71	20.54	22.75	22.78	22.29	21.18	20.81	19.33
Na ₂ O	0.4	0.35	0.24	0.41	0.25	0.27	0.28	0.33	0.56	0.47
K ₂ O	-	0.001	-	-	-	-	-	-	-	-
Total	99.52	100.463	100.98	99.38	101.12	101.72	100.9	99.089	100.28	101.25
WO	45.319	45.621	45.031	42.463	44.606	44.523	44.775	44.701	42.635	38.724
EN	44.196	43.71	49.165	46.887	50.497	50.473	47.542	43.109	44.983	45.351
FS	10.485	10.669	5.804	10.65	4.897	5.004	7.683	12.191	12.381	15.925

NW29-4A	NW29-4B	NW29-6A	NW29-6B	NW29-7	NW29-8	NW75-3A	NW75-3B	NW75-4	NW75-5	NW75-6A
54.23	54	50.83	49.17	51.3	54.65	53	52	51.19	51.1	50.31
-	0.27	0.42	0.7	0.49	0.27	0.24	0.29	0.45	0.31	0.55
1.53	1.49	3.91	5.37	3.49	0.92	1.9	2.62	3.39	3.23	3.94
3.97	3.51	6	8.91	7.04	3.84	4.62	6.84	6.74	6.68	7.62
-	-	-	-	-	-	-	-	-	-	-
0.32	1.02	0.65	-	0.39	0.37	0.7	0.22	-	-	-
-	-	-	-	-	-	-	-	-	-	0.19
-	-	-	-	-	-	-	-	-	-	-
17.68	17.4	15.6	14.31	15.69	18.1	17.29	15.8	15.3	15.46	14.68
22.25	22.33	21.89	20.74	21	23	21.47	21.67	22.12	22	21.58
0.31	0.2	0.26	0.52	0.34	0.3	0.31	0.32	0.38	0.28	0.41
-	-	-	-	-	-	-	-	-	-	-
100.29	100.22	99.56	99.72	99.74	101.45	99.53	99.76	99.57	99.06	99.28
44.546	45.313	45.341	43.566	43.455	44.938	43.697	44.231	45.45	45.151	44.862
49.25	49.128	44.959	41.825	45.174	49.206	48.963	44.872	43.741	44.148	42.462
6.204	5.56	9.701	14.609	11.371	5.856	7.34	10.898	10.809	10.701	12.677

NW75-6B	NW75-7	S15-1	S15-2	S15-4	S15-5	S19-1A	S19-1B	S19-2	S19-3	S19-4
50.55	54.11	49.52	50.93	50.17	50.3	51.35	51.8	49.56	51.34	51.03
0.6	-	0.99	0.83	1.07	0.78	0.45	0.52	0.43	0.38	0.57
3.95	1.19	5.61	3.93	3.37	4.4	3.45	2.81	5.18	3.28	3.58
9.35	4.11	7.04	7.22	10.53	7.33	7.31	7.37	8.06	7.61	7.46
-	-	-	-	-	-	-	-	-	-	-
-	0.24	-	-	-	-	0.19	-	0.25	-	-
-	-	-	-	0.37	-	-	0.17	0.22	0.19	-
-	-	-	-	-	-	-	-	-	-	-
14.16	17.43	14.03	15.27	13.55	14.68	115.79	15.56	14.97	16.03	15.36
20.38	22.33	22.13	21.91	19.92	21.7	20.55	20.96	20.9	20.21	21.09
0.4	0.34	0.42	0.31	0.56	0.29	0.36	0.62	0.39	0.54	0.47
-	-	-	-	-	-	-	-	-	-	-
99.39	99.75	99.74	100.4	99.54	99.48	199.45	99.81	99.96	99.58	99.56
43.014	44.848	46.939	44.905	42.128	45.353	10.968	43.219	43.366	41.581	43.678
41.583	48.708	41.406	43.545	39.872	42.689	85.987	44.642	43.219	45.889	44.262
15.403	6.443	11.655	11.55	18.001	11.958	3.045	12.139	13.415	12.53	12.059

S19-6	S19-7	S25-3	S25-4A	S25-5	S26-2	S26-3	S26-6A	S26-6B	S26-7	S26-8
53.06	53.43	51.26	51.42	49.05	51.26	49.72	50.84	50.12	50.49	49.27
-	0.27	0.5	0.91	1.1	1.01	1.07	0.84	0.8	0.97	1.16
1.85	2.24	3.27	2.6	5.34	2.91	4.97	4.17	3.71	3.19	4.47
5.19	5.21	5.26	9.81	7.74	9.82	7.82	7.32	10.06	10.59	9.85
-	-	-	-	-	-	-	-	-	-	-
0.44	0.6	0.25	-	-	-	-	0.21	-	-	-
-	-	-	0.26	-	0.16	0.22	-	0.34	0.18	-
-	-	-	-	-	-	-	-	-	-	-
16.93	17.02	15.62	14.63	14.01	14.72	14.54	15.06	14.61	14.33	13.69
22	21.77	22.38	19.57	21.99	20.76	22.44	22.59	20.25	20.23	20.54
0.34	0.38	0.32	0.62	0.36	0.45	0.41	0.27	0.47	0.59	0.56
-	-	-	-	-	-	-	-	-	-	-
99.81	100.92	98.86	99.82	99.59	101.09	101.19	101.3	100.36	100.57	99.54
44.348	43.964	46.413	40.951	46.271	42.339	45.844	45.861	41.582	41.645	43.447
47.485	47.824	45.072	42.596	41.017	41.771	41.331	42.54	41.742	41.045	40.291
8.166	8.212	8.515	16.453	12.712	15.89	12.825	11.599	16.676	17.309	16.263

S26-9	W24A-1A	W24A-1B	W24A-2A	W24A-2B	W26-1	W26-2A	W26-2B	W26-3A	W26-3B	W26-3C
50.94	52.36	51.07	50.8	51.12	52.11	52.44	51.15	54.41	52.66	50.33
0.88	0.25	0.33	0.32	0.36	0.58	0.3	0.91	-	0.23	0.78
2.55	2.28	3.75	3.89	3.92	5.14	1.89	3.69	1.77	2.66	4.38
9.98	5.64	6.68	7.37	7.27	9.48	8.04	10.1	4.21	4.42	8.6
-	-	-	-	-	-	-	-	-	-	-
-	0.56	0.56	0.34	0.54	-	-	-	0.44	0.35	-
0.24	0.25	0.19	-	-	-	0.32	-	-	0.17	-
-	-	-	-	-	-	-	-	-	-	-
15.01	16.32	16.07	16.09	15.97	12.82	15.55	14.53	16.84	17.75	14.56
20.22	21.77	20.7	15.8	20.26	18.65	21.11	20.49	23.37	23.27	21.4
0.45	0.36	0.47	0.48	0.44	0.42	0.67	0.54	0.19	0.19	0.55
-	-	-	-	-	-	-	-	-	-	-
100.27	99.79	99.82	95.09	99.88	99.2	100.32	101.41	101.23	101.7	100.6
41.194	44.358	42.747	35.958	42.072	42.495	42.841	42.169	46.659	45.139	44.241
42.549	46.269	46.175	50.95	46.144	40.644	43.909	41.607	46.781	47.908	41.881
16.257	9.373	11.078	13.092	11.784	16.86	13.249	16.224	6.561	6.953	13.877

W26-3D	W26-3E	W26-4A	W26-4B	W27-3A	W27-3B	W27-3C	W27-3D	W27-4A	W27-4B	W27-4C
51.75	49.9	54.78	50.71	51.02	51.4	51.15	50.49	51.26	49.36	51.34
0.55	1.22	-	0.92	0.53	0.52	0.53	0.63	0.57	0.81	0.76
3.82	4.65	0.99	3.4	3.65	2.79	3.19	3.61	3.17	4.7	2.96
7.36	10.64	3.41	10.22	8.95	9.72	8.97	10.31	9.25	9.32	10.41
-	-	-	-	-	-	-	-	-	-	-
0.3	0.22	0.72	-	-	-	-	-	0.24	-	-
-	-	-	0.18	-	-	0.18	0.38	-	-	0.32
-	-	-	-	-	-	-	-	-	-	-
15.71	13.67	17.94	14.08	14.8	14.97	14.63	14	15.11	14.39	14.28
21.56	20.05	23.2	19.86	20.8	19.98	20.65	19.61	20	20.41	19.87
0.55	0.53	0.28	0.6	0.45	0.51	0.4	0.55	0.31	0.45	0.55
-	-	-	-	-	-	-	-	-	-	-
101.6	100.88	101.32	99.97	100.2	99.89	99.7	99.56	99.91	99.44	100.49
43.854	42.322	45.648	41.749	42.994	41.284	42.887	41.339	41.456	42.782	41.295
44.461	40.148	49.114	41.183	42.566	43.039	42.276	41.064	43.578	41.969	41.293
11.685	17.53	5.237	17.068	14.44	15.677	14.837	17.598	14.966	15.249	17.413

W27-4D	W27-7	W28-3A	W28-3B	W28-3C	W28-3D	W28-4A	W28-4B	W28-4C	W28-4D	W29A-1
50.56	54.19	52.99	51.54	51.42	50.88	53.47	51.64	51.75	51.61	50.68
0.63	0.24	0.41	0.43	0.51	0.78	-	0.64	0.56	0.59	0.71
3.79	1.26	2.89	2.88	2.75	4.28	1.7	3.52	2.96	2.88	4.22
9.7	3.69	9.17	8.51	9.18	7.95	4.97	9.02	8.75	8.66	8.45
-	-	-	-	-	-	-	-	-	-	-
-	0.97	-	-	-	-	0.55	-	-	0.54	0.28
0.2	-	0.31	0.28	0.23	-	-	-	0.31	0.26	0.28
-	-	-	-	-	-	-	-	-	-	-
14.63	17.94	16.32	15.52	15.53	15.2	16.97	15.83	16.05	16.05	14.89
20.22	22.61	19.91	20.66	20.08	21.6	22.52	20.51	20.09	20.24	20.76
0.58	0.32	0.37	0.3	0.52	0.53	0.33	0.45	0.53	0.53	0.49
-	-	-	-	-	-	-	-	-	-	-
100.31	101.22	102.37	100.12	100.22	101.22	100.51	101.61	100.82	101.36	100.76
41.859	44.815	39.804	42.062	40.95	44.123	45.03	41.371	40.589	40.858	42.986
42.14	49.476	45.397	43.964	44.067	43.202	47.213	44.428	45.118	45.081	42.899
16.001	5.709	14.799	13.974	14.984	12.676	7.757	14.201	14.294	14.06	14.115

W29A-10	W29A-11A	W29A-11B	W29A-3A	W29A-3B	W29A-4A	W29A-4B	W29A-5	W29A-6	W29A-7	W29A-8
52.97	54.29	51.48	54.39	54.14	53.25	50.06	52.44	51.74	51.19	50.56
0.24	-	0.32	0.18	0.23	-	0.53	0.18	0.34	0.58	0.62
1.89	1.29	2.92	1.17	0.93	1.91	4.19	2.35	2.35	3.15	3.25
6.39	3.53	7.66	4.02	4.26	5.35	9.4	6.43	8.97	8.8	10.04
-	-	-	-	-	-	-	-	-	-	-
0.29	0.68	-	0.59	0.68	0.4	-	0.4	-	-	-
-	-	0.18	-	-	-	-	-	-	0.22	-
-	-	-	-	-	-	-	-	-	-	-
16.29	17.73	15.8	17.57	17.19	16.8	14.56	16.19	15.48	14.61	14.14
21.45	21.98	20.01	22.26	22.39	22.04	20.79	21.63	19.75	20.77	20.2
0.39	0.25	0.4	0.3	0.26	0.41	0.55	0.38	0.47	0.44	0.6
-	-	-	-	-	-	-	-	-	-	-
99.91	99.75	98.77	100.48	100.08	100.16	100.08	100	99.1	99.76	99.41
43.683	44.49	41.588	44.659	45.111	44.443	42.967	43.985	40.899	43.144	42.338
46.159	49.933	45.69	49.046	48.19	47.136	41.869	45.809	44.603	42.226	41.236
10.158	5.577	12.722	6.295	6.699	8.421	15.164	10.206	14.499	14.629	16.425

W29B-1A	W29B-1B	W29B-1C	W29B-1D	W29B-2A	W29B-2B	W29B-2C	W29B-3A	W29B-3B	W29B-6	W29B-7
51.85	51.81	51.12	50.73	53.05	52.14	52.32	54.34	50.46	54.84	54.19
0.35	0.43	0.54	0.57	0.28	0.36	0.35	-	-	-	0.2
3.49	3.41	3.59	4.06	2.36	3.1	2.83	1.01	3.44	1.03	1.5
7.41	7.45	9.63	9.15	5.89	7.08	8.95	3.44	7.63	3.79	4.57
-	-	-	-	-	-	-	-	-	-	-
-	-	-	-	-	-	-	0.46	0.43	0.45	0.32
0.28	0.23	-	0.24	-	0.21	-	-	0.22	-	-
-	-	-	-	-	-	-	-	-	-	-
15.56	15.66	15.04	14.58	16.6	16.04	16.04	18.22	17.57	17.86	17.19
22.16	22.1	10.36	20.84	22.52	21.75	20.53	22.74	18.79	22.76	22.53
0.5	0.49	0.47	0.49	0.37	0.35	0.45	0.3	0.47	0.22	0.29
-	-	-	-	-	-	-	-	0.08	-	-
101.6	101.58	100.75	100.66	101.07	101.03	101.47	100.51	99.09	100.95	100.79
44.484	44.301	41.719	43.006	44.848	43.71	41.197	44.785	38.062	45.008	45.046
43.461	43.678	42.879	41.864	45.997	44.851	44.785	49.927	49.521	49.142	47.822
12.055	12.021	15.402	15.13	9.156	11.439	14.018	5.288	12.416	5.85	7.132

W29B-1A	W29B-1B	W29B-1C	W29B-1D	W29B-2A	W29B-2B	W29B-2C	W29B-3A	W29B-3B	W29B-6	W29B-7
51.85	51.81	51.12	50.73	53.05	52.14	52.32	54.34	50.46	54.84	54.19
0.35	0.43	0.54	0.57	0.28	0.36	0.35	-	-	-	0.2
3.49	3.41	3.59	4.06	2.36	3.1	2.83	1.01	3.44	1.03	1.5
7.41	7.45	9.63	9.15	5.89	7.08	8.95	3.44	7.63	3.79	4.57
-	-	-	-	-	-	-	-	-	-	-
-	-	-	-	-	-	-	0.46	0.43	0.45	0.32
0.28	0.23	-	0.24	-	0.21	-	-	0.22	-	-
-	-	-	-	-	-	-	-	-	-	-
15.56	15.66	15.04	14.58	16.6	16.04	16.04	18.22	17.57	17.86	17.19
22.16	22.1	10.36	20.84	22.52	21.75	20.53	22.74	18.79	22.76	22.53
0.5	0.49	0.47	0.49	0.37	0.35	0.45	0.3	0.47	0.22	0.29
-	-	-	-	-	-	-	-	0.08	-	-
101.6	101.58	100.75	100.66	101.07	101.03	101.47	100.51	99.09	100.95	100.79
44.484	44.301	41.719	43.006	44.848	43.71	41.197	44.785	38.062	45.008	45.046
43.461	43.678	42.879	41.864	45.997	44.851	44.785	49.927	49.521	49.142	47.822
12.055	12.021	15.402	15.13	9.156	11.439	14.018	5.288	12.416	5.85	7.132

W30-10A	W30-10B	W30-1A	W30-1B	W30-2	W30-3	W30-4	W30-5	W30-7A	W30-7B	W30-9
54.09	51.28	51.57	50.34	50.22	50.17	48.21	50.05	45.62	49.53	50.69
-	0.33	0.3	0.45	0.45	0.38	0.39	0.45	0.45	0.39	0.54
1.05	2.97	2.81	4.28	4.02	3.9	3.95	4.48	3.78	3.98	3.58
4.06	8.73	8.41	8.7	8.64	9.48	7.64	9.12	8.07	9.39	8.89
-	-	-	-	-	-	-	-	-	-	-
0.44	-	0.23	0.22	0.29	-	0.28	0.22	0.2	-	0.22
-	0.21	0.26	0.22	0.25	0.3	-	0.24	0.19	0.26	0.23
-	-	-	-	-	-	-	-	-	-	-
18.04	15.89	15.41	15.01	14.86	14.46	14.93	15.03	13.52	15.16	14.9
22.62	20.7	21.73	21.37	21.31	21.06	18.97	20.95	19.23	19.51	21.56
0.33	0.56	0.5	0.41	0.52	0.45	0.43	0.55	0.49	0.43	0.54
-	-	-	-	-	-	-	-	-	-	-
100.63	100.67	101.22	100.57	100.56	100.2	94.8	101.09	91.55	98.65	101.15
44.449	41.575	43.511	43.418	43.554	43.141	41.504	42.606	43.222	40.529	43.633
49.324	44.405	42.933	42.432	42.258	41.215	45.449	42.53	42.282	43.818	41.956
6.227	14.019	13.556	14.15	14.187	15.644	13.047	14.863	14.496	15.653	14.411

W31-1A	W31-1B	W31-1C	W31-1D	W31-2A	W31-2B	W31-2C	W31-2D	W31-3A	W31-3B	W31-3C
53.79	54.1	53.66	54.1	51.23	50.63	51.79	51.76	51.53	51.18	50.9
-	-	0.28	-	0.47	0.64	0.48	0.28	0.39	0.44	0.44
1.54	0.95	1.86	1.51	3.54	3.51	2.6	2.75	3.09	3.07	3.6
5.32	4.37	4.93	4.74	8.06	10.57	9.65	9.78	9.14	9.2	9.64
-	-	-	-	-	-	-	-	-	-	-
0.24	0.26	0.31	0.31	0.27	0.53	0.27	-	-	-	-
0.23	-	-	-	-	0.24	0.32	-	0.24	0.22	-
-	-	-	-	-	-	-	-	-	-	-
16.51	17.67	17.18	17.15	14.8	13.44	14.7	14.73	14.46	14.67	14.43
22.59	22.36	22.06	22.47	21.84	20.13	20.57	20.48	20.67	20.56	20.46
0.26	-	0.2	0.36	0.53	0.49	0.45	0.34	0.6	0.42	0.42
-	-	-	-	-	-	-	-	-	-	-
100.48	99.71	100.48	100.64	100.74	100.18	100.83	100.12	100.12	99.76	99.89
45.274	44.403	44.286	44.911	44.824	42.585	42.144	42.132	42.961	42.544	42.57
46.039	48.823	47.988	47.694	42.264	39.56	41.905	42.163	41.817	42.237	41.775
8.687	6.774	7.725	7.395	12.912	17.855	15.951	15.704	15.222	15.219	15.656

W31-3D	W31-4A	W31-4B	W31-4C	W31-4D	W31-6	W34-1A	W34-1B	W34-2A	W34-2B	W34-3A
51.44	53.72	54.26	54.33	54.29	54.73	50.46	51.56	52.67	51.03	49.9
0.41	0.26	0.22	0.21	0.26	-	0.43	0.55	0.5	0.63	0.61
3.88	1.74	1.27	1.24	1.44	0.87	3.57	2.44	7.81	3.71	3.08
7.79	5	4.59	4.32	4.84	3.65	9.66	9.88	8.09	8.66	9.76
-	-	-	-	-	-	-	-	-	-	-
0.22	0.38	0.28	0.49	0.28	0.47	0.25	-	0.2	0.3	-
-	-	-	-	0.22	-	-	0.3	-	0.25	0.28
-	-	-	-	-	-	-	-	-	-	-
15.22	16.74	17.53	17.4	17.42	18.2	16.08	15.45	12.16	16.69	14.72
21.29	22.65	22.79	22.76	22.55	23.03	19.27	19.91	15.75	18.16	19.8
0.38	0.2	0.35	0.37	0.38	0.32	0.48	0.44	2.37	0.44	0.58
-	-	-	-	-	-	-	-	0.52	0.29	-
100.63	100.69	101.29	101.12	101.68	101.27	100.2	100.53	100.07	100.16	98.73
43.854	45.441	44.894	45.211	44.442	44.978	39.18	40.34	40.401	37.568	41.146
43.621	46.729	48.048	48.091	47.769	49.457	45.49	43.555	43.401	48.04	42.562
12.525	7.83	7.058	6.698	7.788	5.564	15.33	16.105	16.198	14.392	16.291

W34-3B	W34-4A	W34-4B	W34-5	W34-6A	W34-6B	W34-7A	W34-7B	W36-1	W36-3	W36-4
50.9	51.69	51.03	50.69	54	50.3	53.45	51.14	51.48	52.75	47.47
0.47	0.34	0.54	0.58	0.22	0.57	0.22	0.57	0.51	0.39	0.95
3.92	2.89	2.62	3.83	1.27	3.54	1.43	2.63	3.72	2.3	6.49
8.78	8.43	10.72	8.6	5.86	11	4.65	10.43	8.4	6.33	9.44
-	-	-	-	-	-	-	-	-	-	-
0.24	-	-	0.21	0.3	-	0.68	-	-	0.18	-
0.24	0.21	-	0.19	-	0.18	-	0.29	0.19	-	0.2
-	-	-	-	-	-	-	-	-	-	-
15.46	16.1	15.52	15.62	17.72	15.16	17.52	15.34	15.22	16.58	12.92
20.42	20.67	19.21	21.12	21.47	19.09	22.78	20.03	20.68	21.49	20.95
0.61	0.49	0.53	0.43	0.27	0.51	0.28	0.45	0.47	0.4	0.47
-	-	-	-	-	-	-	-	-	-	-
101.04	100.82	100.17	101.27	101.11	100.35	101.01	100.88	100.67	100.42	98.89
41.696	41.492	39.067	42.481	42.348	39.029	44.854	40.266	42.583	43.414	45.099
43.923	44.967	43.916	43.715	48.631	43.126	47.999	42.907	43.607	46.604	38.699
14.381	13.542	17.017	13.804	9.022	17.845	7.147	16.827	13.81	9.982	16.202

W36-5	W37-1	W37-4	W37-5	W37-6	W37-8	W37-9
51.2	49.71	50.88	53.47	47.25	49.85	48.16
0.52	0.62	0.38	0.27	0.85	0.6	0.68
3.07	4.79	3.75	2.07	6.51	4.55	6.05
9.86	7.87	7.95	4.9	9.73	9.44	8.88
-	-	-	-	-	-	-
-	0.3	0.27	0.4	-	0.19	0.29
0.25	-	-	0.2	-	0.25	0.17
-	-	-	-	-	-	-
14.16	15.07	16.23	17.31	13.46	15.34	14.1
20.39	21.59	20.86	22.81	21.22	20.47	21.47
0.57	0.35	0.33	0.36	0.466	0.33	0.38
-	-	-	-	-	-	-
100.02	100.3	100.65	101.79	99.48	101.02	100.18
42.492	44.332	42.016	44.833	44.633	41.454	44.586
41.058	43.055	45.485	47.339	39.392	43.224	40.741
16.45	12.614	12.499	7.828	15.975	15.322	14.673

Sample	W31-8	W31-7	W27-6a	W27-6b	W27-4	S25-1	W36-6	NW29-1	NW29-2	NW92	S26
SiO ₂	68.77	69.05	56.46	68.83	54.04	54.35	56.47	51.93	52.46	59.81	64.66
Al ₂ O ₃	20.25	20.33	28.25	20.33	28.69	28.15	26.34	30.2	30.36	23.16	20.2
FeO	-	-	2.2	-	0.94	1.05	-	1.12	1.25	1.97	-0.47
MgO	-	-	0.41	-	0.19	-	1.63	0.37	-	0.66	-
CaO	0.83	0.91	1.45	0.38	12.06	11.49	9.88	12.44	12.51	6.18	2.21
Na ₂ O	8.51	9.24	4.1	11.23	4.28	4.55	5.34	3.83	3.99	3.31	8.72
K ₂ O	-	0.07	5.71	-	0.42	0.45	0.53	0.42	0.23	5.09	2.75
P ₂ O ₅	-	-	-	-	-	-	-	-	-	-	1.01
BaO	-	-	-	-	-	-	-	-	-	0.37	-
Total	98.36	99.6	98.49	100.77	100.62	100.04	100.19	100.31	100.8	100.55	100.02
Ab	17.9	94.4	46.8	11.9	38.2	40.6	47.9	34.9	36.1	32.9	74.2
An	1	5.1	9.3	0.2	59.4	56.7	49	62.6	62.5	33.9	10.4
Or	81.2	0.5	43.9	87.9	2.5	2.6	3.1	2.5	1.4	33.2	15.4

Sample	CS3-3	CS3-8	CS3-9
SiO ₂	39.778	39.968	40.184
FeO	19.114	19.084	19.117
MnO	0.294	0.352	0.383
MgO	44.417	44.437	42.966
Na ₂ O	0.458	0.346	0.33
Total	104.061	104.187	102.98
Fo	80.31	80.29	79.7
Fa	19.69	19.71	20.3

C.1 Accuracy and Precision

C.1.1 ICP-MS Data

The samples are compared to the Canadian Centre for Mineral and Energy Technology, Mines and Resources standard MRG-1, which is a gabbro from Mount Royal, Montreal. Standard values are from Govindaraju (1994). Column A is the assumed true value of MRG-1. Column B is the measured value on the Takla Group sample. Column C is the difference A - B. Column D is the accuracy, which is the difference expressed as a percentage of the true value of the standard, i.e.

$$100 * (A-B) / A.$$

Column E is the mean of two readings on sample S-153. Column F is the standard deviation for sample S-153 calculated from the normal expression for standard deviation, i.e.

$$\text{square root} ((\text{sum} (\text{mean} - \text{reading}) (\text{mean} - \text{reading})) / (N - 1)) \text{ for } N \text{ readings.}$$

Column G is the standard deviation expressed as a percentage of the mean, i.e.

$$100 * \text{standard deviation} / \text{mean.}$$

Columns H, I and J are as E, F and G for sample S-74.

Element	A Standard	B Measured	C Error	D Accuracy
Li	4.20	3.60	0.60	14.3%
Rb	8.50	7.55	0.95	11.2%
Sr	266.00	261.34	4.66	1.8%
Y	14.00	10.96	3.04	21.7%
Zr	108.00	91.10	16.90	15.6%
Nb	19.20	20.60	-1.40	-7.3%
Mo	0.87	55.34	-54.47	-62.61%
Cs	0.57	0.57	0.00	0.0%
Ba	61.00	46.93	14.07	23.1%
La	9.89	9.00	0.89	9.0%
Ce	26.00	26.80	-0.80	-3.1%
Pr	3.40	3.76	-0.36	-10.6%
Nd	19.20	18.22	0.98	5.1%
Sm	4.50	4.44	0.06	1.3%
Eu	1.39	1.44	-0.05	-3.6%
Gd	4.00	4.08	-0.08	-2.0%
Tb	0.51	0.55	-0.04	-7.8%
Dy	2.90	3.07	-0.17	-5.9%
Ho	0.49	0.52	-0.03	-6.1%
Er	1.12	1.29	-0.17	-15.2%
Tm	0.11	0.15	-0.04	-36.4%
Yb	0.60	0.82	-0.22	-36.7%
Lu	0.12	0.11	0.01	8.3%
Hf	3.76	3.75	0.01	0.3%
Ta	0.80	0.89	-0.09	-11.2%
Tl	0.06	0.05	0.01	16.7%

Element	A	B	C	D
Pb	10.00	4.89	5.11	51.1%
Bi	0.01	0.15	-0.14	-14.00%
Th	0.93	0.82	0.11	11.8%
U	0.24	0.32	-0.08	-33.3%

Element	E Sample S- 153	F Std. Dev.	G Std. Dev. as % of mean	H Sample S- 74	I Std. Dev.	J Std. Dev. as % of mean
Li	11.43	+/- 0.71	6.2%	32.21	+/- 0.50	1.6%
Rb	2.23	+/- 0.01	0.6%	27.24	+/- 0.54	2.0%
Sr	302.52	+/- 2.11	0.7%	348.24	+/- 7.95	2.3%
Y	19.60	+/- 0.07	0.4%	16.81	+/- 0.45	2.7%
Zr	83.65	+/- 1.15	1.4%	55.72	+/- 0.33	0.6%
Nb	4.45	+/- 0.01	0.2%	3.15	+/- 0.08	2.5%
Mo	1.11	+/- 0.13	12.2%	0.65	+/- 0.06	9.9%
Cs	0.11	+/- 0.01	12.9%	2.99	+/- 0.03	0.9%
Ba	63.11	+/- 1.44	2.3%	509.79	+/- 0.86	0.2%
La	9.32	+/- 0.12	1.3%	7.67	+/- 0.07	0.9%
Ce	21.76	+/- 0.07	0.3%	17.30	+/- 0.08	0.5%
Pr	2.94	+/- 0.05	1.7%	2.42	+/- 0.01	0.6%
Nd	13.22	+/- 0.24	1.8%	11.45	+/- 0.18	1.6%
Sm	3.37	+/- 0.11	3.2%	3.11	+/- 0.02	0.7%
Eu	1.09	+/- 0.04	3.9%	1.25	+/- 0.00	0.0%
Gd	3.81	+/- 0.04	1.1%	3.56	+/- 0.02	0.6%
Tb	0.60	+/- 0.00	0.0%	0.56	+/- 0.02	3.8%
Dy	3.66	+/- 0.01	0.4%	3.45	+/- 0.01	0.2%
Ho	0.77	+/- 0.02	2.8%	0.72	+/- 0.01	1.0%
Er	2.22	+/- 0.03	1.3%	2.02	+/- 0.04	2.1%
Tm	0.33	+/- 0.01	2.2%	0.28	+/- 0.01	2.6%
Yb	2.13	+/- 0.02	1.0%	1.74	+/- 0.04	2.0%
Lu	0.31	+/- 0.00	0.0%	0.25	+/- 0.00	0.0%
Hf	2.53	+/- 0.04	1.7%	1.74	+/- 0.05	2.9%
Ta	0.43	+/- 0.01	1.7%	0.29	+/- 0.01	2.5%
Tl	0.02	+/- 0.01	47.1%	0.11	+/- 0.02	20.2%
Pb	2.79	+/- 0.04	1.5%	2.76	+/- 0.09	3.3%
Bi	0.02	+/- 0.01	70.7%	0.06	+/- 0.01	12.9%
Th	1.23	+/- 0.03	2.3%	0.90	+/- 0.02	2.4%
U	0.65	+/- 0.01	1.1%	0.57	+/- 0.01	1.2%

C.1.2 XRF Data

Major and trace element XRF values are compared to the United States Geological Survey (USGS) standard diabase W-2. Trace elements are compared again to USGS standard andesite AGV-1. Column A is the assumed true value of the standard W-2. Column B is the

mean of 14 measured analyses of this standard. Column C is the standard deviation. Column D is the difference between the standard value and the mean measured value. Column E is the assumed true value of the standard AGV-1. Column F is the mean of measured 14 analyses of this standard. Columns G and H are as C and D.

W-2

Element	A Standard	B Mean	C Std. Dev.	D Difference
SiO ₂	52.44	52.52	+/- 0.10	0.08
TiO ₂	1.06	1.05	+/- 0.01	0.01
Al ₂ O ₃	15.35	15.21	+/- 0.12	0.14
Fe ₂ O ₃	10.76	10.31	+/- 0.08	0.45
MnO	0.10	0.16	+/- 0.00	0.06
MgO	6.37	6.50	+/- 0.10	0.13
CaO	10.87	10.97	+/- 0.07	0.10
Na ₂ O	2.14	2.40	+/- 0.24	0.26
K ₂ O	0.63	0.64	+/- 0.01	0.01
P ₂ O ₅	0.13	0.12	+/- 0.01	0.01
Ba	182.0	180.8	+/- 5.8	1.2
Rb	20.0	21.8	+/- 2.1	1.8
Sr	194.0	193.6	+/- 4.2	0.4
Y	24.0	18.0	+/- 1.7	6.0
Zr	94.0	90.2	+/- 2.2	3.8
Nb	7.9	5.5	+/- 0.7	2.4
Ga	20.0	18.4	+/- 1.4	1.6
Zn	77.0	82.3	+/- 1.1	5.3
Cu	103.0	109.3	+/- 3.8	6.3
Ni	70.0	71.3	+/- 2.1	1.3
V	262.0	262.3	+/- 6.4	0.3
Cr	93.0	89.8	+/- 3.8	3.3

AGV-1

Element	A Standard	B Mean	C Std. Dev.	D Difference
Ba	1226.0	1244.1	+/- 11.6	18.1
Rb	67.3	67.6	+/- 2.1	0.3
Sr	662.0	666.4	+/- 5.0	4.4
Y	20.0	19.4	+/- 1.0	0.6
Zr	227.0	247.5	+/- 9.2	20.5
Nb	15.0	12.0	+/- 1.1	3.0
Ga	20.0	19.1	+/- 1.9	0.9
Zn	88.0	89.1	+/- 1.5	1.1
Cu	60.0	60.9	+/- 5.9	0.9
Ni	16.0	17.1	+/- 1.7	1.1
V	121.0	123.4	+/- 3.1	2.4
Cr	10.1	16.0	+/- 3.7	5.9

XRF analyses are recalculated to anhydrous values, however original major oxide analysis totals are included, as well as loss on ignition values.

Sample	NW-1C	NW-56	NW-69	NW-73	NW-24A	NW-75	NW-76	NW-77	NW-92	NW-93	NW14-B	NW24-A
SiO2	50.64	50.76	51.51	50.05	48.55	47.08	52.07	55.14	55.75	49.54	49.78	48.52
TiO2	0.93	1.12	1.29	1.05	0.70	1.00	1.05	1.11	1.21	0.98	0.94	0.70
Al2O3	17.63	14.69	17.82	13.87	10.43	15.20	19.17	17.41	18.13	14.79	13.00	10.45
Fe2O3	1.01	1.28	1.06	1.27	1.27	1.42	0.98	0.91	0.95	1.32	1.28	1.28
FeO	8.22	10.38	8.60	10.31	10.30	11.47	7.96	7.34	7.69	10.67	10.33	10.35
MnO	0.18	0.21	0.18	0.22	0.20	0.25	0.20	0.15	0.17	0.21	0.20	0.20
MgO	5.93	6.27	5.15	8.32	14.17	8.24	4.25	3.64	3.20	7.63	9.69	14.14
CaO	10.05	10.86	7.61	10.13	12.48	9.67	7.17	8.35	7.58	9.93	11.44	12.47
Na2O	2.70	2.85	4.11	2.38	1.21	3.24	5.00	4.51	3.33	2.26	1.79	1.22
K2O	2.43	1.35	2.19	2.19	0.50	2.19	1.74	1.04	1.71	2.45	1.37	0.50
P2O5	0.29	0.23	0.48	0.22	0.18	0.23	0.42	0.42	0.28	0.25	0.19	0.18
Total	96.66	96.48	94.14	97.00	95.64	90.70	93.28	92.95	97.67	97.32	96.24	95.83
LOI	2.20	2.40	4.80	1.90	3.40	4.00	5.80	5.80	1.60	1.40	3.10	3.40
Cr	158	86	75	271	971	111	35	57	10	125	345	966
Ni	72	37	36	81	233	33	21	30	7	36	103	233
Co	30	40	27	51	61	51	25	22	26	44	48	61
V	307	332	331	310	242	351	331	317	213	343	299	247
Cu	-	-	-	-	-	-	-	-	-	-	-	-
Pb	-	-	24	-	-	8	-	-	-	-	-	-
Zn	98	106	130	102	94	139	165	93	98	172	104	95
K	-	-	-	-	-	-	-	-	-	-	-	-
Rb	49	32	34	40	7	61	44	30	27	48	25	7
Ba	537	278	595	772	203	712	287	148	933	923	352	182
Sr	420	318	612	540	189	789	351	460	469	384	302	1232
Ga	-	-	-	-	-	-	-	-	-	-	-	-
Nb	2.1	6.2	9.6	5.2	3.1	2.2	9.6	7.5	6.1	4.1	4.2	3.1
Zr	48	70	110	56	33	41	84	84	117	47	50	33
Ti	-	-	-	-	-	-	-	-	-	-	-	-
Y	14	18	23	16	13	15	19	17	25	14	15	13
Th	2.07	2.07	5.31	2.06	2.09	4.41	1.07	3.23	2.05	1.03	1.04	3.13
U	-	-	1.06	-	2.09	1.10	-	-	-	-	-	-
La	8.28	-	17.00	-	25.09	-	28.94	8.61	17.40	17.47	7.27	7.30
Ce	31.04	49.75	26.56	23.71	-	-	-	-	-	-	-	-
Nd	7.24	20.73	12.75	8.25	5.23	12.13	30.02	17.21	15.36	2.05	4.16	8.35

NW-26	NW-77	NW-29	NW-41	NW-44	S-15	S-19	S-32	S-42	S-67	S-74	S-153	CS-2
51.38	55.15	47.95	59.98	58.69	49.52	49.43	49.54	49.22	49.96	51.35	57.01	49.56
1.39	1.11	0.80	0.69	0.69	1.43	0.66	1.06	1.33	1.19	1.06	0.76	0.75
17.91	17.48	10.51	17.67	17.61	17.28	10.21	19.08	14.66	15.51	16.30	18.92	20.20
1.14	0.90	1.28	0.88	0.82	1.30	1.33	1.21	1.31	1.19	1.13	0.81	0.87
9.25	7.28	10.39	7.10	6.66	10.55	10.79	9.79	10.64	9.67	9.12	6.59	7.07
0.20	0.15	0.19	0.09	0.15	0.18	0.20	0.22	0.22	0.36	0.25	0.19	0.13
4.98	3.65	14.32	3.50	2.56	5.77	11.84	5.18	8.77	8.46	7.78	4.23	5.94
7.71	8.33	12.46	3.01	7.29	8.21	12.67	9.26	8.05	9.52	6.49	4.15	12.33
4.24	4.49	1.31	4.83	3.19	4.33	2.66	3.25	4.13	2.28	4.21	6.99	2.78
1.42	1.04	0.61	2.05	2.15	1.22	0.03	1.07	1.48	1.66	2.08	0.10	0.32
0.38	0.42	0.19	0.21	0.21	0.23	0.17	0.35	0.18	0.19	0.22	0.24	0.04
97.31	93.13	95.42	97.56	96.49	97.26	96.12	96.28	95.86	94.17	94.50	97.73	97.97
1.90	-	3.20	2.30	2.30	3.40	3.70	2.80	5.40	6.30	5.10	3.00	1.30
42	55	833	13	16	30	657	14	201	159	136	5	106
27	32	223	13	8	29	151	21	50	41	47	9	78
31	19	65	22	21	-	-	-	-	-	-	-	-
270	319	260	161	187	408	285	297	419	322	336	163	255
-	-	-	-	-	138	85	38	63	518	3123	351	29
-	11	-	-	7	-	-	-	-	-	-	-	-
91	91	96	38	138	108	93	125	120	99	97	103	51
-	-	-	-	-	10104	262	8890	12268	13811	17304	856	2647
29	29	14	35	58	17	-	26	18	18	25	-	-
525	161	203	923	1223	303	5	406	601	886	610	40	159
571	453	187	592	549	298	197	649	253	326	387	317	644
-	-	-	-	-	21	13	25	21	18	20	23	20
9.2	5.4	4.2	4.1	4.1	5.2	-	5.2	6.3	6.4	5.3	6.2	-
131	85	37	95	87	74	41	97	78	74	76	105	24
-	-	-	-	-	8544	3977	6357	7974	7142	6344	4572	4502
25	17	13	22	20	22	13	25	23	25	25	27	7
2.06	2.15	4.19	4.10	4.15	-	-	-	-	-	-	-	-
-	-	-	4.10	1.04	-	-	-	-	-	-	-	-
7.19	5.37	4.19	6.15	12.44	-	-	-	-	-	-	-	-
-	-	-	-	-	-	-	-	-	-	-	-	-
7.19	24.70	16.77	14.35	8.29	-	-	-	-	-	-	-	-

CS-3	CS-9	CS-14	CS-29A	CS-30	CS-31	CS-34A	CS-36	W-26	W-27	W-28	W-29A	W-29B
44.61	48.38	48.22	48.55	49.46	49.70	49.90	47.87	49.04	48.98	56.38	49.43	50.96
0.61	0.64	0.55	0.61	0.66	0.66	0.65	0.66	1.02	0.92	0.78	0.84	0.73
3.23	4.10	8.70	8.35	8.79	9.60	11.16	9.47	16.38	13.37	12.44	12.48	11.04
1.64	1.13	1.16	1.18	1.39	1.28	1.20	1.43	1.19	1.34	0.89	1.41	1.25
13.30	9.17	9.43	9.57	11.23	10.38	9.74	11.61	9.67	10.83	7.19	11.39	10.09
0.20	0.18	0.17	0.19	0.19	0.20	0.19	0.20	0.22	0.21	0.23	0.19	0.21
18.79	16.31	9.12	11.00	12.00	12.63	11.94	13.35	8.17	7.80	5.58	8.40	10.12
17.55	19.99	19.04	17.58	13.11	12.88	11.00	12.64	10.16	13.40	10.15	11.96	12.17
0.06	0.10	2.72	2.64	1.91	1.95	1.76	1.41	2.76	1.98	4.60	1.87	2.66
-	-	0.72	0.17	1.09	0.55	2.31	1.20	1.17	0.94	1.57	1.79	0.60
-	-	0.16	0.15	0.16	0.16	0.14	0.17	0.21	0.24	0.19	0.24	0.19
100.09	98.13	93.26	94.20	98.44	96.49	97.60	98.20	96.99	99.04	98.27	97.45	97.41
0.70	0.60	6.70	6.90	3.40	3.30	2.30	2.30	3.80	1.70	1.50	3.50	2.40
759	676	908	607	639	560	562	944	145	225	250	234	438
146	106	222	145	155	136	163	222	50	61	47	52	86
-	-	-	-	-	-	-	-	-	-	-	-	-
239	201	211	216	271	282	263	285	303	323	240	314	288
12	22	94	112	110	112	112	110	36	147	182	152	90
-	-	-	-	-	-	-	-	-	-	-	-	-
54	51	65	69	89	87	76	83	91	95	57	94	87
-	-	5937	1425	9050	4526	19173	9933	9689	7804	13028	14838	4999
-	-	10	-	24	7	48	26	33	11	24	34	12
-	13	181	33	275	136	1138	217	267	303	242	360	119
29	31	252	185	256	262	535	225	411	335	157	288	246
9	8	10	12	14	14	13	11	17	18	10	16	15
-	-	-	-	-	-	-	-	-	-	-	-	-
14	19	36	44	41	42	40	39	83	77	66	65	63
3647	3827	3312	3666	3947	3960	3912	3958	6123	5514	4673	5046	4357
9	10	13	16	15	14	14	13	21	21	18	18	17
-	-	-	-	-	-	-	-	-	-	-	-	-
-	-	-	-	-	-	-	-	-	-	-	-	-
-	-	-	-	-	-	-	-	-	-	-	-	-
-	-	-	-	-	-	-	-	-	-	-	-	-
-	-	-	-	-	-	-	-	-	-	-	-	-

W-30	W-31	W-32	W-33	W-34	W-35	W-36	W-37	W-39	W-41	W-42	W-43	W-44
48.88	51.39	50.68	48.04	50.28	48.20	50.55	50.72	56.55	51.53	50.35	49.55	54.04
0.77	0.75	0.77	0.99	1.07	0.63	0.91	0.87	0.84	1.11	1.04	1.12	0.88
10.67	11.95	12.18	12.26	12.06	10.00	13.76	14.89	14.61	17.23	20.45	17.27	18.74
1.37	1.20	1.31	1.40	1.47	1.37	1.30	1.21	0.86	1.14	0.98	1.13	0.98
11.13	9.75	10.57	11.38	11.94	11.07	10.49	9.80	7.00	9.25	7.94	9.11	7.96
0.24	0.19	0.21	0.24	0.22	0.21	0.18	0.17	0.11	0.19	0.19	0.18	0.19
11.52	7.88	9.66	9.12	8.35	13.99	7.44	7.31	4.73	5.14	4.26	4.14	4.20
12.14	12.23	10.50	11.90	10.06	10.96	10.13	10.22	9.85	9.94	9.79	12.81	7.72
1.66	3.13	2.48	1.06	3.83	1.27	3.34	3.36	3.12	3.65	4.41	3.91	3.69
1.43	1.30	1.38	3.39	0.39	2.09	1.60	1.17	1.98	0.53	0.24	0.53	1.28
0.19	0.23	0.26	0.23	0.32	0.21	0.30	0.29	0.34	0.30	0.34	0.26	0.31
97.33	96.99	98.95	98.55	98.24	97.27	98.48	96.95	92.07	95.56	94.42	94.78	94.35
3.20	3.10	2.20	3.00	1.90	4.10	2.10	2.50	8.50	3.70	4.60	3.40	3.90
446	223	325	161	198	806	127	98	115	63	12	61	15
106	47	94	46	56	219	39	39	58	30	16	40	19
-	-	-	-	-	-	-	-	-	-	-	-	-
283	294	320	246	310	267	379	394	277	335	284	380	246
103	192	83	79	163	106	50	25	108	45	21	69	46
-	-	-	-	-	-	-	-	-	-	-	-	-
103	96	99	108	125	99	96	104	122	116	114	52	98
11830	10815	11459	28149	3253	17366	13303	9694	16446	4389	1951	4424	10652
29	22	32	59	6	33	29	24	43	6	-	6	35
422	419	230	754	124	357	442	318	595	187	50	-	148
297	356	324	195	228	186	577	479	483	206	208	131	500
16	13	16	15	14	14	14	18	18	21	26	25	17
-	-	-	-	-	-	-	-	5.5	5.3	5.3	-	5.3
58	64	74	70	88	47	79	71	99	78	108	69	101
4614	4498	4597	5914	6431	3806	5482	5189	5315	6655	6213	6709	5257
18	20	19	25	23	12	18	20	23	23	26	19	20
-	-	-	-	-	-	-	-	-	-	-	-	-
-	-	-	-	-	-	-	-	-	-	-	-	-
-	-	-	-	-	-	-	-	-	-	-	-	-
-	-	-	-	-	-	-	-	-	-	-	-	-
-	-	-	-	-	-	-	-	-	-	-	-	-

W-73B	W-75	W-77	W-79	WIL-26	WIL-29	WIL-30	WIL-32	WIL-33	WIL-34	WIL-35
51.55	47.67	50.22	49.18	59.73	58.15	55.92	57.84	53.61	54.03	52.43
0.99	1.16	1.33	1.30	0.72	0.95	0.69	0.84	0.73	0.78	0.76
16.97	15.44	16.28	17.47	16.93	17.92	19.65	17.94	19.43	19.05	20.87
1.09	1.24	1.24	1.13	0.86	0.90	0.81	0.88	0.96	0.99	0.91
8.81	10.05	10.07	9.17	6.93	7.28	6.55	7.10	7.79	8.02	7.34
0.17	0.26	0.17	0.22	0.16	0.22	0.20	0.21	0.18	0.18	0.17
5.27	6.92	6.70	5.08	2.13	3.61	3.36	3.19	4.30	4.23	3.03
9.74	13.38	10.29	12.03	7.52	3.54	5.26	6.85	8.54	7.35	8.47
4.11	3.23	2.58	3.37	4.57	7.04	5.00	3.77	3.46	4.15	5.61
0.96	0.50	0.90	0.80	0.24	0.17	2.32	1.20	0.86	1.07	0.23
0.35	0.16	0.22	0.25	0.22	0.23	0.23	0.19	0.15	0.15	0.16
96.95	93.57	96.71	94.39	97.12	97.75	95.80	96.13	96.27	95.95	95.05
3.30	4.90	2.70	5.10	2.20	2.30	3.30	2.80	2.80	3.60	4.00
110	111	53	31	25	-	5	-	5	8	5
42	51	37	25	17	-	5	6	8	7	8
-	-	-	-	-	-	-	-	-	-	-
339	335	381	285	218	238	148	191	233	205	214
199	83	121	93	191	51	38	74	43	89	72
-	-	-	-	-	-	-	-	-	-	-
86	93	90	98	66	109	95	87	97	89	67
7954	4127	7465	6663	1981	1370	19290	9922	7132	8903	1937
14	10	20	19	-	-	53	21	16	22	-
173	130	233	102	163	58	2058	1220	815	896	81
114	555	441	346	707	205	550	414	401	367	213
18	18	18	20	21	18	20	17	19	18	19
5.2	-	-	-	6.2	7.2	6.3	5.2	-	-	-
66	69	78	89	108	84	115	93	78	74	60
5932	6933	7961	7764	4293	5688	4161	5029	4397	4665	4578
22	17	23	26	24	21	22	22	18	19	18
-	-	-	-	-	-	-	-	-	-	-
-	-	-	-	-	-	-	-	-	-	-
-	-	-	-	-	-	-	-	-	-	-
-	-	-	-	-	-	-	-	-	-	-
-	-	-	-	-	-	-	-	-	-	-

Sample	S-32	S-74	CS-2	CS-9	W-26	W-28	W-31
Cr	14	136	106	676	145	250	223
Ni	21	47	78	106	50	47	47
V	297	336	255	201	303	240	294
Cu	38	3123	29	22	36	182	192
Pb	3	3	1	3	1	2	2
Zn	125	97	51	51	91	57	96
Bi	0.02	0.06	0.00	0.01	0.02	0.03	0.01
Mo	0.64	0.73	0.11	0.08	0.46	0.49	0.48
K	8890	17304	2647	0	9689	13028	10815
Rb	26	29	4	0	34	23	24
Cs	0.32	3.18	0.14	0.00	4.28	0.10	0.25
Ba	362	544	143	3	252	214	385
Sr	630	366	613	32	420	150	343
Tl	0.05	0.12	0.02	0.00	0.05	0.05	0.04
Ga	25	20	20	8	17	10	13
Li	16.06	34.04	4.79	3.86	14.03	3.08	10.75
Ta	0.46	0.30	0.30	0.27	0.71	0.63	0.35
Nb	4.5	3.3	0.6	0.4	3.6	2.7	2.5
Hf	2.46	1.81	0.47	0.61	1.85	1.62	1.53
Zr	81	60	11	11	63	56	45
Ti	6357	6344	4502	3827	6123	4673	4498
Y	18	18	6	7	17	15	14
Th	1.52	0.97	0.07	0.03	0.82	0.80	1.10
U	0.65	0.61	0.04	0.02	0.48	0.50	0.38
La	12.94	8.25	2.14	0.79	5.85	5.96	6.86
Ce	28.56	18.55	5.02	2.78	14.61	13.95	15.19
Pr	3.78	2.60	0.78	0.58	2.09	2.03	2.19
Nd	17.20	12.10	3.90	3.55	9.88	9.62	10.15
Sm	4.11	3.31	1.22	1.36	2.81	2.64	2.78
Eu	1.53	1.33	0.59	0.48	1.02	0.90	0.88
Gd	4.42	3.79	1.44	1.73	3.41	2.92	2.86
Tb	0.63	0.59	0.22	0.29	0.51	0.45	0.46
Dy	3.75	3.69	1.32	1.77	3.25	2.92	2.93
Ho	0.75	0.76	0.27	0.32	0.68	0.61	0.56
Er	2.11	2.12	0.69	0.86	1.92	1.73	1.61
Tm	0.31	0.30	0.09	0.11	0.26	0.26	0.21
Yb	1.96	1.89	0.61	0.70	1.74	1.61	1.39
Lu	0.30	0.27	0.08	0.10	0.26	0.24	0.21

W-35	W-36	W-37	W-39	S-74D	S-153	S-153D
806	127	98	115	136	5	5
219	39	39	58	47	9	9
267	379	394	277	336	163	163
106	50	25	108	3123	351	351
2	1	1	1	3	3	3
99	96	104	122	97	103	103
0.03	0.00	0.02	0.09	0.06	0.03	0.02
0.20	0.32	0.29	1.64	0.64	1.04	1.24
17366	13303	9694	16446	17304	856	856
33	26	25	45	30	2	2
0.42	0.67	1.80	1.12	3.22	0.10	0.12
305	386	274	555	546	66	64
183	562	460	494	378	310	313
0.03	0.05	0.06	0.24	0.10	0.01	0.02
14	14	18	18	20	23	23
11.82	12.99	24.01	26.35	34.81	12.30	11.26
0.21	0.31	0.32	0.34	0.31	0.44	0.43
1.7	3.3	2.5	4.9	3.4	4.6	4.6
1.13	1.67	1.53	2.23	1.89	2.64	2.58
34	47	46	72	59	85	87
3806	5482	5189	5315	6344	4572	4572
11	15	15	19	18	20	20
1.09	1.22	1.79	1.77	0.94	1.29	1.25
0.61	0.51	0.87	3.05	0.62	0.65	0.66
6.39	7.55	10.68	12.11	8.15	9.54	9.70
14.07	17.65	24.26	23.24	18.43	22.37	22.48
1.98	2.59	3.44	3.28	2.57	2.99	3.06
9.01	12.53	15.85	14.27	12.38	13.45	13.80
2.45	3.40	3.79	3.49	3.34	3.55	3.39
0.79	1.00	1.15	1.15	1.34	1.09	1.15
2.54	3.56	3.49	3.53	3.82	3.89	3.96
0.39	0.50	0.50	0.55	0.62	0.62	0.62
2.24	3.18	3.19	3.55	3.67	3.76	3.78
0.45	0.63	0.58	0.69	0.77	0.81	0.77
1.30	1.75	1.64	2.08	2.19	2.27	2.30
0.18	0.24	0.25	0.32	0.29	0.33	0.34
1.13	1.51	1.45	2.07	1.83	2.18	2.21
0.18	0.22	0.20	0.30	0.27	0.32	0.32

Appendix D: XRF Data of Minehan (1989)

Oxide values are recalculated to anhydrous form.

Sample	KM30	KM33	KM15	KM35	KM37	KM18	KM34	KM36	KM27	KM25
SiO ₂	37.38	42.99	44.43	46.71	47.82	48.08	49.56	49.80	50.31	51.56
TiO ₂	0.61	0.58	0.87	0.93	0.90	1.38	0.96	0.51	0.93	0.70
Al ₂ O ₃	12.82	10.91	14.38	16.24	18.98	19.17	16.91	8.64	22.21	13.15
Fe ₂ O ₃	2.01	1.99	2.71	2.06	2.37	2.92	2.16	2.25	2.25	2.38
FeO	6.40	6.36	8.64	6.58	7.57	9.31	6.88	7.17	7.18	7.59
MnO	0.33	0.26	0.21	0.22	0.16	0.18	0.20	0.18	0.17	0.16
MgO	6.62	8.16	7.56	6.42	7.98	7.96	5.80	14.80	3.96	10.30
CaO	31.28	27.05	18.52	18.17	10.08	9.65	14.53	15.79	7.99	12.17
Na ₂ O	1.88	1.04	1.87	2.00	2.77	1.21	2.31	0.46	4.61	1.34
K ₂ O	0.51	0.49	0.58	0.39	1.28	0.04	0.47	0.31	0.29	0.55
P ₂ O ₅	0.15	0.17	0.23	0.27	0.10	0.10	0.24	0.09	0.09	0.09
LOI	17.73	11.70	7.50	5.85	4.53	5.58	2.42	4.04	2.56	1.78
Cr	186	759	237	289	111	165	251	220	0	819
Ni	42	66	50	34	31	26	52	166	0	150
V	183	231	286	243	296	423	267	208	231	273
Rb	10	10	13	0	21	0	13	8	10	13
Ba	177	228	229	403	251	74	478	312	297	258
Sr	206	243	235	0	215	431	341	98	2295	303
Nb	0.0	5.0	0.0	0.0	5.0	5.0	5.0	0.0	5.0	0.0
Zr	46	53	63	0	55	73	91	44	75	60
Y	9	10	13	0	14	20	22	7	18	14

KM24	KM23	KM13	KM31	KM22	KM32	KM26	KM11	KM28	KM9	KM19	KM3
51.67	52.13	53.84	55.19	55.55	56.03	56.93	29.63	59.35	61.07	61.35	63.35
0.93	1.15	0.74	0.88	0.73	0.58	0.93	0.25	0.68	0.74	0.50	0.71
16.09	17.58	20.41	18.38	19.22	12.11	18.56	59.16	16.67	16.78	17.50	17.55
2.39	2.61	2.13	1.35	1.91	1.46	2.09	0.78	2.00	1.29	1.34	1.08
7.63	8.35	6.77	4.31	6.08	4.68	6.65	2.50	6.38	4.13	4.28	3.43
0.13	0.19	0.17	0.14	0.13	0.16	0.19	0.06	0.15	0.09	0.13	0.08
8.40	5.09	4.01	3.78	3.94	5.24	2.90	0.96	3.07	4.18	2.32	2.61
10.24	10.10	6.53	9.56	7.71	17.69	7.76	3.53	8.72	6.47	6.45	5.24
1.59	2.19	3.97	5.82	3.76	1.68	2.73	2.14	2.39	3.80	3.50	3.92
0.80	0.46	1.18	0.51	0.80	0.17	0.93	0.91	0.24	1.29	2.24	1.70
0.12	0.13	0.26	0.08	0.17	0.20	0.35	0.10	0.35	0.15	0.40	0.34
2.07	1.20	1.98	4.36	1.84	5.92	0.80	4.41	2.65	1.97	1.51	1.12
459	132	21	110	27	924	0	16	58	150	48	51
114	22	12	63	0	63	0	0	12	67	11	27
276	295	168	269	222	222	150	60	180	124	125	103
19	12	28	12	22	6	21	17	9	27	64	34
302	222	502	210	560	505	526	1128	151	827	1359	1217
274	271	684	273	398	336	487	568	249	572	2247	675
0.0	7.0	0.0	5.0	5.0	0.0	8.0	4.0	11.0	19.0	20.0	17.0
65	90	61	62	86	53	147	63	105	144	170	173
16	25	13	12	16	12	32	8	14	11	12	10

KM7	KM2	KM4	KM8	KM6	KM17	KM14	KM20	KM1	KM12	KM16	KM5	KM10	KM21
63.46	65.81	65.90	66.03	66.15	66.24	66.41	66.69	66.75	67.24	67.35	67.55	68.19	69.75
0.49	0.57	0.50	0.53	0.50	0.50	0.57	0.39	0.48	0.44	0.50	0.45	0.27	0.33
17.66	16.98	16.98	17.15	16.84	16.77	17.44	16.24	17.12	16.66	16.99	16.73	18.55	16.34
1.08	0.93	0.92	0.94	0.91	0.92	1.02	1.00	0.82	0.84	0.93	0.86	0.66	0.66
3.43	2.96	2.95	3.01	2.92	2.93	3.26	3.18	2.62	2.67	2.96	2.75	2.09	2.10
0.09	0.07	0.07	0.07	0.07	0.07	0.08	0.09	0.00	0.06	0.06	0.07	0.07	0.06
2.39	2.01	2.33	2.31	2.23	1.88	1.96	2.15	1.72	2.00	1.79	1.71	0.59	1.12
5.86	4.84	5.02	5.84	4.63	4.65	3.55	5.06	4.93	4.52	3.93	4.75	2.53	3.86
4.01	3.82	3.88	3.40	4.35	4.23	4.02	3.64	3.72	3.30	3.85	3.80	4.29	4.01
1.35	1.73	1.22	0.53	1.16	1.59	1.36	1.37	1.66	2.14	1.46	1.17	2.61	1.65
0.16	0.26	0.23	0.18	0.23	0.22	0.32	0.18	0.17	0.14	0.18	0.15	0.15	0.12
3.52	2.26	0.95	1.49	2.43	1.62	2.21	2.60	1.54	4.69	1.94	0.61	1.45	0.75
77	38	95	63	75	49	51	89	92	63	16	29	0	39
14	21	26	15	35	14	16	18	66	23	12	11	0	11
101	78	68	84	78	76	78	81	65	69	82	65	28	45
29	30	28	13	22	37	26	30	34	39	29	30	54	39
1115	851	810	444	809	967	962	1041	674	577	1006	781	1168	907
604	479	499	444	473	543	560	642	450	313	485	430	483	393
6.0	15.0	11.0	10.0	12.0	11.0	14.0	8.0	10.0	9.0	11.0	10.0	8.0	11.0
111	144	142	123	160	160	154	110	138	122	151	149	130	111
6	8	7	6	9	9	10	10	7	6	10	7	8	9